EXPERIMENTAL INVESTIGATION OF THE AXISYMMETRIC TURBULENT BUOYANT PLUME

by

Paul D. Beuther

A dissertation submitted to the Faculty
of the Graduate School of State University
of New York at Buffalo in partial fulfillment
of the requirements for the degree of
Doctor of Philosophy

May 1980

Table of Contents

Chapter		Page No.
	Acknowledgements	
	List of Figures	i
	Nomenclature	iv
	Abstract	viii
1	Introduction	1
2	Background	3
	2.1 Theoretical Review	3
	2.2 Previous Experimental Investigations	8
	2.3 Review of Turbulence Models	10
	2.4 Taylor's Hypothesis	13
3	Description of the Experiment	17
	3.1 Introduction	17
	3.2 Description of the Plume Facility	19
	3.3 Measurement Technique	22
	3.4 Calibration	27
4	Description of Signal Processing/Data Analysis	38
	4.1 Data Acquisition	38
	4.2 Data Conversion	42
5	Presentation and Discussion of Results	51
	5.1 Moments of Velocity and Temperature	51
	5.2 Moments of Velocity and Temperature Derivatives	81
	5.3 Spectra	88
	5.4 Turbulent Energy and Fluctuating Temperature Balance	108
6	Summary and Conclusions	116
Appendix		
A1	Governing Equations for an Axisymmetric	121
A2	Description of Homemade Electronic Hardware	125
A3	Angle Calibration Technique	132
Bibliography		140

ACKNOWLEDGMENTS

I thank all those who have helped me with this dissertation, especially to Dr. William K. George, whose original invitation to Buffalo and subsequent guidance has had a major influence on my education. I also express my thanks to my wife Collette and my colleagues at Owens-Corning Fiberglas for their support and encouragement while I was finishing this disertation. Finally, a special note of thanks goes to Eileen Graber for typing the manuscript.

The research was supported by the National Science Foundation, Meterology Program under Grant Nos. ATM 76-01257 and ATM 78-08442 and Fluid Dynamics Program under Grant No. ENG 76-17466, and the Air Force Office of Scientific Research, Fluid Dynamics Branch under Contract No. F 49620-78-C-0047.

List of Figures and Tables

Figure No.	Page No.	Figure Title
1.	7	Plume Orientation
2.	18	Plume Facility
3.	20	Plume Heater
4.	23	x-wire Geometry
5.	25	Block Diagram of Data Acquisition
6.	29	Velocity Calibration Data
7.	33	Angle Calibration Geometry
8.	35	Angle Calibration Data
9.	36	Angle Calibration Velocity Mapping
10a.	41	"Plume" Flow Chart for Data Acqusition
10b.	43	"Deriv" Flow Chart for Data Conversion
11	45	2-D Probability Plot for u and v
12.	47	Ambient Temperature Data
13.	49	Ambient Temperature Gradient Data
14.	50	Buoyancy Force as a Function of Height
15.	55	Mean Velocity Profiles
16.	56	Mean Temperature Difference Profiles
17.	59	Velocity Fluctuation Profiles
18.	60	Temperature Fluctuation Profiles
19.	61	Reynolds Stress Profile
20.	63	Turbulent Heat Flux Profiles
21.	65	Mean Momentum Balance
22.	66	Mean Temperature Balance
23	69	$\overline{u^3}$ Profile
24.	70	$\overline{v^3}$ Profile

Figure No.	Page No.	Figure Title
25	71	$\overline{u^2v}$ Profile
26	72	$\overline{uv^2}$ Profile
27.	73	$\overline{ut^2}$ Profile
28.	74	$\overline{vt^2}$ Profile
29.	75	$\overline{t^3}$ Profile
30.	76	$\overline{u^2t}$ Profile
31.	77	$\overline{v^2t}$ Profile
32.	78	$\overline{u^4}$ Profile
33.	79	$\overline{v^4}$ Profile
34.	80	$\overline{u^2v^2}$ Profile
35.	82	Comparison of $\overline{u^2v^2}$ to Gaussian Predictio
36.	94	Validity of Taylor's Hypothesis
37.	96	Vertical Velocity Spectra
38.	97	Vertical Velocity Derivative Spectra
39.	98	Comparison of Vertical Velocity and Vertical Velocity Derivative Spectra
40.	99	Radial Velocity Spectra
41.	100	Comparison of Vertical and Radial Velocity Spectra
42.	101	Comparison of Radial Velocity and Radial Velocity Derivative Spectra
43.	104	Temperature Spectra
44.	105	Temperature Spectra x $k^{+5/3}$
45.	106	Temperature Derivative Spectra
46.	107	Comparison of Temperature and Temperatur Derivative Spectra.
47.	112	Turbulent Kinetic Energy Balance
48.	113	Turbulent Temperature Fluctuation Balanc

Figure No.	Page No.	Figure Title
A2.1	126	Schematic of Temperature Anemometer
A2.2	128	Schematic of Amplifier and Differentiator
A2.3	129	Transfer Function of Differentiator
A2.4	131	Schematic of Probe Traverser Control
A3.1	135	Angle Calibration Geometry

Table No.	Page No.	Table Title
I	57	Effects of Stratification on Mean Velocity and Temperature Profiles
II	67	Fitted Curves for 1st and 2nd Moment.
III	67	Fitted Curves For 3rd Moment
IV	87	Derivative Measurements
V	87	Similarity Scaling of Derivative Measurements
VI	92	Comparison of Universal Constant of Temperature Spectra
VII	114	Comparison of Calculated and Measured Dissipation

b	Effective plume width; $U(b)/U(0) = 1/e$
c	Bit resolutin of A/D
d	Diameter of hot-wire sensor
$d_1(\eta)$	Similarity function for $\lambda\overline{\left(\frac{\partial u_z}{\partial t}\right)^2}$
$d_2(\eta)$	Similarity function for $\lambda\overline{\left(\frac{\partial u_r}{\partial t}\right)^2}$
$d_3(\eta)$	Similarity function for $\gamma_o^2\beta^2\lambda\overline{\left(\frac{\partial t}{\partial t}\right)^2}$
e_o	Output voltage of differentiator
e_1	Input voltage for differentiator
$E(k)$	Velocity fluctuation spectrum function
E_t	Output voltage of temperature anemometer
$E_t(k)$	Temperature fluctuation spectrum function
F_o	Buoyancy flux
F_{11}	3-D spectrum of axial velocity fluctuations
F_{22}	3-D spectrum of radial velocity fluctuations
F_t	3-D spectrum of temperature fluctuations
F_{11}^1	1-D spectrum of axial velocity fluctuations
F_{22}^1	1-D spectrum of radial velocity fluctuations
F_t^1	1-D spectrum of temperature fluctuations
$f(\eta)$	Similarity function for mean axial velocity
f_n	Sampling rate of A/D converter
g_o	Gravitational acceleration
$g(\eta)$	Similarity function for mean buoyancy
$h_{ij}(\eta)$	Similarity functions for second moments $i,j = 1,2,3$ for u_z, u_r, t respectively.
I	Current through hot-wire sensor
$\underset{\sim}{k}$	wavenumber vector
k	Chapter 3: Anglecalibration constant
k	Chapter 5: Magnitude of $\underset{\sim}{k}$

$k(\eta)$	Similarity variable for mean radial velocity
k_1	Wavenumber in axial direction
L	Hot-wire sensor length
ℓ	Turbulence length scale based on dissipation
M	Mass flux
N^2	Brunt-Vasaila frequency, $-\frac{g_o}{\rho_o}\frac{d\rho_\infty}{dz}$
Nu	Nusselt number
P	Mean static pressure
P(u)	Probability density of velocity flucuations
Pr	Prandtl number
P_T	Turbulent Prandtl number
p	Turbulent static pressure
$R(\tau)$	Time auto-covariance function
R_d	Reynolds number based on the diameter of the hot-wire sensor
$R_{ij}(\underset{\sim}{r})$	Spatial velocity covariance function
R_ℓ	Reynolds number based on the turbulent length and velocity scales
R_T	Turbulent Reynolds number
R_w	Resistance of hot-wire sensor
$\underset{\sim}{r}$	Spatial separation vector in covariance function
r	radial space coordinate
S_{dt}	Frequency spectrum of temperature derivatives
S_{du}	Frequency spectrum of axial velocity derivatives
S_{dv}	Frequency spectrum of radial velocity derivatives
S_t	Frequency spectrum of temperature fluctuations
S_u	Frequency spectrum of axial velocity fluctuations
S_v	Frequency spectrum of radial velocity fluctuations

T	Temperature
T_f	Film temperature
T_g	Gas temperature
T_w	Wire temperature
t	Temperature fluctuation
U_o	Magnitude of velocity
U_1	Mean axial velocity
U_2	Mean radial velocity
U_c	Convection velocity
U_{eff}	Effective velocity measured by hot-wire
U_r	Mean radial velocity
U_z	Mean axial velocity
U	Mean azimuthal velocity
u	Axial velocity fluctuation
u_1	Axial velocity fluctuation
u_2	Radial velocity fluctuation
u_3	Azimuthal velocity fluctuation
u_r	Radial velocity fluctuation
u_z	Axial velocity fluctuation
u_ϕ	Azimuthal velocity fluctuation
v	Radial velocity fluctuation
$\underset{\sim}{x}$	Spatial coordinate vector
z	Axial space coordinate
α	Chapter 2: Entrainment coefficient
α	Chapter 5: Constant in velocity spectrum function
α_1	Constant in 1-D velocity spectrum

β Chapter 2: Coefficient of thermal expansion

β Chapter 5: Constant in temperature spectrum function

β_1 Constant in 1-D temperature spectrum

γ Thermal diffusivity

γ_T Eddy diffusivity

ϵ Dissipation of turbulent kinetic energy

ϵ_t Dissipation of turbulent temperature fluctuations

η Non-dimensional radial coordinate, r/z

Θ Angle between x-wire sensors

κ Thermal conductivity

λ Taylor microscale

λ_t Taylor microscale for temperature fluctuations

μ Dynamic viscosity

ν Kinematic viscosity

ν_T Eddy viscosity

ρ Density

$\rho_{ijk}(\underline{r})$ Correlation functions of third moments

ρ_∞ Density of ambient air in plume

ρ_o Density of ambient air at base of plume

τ Time separation in auto-covariance function

$\underline{\Phi}_{11}$ Non-dimensional 1-D axial velocity spectrum

$\underline{\Phi}_{zz}$ Non-dimensional 1-D radial velocity spectrum

$\underline{\Phi}_t$ Non-dimensional 1-D temperature spectrum

ϕ angle between velocity vector and normal of hot-wire sensor

ω circular frequency

Abstract

The investigation consists of a detailed experimental study of the turbulent energy balance and eddy structure in a turbulent axisymmetric hot air plume in a stably stratified environment. Data is obtained at various positions in the plume for exit flow conditions corresponding to a densimetric Froude number of about unity. The measurement techniques use hot wire anemometry methods to produce instantaneous velocity and temperature signals which are simultaneously sampled using an analog-to-digital converter. Data is acquired and analyzed using an on-line PDP 11 minicomputer. A computer controlled traversing apparatus is utilized to simplify data acquisition.

Measurements are taken of the turbulent and mean quantities needed to specify the energy budget. Also acquired are the power spectral densities, and single and joint probability densities of velocity and temperature. Whether or not local isotropy exists at small scales is determined and the applicability of Taylor's hypothesis to the dissipative scales is tested. The data is compared with current computer models to verify their credibility. From these measurements and models the structural characteristics of the turbulence are inferred.

Chapter 1. Introduction

This paper attempts to gain insight into the laws of nature that govern turbulent fluid motion affected by buoyancy forces. Measurements of temperature and two components of velocity have been taken using a minature x-wire for velocity and a cold resistance wire for temperature in a hot air axisymmetric turbulent plume. There is a severe shortage of good quality data in buoyancy driven flows and the plume, one of the simplest examples of such flows, lends itself well to laboratory study. This paper marks the first time measurements of the turbulent kinetic energy budget and temperature fluctuation budget have been published for a plume. Spectral measurements of velocity and temperature, along with their time derivatives are also presented.

The data presented represent a range of thermal stratification of the ambient environment, and is compared with previous data taken under neutral ambient conditions. For small degrees of stratification it is shown that the data can still be scaled in similarity variables if the local value of the buoyancy heat flux is used for scaling. However, for severe changes in stratification such a scaling is not possible, since the shape of the velocity profile changes with increasing thermal stratification.

A surprising discovery in this investigation is the seriousness of the problem of drop-out* from the velocity x-wire due to the high intensity of the velocity fluctuations. Often overlooked in the past, the magnitude of this problem in this investigation (greater than 50% at some locations) sheds doubt on many previous investigations. The high turbulence intensity also creates a serious problem in measuring the dissipation of the turbulent velocity fluctuations. This is due, in part, to a breakdown of Taylor's hypothesis which assumes that a velocity field is frozen in

* Drop-out is the loss of information occurring when the velocity vector is outside the angle of acceptance of the x-wire.

space and is being swept by the probe at a constant velocity. Since this is not the case in high intensity flows correction schemes for the dissipation need to be employed. This investigation has looked at schemes developed by Lumley (1965a) and Wyngaard and Clifford (1977), both of which indicate that the magnitude of this correction can easily exceed 50% at many parts of the flow. This correction must also be employed in a calculating spectral density functions of velocity and temperature.

The prime goal of this investigation is to provide a reliable set of data in a buoyancy dominated flow that can be used for comparison in future and present models of buoyancy dominated turbulent flows. Later this data will be compared with some models already in existence. Hopefully this data will spur new turbulence models for these types of flows.

Chapter 2. Background

2.1 Theoretical Review

Buoyancy dominated turbulent flows are a common occurrence in the environment, but have never been well understood. One reason for this can be attributed to the added complexity involved in measuring both velocity and buoyancy simultaneously. It has only been in the last decade that significant progress has been made, particularly with regard to meteorological phenomena, but much more is still left undone. The mechanics of even the simplest of these flows, the plume, are still a mystery. In fact, no simple turbulent flow, even without buoyancy, is well understood.

Turbulence is a condition of instability in a fluid flow, characterized by the seemingly random motion of the fluid and high levels of fluctuating vorticity. Turbulence is related to the Reynolds number; all flows eventually become turbulent as the Reynolds number becomes large. The non-deterministic nature of these flows necessitates a statistical method of analysis. Modern turbulence research began in the late 19th century when Osborne Reynolds (1895) developed a set of equations governing turbulent motion. Unfortunately, the equations are unable to be solved because there are more unknowns than equations. This is commonly called the closure problem of turbulence. In order to relate terms such as the Reynolds stress tensor, $\overline{uv}$, to the other known parameters and close the equations, one must resort to intuitive reasoning and ad hoc assumptions. The simplest model is the eddy viscosity which assumes the Reynolds stress, $\overline{uv}$, or turbulent heat flux, $\overline{vt}$, to be proportional to the mean gradient of velocity or temperature. This has had good success in flows that can be characterized by only one time scale, such as most free shear flows. Other methods will be discussed later in this chapter.

Plumes are a specific class of buoyancy dominated turbulent flows which are produced by a density difference between the flow and its environment. If this density difference is supplied at a constant rate to a uniform environment, the buoyancy flux defined by equation (2.1) will be constant for all heights (c.f. Turner, 1973). Because of this, plumes constantly entrain ambient fluid, and the net momentum defined by equation (2.2) increases with height.

$$F_o = 2\pi \int \widetilde{u}\, \overline{g_o \frac{\Delta\rho}{\rho}}\, r dr \qquad (2.1)$$

$$M = 2\pi \int \overline{\widetilde{u}^2}\, r dr \qquad (2.2)$$

The radial velocity of the entrained air is directly proportional to the mean centerline vertical velocity. A detailed discussion of entrainment processes of various free shear flows can be found in Townsend (1970).

Examples of plume-like flows abound, but the classical example is the plume rising off the lighted cigarette in a still room. Another common example is that of the plume issuing from a smokestack. However, plumes do not have to be rising; a denser fluid released into a lake or river results in an upside down density driven plume. These flows can all be analyzed in the same fashion, since they are all governed by the same process.

If the Reynolds number of the plume becomes large enough that the viscosity and molecular diffusivity become unimportant, the only parameters governing the flow dynamics in a neutral environment are the buoyancy flux, F_o, the height, z, and the radial component, r. Simple dimensional analysis leads to

$$u \propto F_o^{1/3} z^{-1/3} F(r/z) \qquad (2.3)$$

$$g_o \frac{\Delta\rho}{\rho} \propto F_o^{2/3} z^{-5/3}\, g(r/z) \qquad (2.4)$$

However, a neutral environment is not a common occurrence in nature. With the exception of an hour or two at dawn and dusk, the atmosphere over land is usually far from neutral. For the case of a plume in a stable environment, similarity type solutions as found above expressing plume properties in powers of height above the source cannot be found. In fact, at some height the buoyant fluid will eventually come to rest. Morton, Taylor and Turner, (1956) developed a set of non-dimensional functions corresponding to height, radius, vertical velocity, and buoyancy parameter. These parameters are dependent upon the ambient density gradient. They are summarized below in equations (2.5) - (2.8).

Height : $$z = 0.41\,\alpha^{-1/2} F_o^{1/4} N^{-3/4} z_1 \qquad (2.5)$$

Plume Width: $$b = 0.82\,\alpha^{1/2} F_o^{1/4} N^{-3/4} b_1 \qquad (2.6)$$

Velocity : $$u = 1.16\,\alpha^{-1/2} F_o^{1/4} N^{1/4} u_1 \qquad (2.7)$$

Buoyancy : $$g\frac{\Delta\rho}{\rho} = 0.82\,\alpha^{-1/2} F_o^{1/4} N^{5/4} \Delta_1 \qquad (2.8)$$

α is the entrainment coefficient and N^2 is the Brunt-Väisälä frequency of gravity waves in a stable atmosphere. For $z_1 < 2$ the plume spreads nearly linearly, and the solutions are similar to those in a neutral environment. Above this height the plume begins to spread out radially and eventually reaches a maximum height at $z_1 = 2.5$.

For an unstable environment, Batchelor (1954) showed that power law similarity solutions exist when the ambient density gradient is of the form

$$\frac{g_o}{\rho_o}\frac{d\rho_\infty}{dz} = C z^p \qquad (2.9)$$

where $C \geq 0$

The equations governing the motions of an axisymmetric plume are obtained by decomposing the Navier-Stokes equations into mean and fluctuating quantities and averaging. The resulting Reynolds equations for momentum, continuity and temperature are written below (See Figure 1).

$$\bar{u}_j \frac{\partial \bar{u}_i}{\partial x_j} + \frac{\partial}{\partial x_j}(\overline{u_i u_j}) = -\frac{1}{\rho}\frac{\partial P}{\partial x_i} + \nu \frac{\partial^2 \bar{u}_i}{\partial x_j^2} - g_o \frac{\Delta \rho}{\rho_\infty} \delta_{i3} \tag{2.10}$$

$$\frac{\partial \bar{u}_i}{\partial x_i} = 0 \tag{2.11}$$

$$\bar{u}_j \frac{\partial T}{\partial x_j} + \frac{\partial}{\partial x_j}(\overline{u_j t}) = \gamma \frac{\partial^2 T}{\partial x_j \partial x_j} \tag{2.12}$$

These equations assume the fluid to be incompressible and that the density fluctuations are small. The latter assumption allows use of the Boussinesq approximation to ignore the density fluctuations except in the buoyancy term of the momentum equation. If the density differences arise from thermal expansion and the temperature differences are sufficiently small, the buoyancy term can be written as:

$$g_o \frac{\Delta \rho}{\rho_\infty} = -g_o \beta \Delta T \tag{2.13}$$

where β is the coefficient of thermal expansion. For an ideal gas, $\beta \sim \frac{1}{T}$.

By rewriting in cylindrical coordinates, discarding all viscous and molecular diffusion terms and all mean gradients in the azimuthal direction, the dominant terms in the equations yield the following. (See Appendix A1 for a detailed derivation of all equations governing the motion of plumes).

Figure 1. Plume Orientation

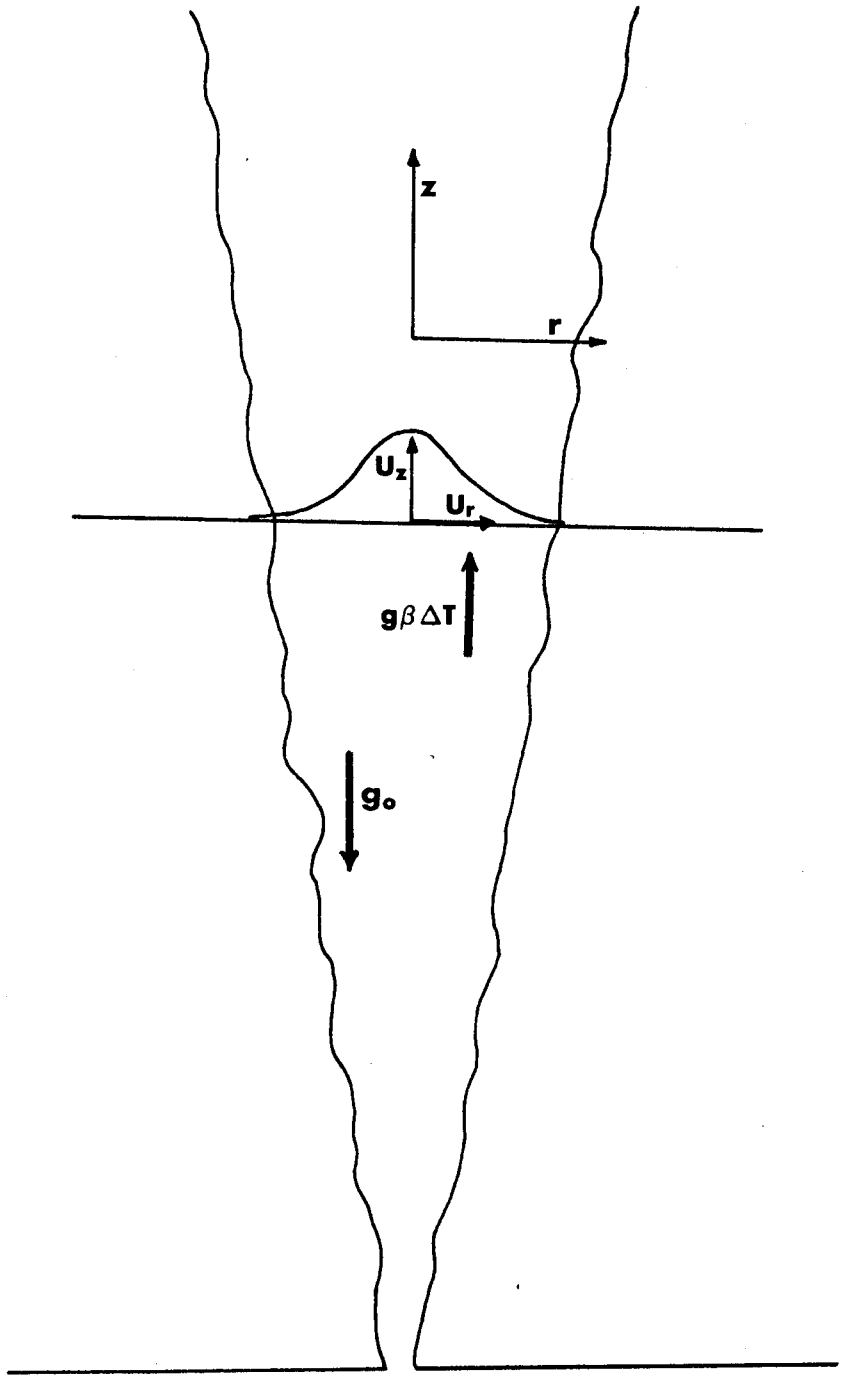

$$\bar{u}_z \frac{\partial \bar{u}_z}{\partial z} + \bar{u}_r \frac{\partial \bar{u}_z}{\partial r} + \frac{1}{r}\frac{\partial}{\partial r}\left(r \overline{u_z u_r}\right) = g_o \beta \Delta T \qquad (2.14)$$

$$\frac{\partial}{\partial z} \bar{u}_z + \frac{1}{r}\frac{\partial}{\partial r}(r \bar{u}_r) = 0 \qquad (2.15)$$

$$\bar{u}_z \frac{\partial T}{\partial z} + \bar{u}_r \frac{\partial T}{\partial r} + \frac{\partial}{\partial z}(\overline{u_z t}) + \frac{1}{r}\frac{\partial}{\partial r}(r \overline{u_r t}) = 0 \qquad (2.16)$$

For the case of a uniform environment similarity forms can be developed.

2.2 Previous Experimental Investigations

During the past forty years there have been several studies of turbulent plumes, beginning with Schmidt (1941). The first detailed study of the turbulent plume was undertaken by Rouse, Yih, and Humphreys (1952)(c.f. Yih 1953). They used a wind vane anemometer and thermocouples to measure mean velocity and temperature profiles in a gas burner generated plume. They found the temperature profile to be wider than that of the velocity profile,* a result which has prompted the development of many convincing theories explaining this behavior. The result has been refuted by several more recent investigations (See below). The discrepancy is most likely due to the inability of the wind vane anemometer to respond to the low velocities at the outer edges of the plume. Despite the uncertainty associated with the measurements, they have been the primary data reference on plumes until very recently.

In 1974 George, Alpert and Tamanini (1977) extended the work of Rouse, Yih and Humphreys by measuring a hot air turbulent plume with a two-wire

* A sufficient relative measure of profile width is obtained by normalizing both profiles by their centerline (maximum) values and plotting them togethe

probe (one operated in the constant temperature mode and the other operated as a resistance thermometer.) They measured mean and rms fluctuating quantities, velocity-temperature correlation and the joint probability distribution. All data satisfactorily collapsed using the conventional similarity scaling. The shape of the profile of mean temperature displayed good agreement with the results of Rouse et al., but it was 20% lower at the centerline. The mean velocity had a lower centerline value and a much wider profile than did the data of Rouse et al. The authors observed that when the profiles of temperature and velocity were compared, normalized to center-line values, the velocity profile was wider than that of the temperature profile. This is opposite to the result found by Rouse, et al. In this investigation, the turbulent heat flux was included in the calculation of the total buoyancy flux. Other previous investigations ignored this contribution which can be as large as 10-15%.

In an independent effort, Nakagone and Hirata (1977) also obtained velocity and temperature data using a two-wire probe. Unfortunately, the mean data is not presented in a manner conducive to quantitative comparison with other experiments. In agreement with the results of George et al., Nakagone and Hirata found the velocity profile to be wider than the temperature profile. Both of the experiments measured rms temperature and velocity intensities of roughly 33% and 26% respectively when scaled to the centerline mean value. None of the above investigations directly measured the buoyancy flux at the plume source, but instead relied on the integration of the measured velocity and temperature profiles to obtain these values.

In addition to the above, Kotsovinos (1977) did work in a two-dimensional plume using a Laser Doppler Anemometer. He measured profiles of first and second moments, and reported center-line turbulent intensities in the

neighborhood of 50-60%. These results have not been substantiated by other techniques or investigators as yet.

2.3 Review of Turbulence Models

Turbulence models have become more numerous and have been greatly improved during the past decades. As mentioned previously, the main obstacle in turbulence modeling is the closure problem. The methods of overcoming this are diverse and often complicated. However, even the most complete model operates under numerous restrictions, and often requires the accompaniment of good intuitive analysis. This section will be devoted to reviewing several of these models as they have been applied to turbulent plumes and other buoyancy dominated flows.

Eddy Viscosity: The eddy viscosity is one of the oldest models for the Reynolds stress, evolving out of Prandtl's mixing length theories. An eddy viscosity model assumes Reynolds stress, $\overline{uv}$ (or the cross-stream heat flux, $\overline{vt}$) to be proportional to the gradient of the mean axial velocity (or temperature). For example,

$$\overline{uv} = \nu_T \frac{\partial u}{\partial r} \tag{2.17}$$

$$\overline{vt} = \gamma_T \frac{\partial T}{\partial r} \tag{2.18}$$

where ν_t is the eddy viscosity and γ_t is the eddy diffusivity.

Models such as these are often referred to as gradient transport models. Although they are often justified on a mixing length type of argument, the reason they work is that in single time scale flows the time scale of the turbulence is the same as that of the mean flow. The success of these models follows from a dimensional necessity; there is no other possibility. For flows with more than one time scale (three-dimensional flows, flows with suction, impinging flows) the gradient transport model fails. However,

most free shear flows (jets, wakes, plumes) are single time-scale flows in which a gradient transport gives reasonable results.

By combining the two gradient transport equations above with the three equations for momentum, temperature, and continuity, the resulting set of equations can be solved. Yih (1977) has found an exact solution of these equations for a turbulent plume for the case of a turbulent Prandtl number equal to 1.1 or 2.0. The definition of the turbulent Prandtl number is the same as the ordinary Prandtl number except the eddy viscosity and eddy diffusivity are substituted for the molecular values. Yih's solutions for the velocity and temperature similarity profiles are given by:

Velocity: $$f(\eta) = \frac{f_1}{[1+A\eta^2]^2} \tag{2.19}$$

Temperature: $$g(\eta) = \frac{g_1}{[1+A\eta^2]^m} \tag{2.20}$$

where $\eta \equiv r/z$ and $m = 3$ and $m = 4$ for turbulent Prandtl number equal to 1.1 and 2.0 respectively.

Yih's solutions were extended to other values of Prandtl number by Hamilton and George (1976) and Baker, Taulbee and George (1979). These were both computational solutions of the same plume equations, although they took into account the turbulent contribution of the vertical heat flux. The results for Prandtl number equal unity are very close to Yih's solution for Prandtl number 1.1.

All three of these investigations assumed a constant eddy viscosity and eddy diffusivity across the flow. As pointed out by Baker (1980) the solutions badly over-estimate the entrainment. This is due to the poor fit to data at large values of radius. A better model might incorporate an eddy viscosity which decays as a function of radius.

Two Equation Models: The next degree of complexity of modeling involves relating the second moments to third moments and closing the equations at this point. This is usually done by using a gradient transport hypothesis for these third moments, but other simplifications are often used to reduce the amount of computing time necessary. This class of models gets its name because the turbulent transport is evaluated from equations involving two turbulence properties, which are determined by finding a solution to the modeled form of their respective equation. The two mos common properties chosen are the turbulent kinetic energy, K, and its dissipation, ε. For the plume and other flows with scalar quantities such as temperature, a third parameter is needed. This is usually the mean-square temperature fluctuation.

Tamanini (1978) and Chen and Rodi (1975) have applied these methods to the turbulent plume in a neutral environment. The predictions of the models agree quite well with the experimental data available. Tamanini noted that the dissipation in the plume is approximately the same as in a forced jet, but the production terms are 20% lower. Also of interest was the unusually high value required for the temperature dissipation.

Normality of Fourth Moments: This method relies on a statistical argument for closure. By assuming the fourth moments are normally distributed, they can be related to the second moments as shown in Equation (2.21). In most flows, this appears to be a good assumption when the flow is fully

$$\overline{u_i u_j u_k u_l} = \overline{u_i u_j}\ \overline{u_k u_l} + \overline{u_i u_k}\ \overline{u_j u_l} + \overline{u_i u_l}\ \overline{u_j u_k} \qquad (2.21)$$

turbulent (see Monin and Yaglom 1975). However at the outer edges of the flow the intermittent nature of the turbulence weakens this assumption considerably. Although it eliminates the need for the gradient transport assumption at fourth order, in practice the resulting set of

equations becomes difficult to solve. The first to attempt such a closure was Millionschikov (1941). A more recent and partially successful attempt is due to Lumley (1975), but restrictions on computer time and storage have limited the number of other attempts. However, several investigators have successfully applied this method to smaller, more manageable problems and have obtained excellent results (c.f. Beuther, George, Arndt 1977).

2.4 Taylor's Hypothesis

Turbulence theory deals mostly with spatial variations of the velocity and scalar fields. However, it is the temporal fluctuations of the Eulerian fields that are usually measured. To convert temporal variations into spatial ones, most investigators resort to Taylor's Frozen Field Hypothesis. (c.f. Taylor 1938). This theory states that the measured fluctuation can be considered as a spatial one being convected by the measurement point at some convection velocity, U_c. As a consequence, the following relations exist.

$$\frac{d}{dz} = \frac{1}{U_c}\frac{d}{dt} \tag{2.22}$$

$$k = \frac{2\pi f}{U_c} \tag{2.23}$$

k is the wave number for a given spatial fluctuation.

In a highly turbulent shear flow, many factors exist which can cause Taylor's hypothesis to fail. Lumley (1965a) outlines several criteria to determine the applicability of the frozen field hypothesis; these are summarized below:

1. Non-uniform Convection Velocity. Equation (2.22) assumes that U_c is a constant value. However, there is no reason for all eddies to be convected at the same speed. It is likely that the smaller fluctuations are convected at a different rate than the larger

fluctuations (c.f. Wills 1964). The effect of these different convection velocities can be ignored if

$$\bar{U} \gg \frac{2\pi}{k} \cdot |\nabla \bar{U}| \qquad (2.24a)$$

In general, this effect is valid only for the small scales.

2. Spectral Aliasing Due to Non-uniform Convection Velocity. This effect can also cause spectral broadening of the velocity spectrum unless the following criteria is met:

$$\frac{2 \frac{d^2}{dk_1^2}(F_{11}^1)\, \pi^2 |\nabla \bar{U}|^2}{3 \bar{U}^2 F_{11}^1} \ll 1 \qquad (2.24b)$$

where F_{11}^1 is the one-dimensional velocity spectrum. This is equivalent to the square of equation 2.24a in the inertial subrange where the spectrum has a power law roll-off.

3. Temporal Variation of the Convected Eddy. In reality, the turbulence is not really a frozen field; it does have a time dependence. This temporal variation can be ignored if

$$F_{11}^1 \lll \frac{\bar{U}^2}{k} \qquad (2.24c)$$

This insures that the eddy does not evolve during the time required for it to be swept past the measuring probe. (The increased number of inequality signs is because the original criteria used to develop this was squared).

4. Fluctuation of the Convection Velocity. Due to the nature of turbulence, the eddies are not being convected at a constant rate. To account for this Lumley developed a model to correct for the errors associated with assuming a constant convection velocity. By approximating the characteristic function by its first two terms

$$EXP[i \underline{k} \cdot \underline{u}] \simeq 1 + \tfrac{1}{2} \overline{(i \underline{k} \cdot \underline{u})^2} \qquad (2.25)$$

Lumley developed the following equation relating the measured one-dimensional velocity spectrum of u_1 to the true spectrum:

$$F^1_{11_m} = F^1_{11} + \frac{\overline{u_1^2}}{2U^2}\left(k_1^2 F''_{11} + 4k_1 F'_{11} + 2F_{11}\right) - \frac{\overline{u_2^2}+\overline{u_3^2}}{U^2}\left(k_1 F'_{11} + F_{11}\right) \quad (2.26)$$

where the primes denote differentiation with respect to k_1. Lumley's analysis was extended by Wyngaard and Clifford (1977) to the u_2 component and to scalar spectra with the following result:

$$F^1_{22m} = F_{22} + \frac{\overline{u_1^2}}{2U^2}\left\{k_1^2 F''_{22} + k_1 F'_{22}\left[4 - 5\frac{\overline{u_2^2}}{\overline{u_1^2}} - \frac{\overline{u_3^2}}{\overline{u_1^2}}\right] + F_{22}\left(2 + \frac{\overline{u_2^2}}{\overline{u_1^2}} - \frac{\overline{u_3^2}}{\overline{u_1^2}}\right) - 2\frac{\overline{u_2^2}}{\overline{u_1^2}}\left(k_1^2 F''_{11} - k_1 F'_{11}\right)\right\} \quad (2.27)$$

$$F^1_{t_m} = F_t + \frac{\overline{u_1^2}}{2U^2}\left(k_1^2 F''_t + 4k_1 F'_t + 2F_t\right) - \frac{\overline{u_2^2}+\overline{u_3^2}}{2U^2}\left(k_1 F'_t + F_t\right) \quad (2.28)$$

The above assume that the convected field is isotropic, although this is not required for the convecting field.

By integrating the solutions to the above equations, relationships relating the true space derivatives and those inferred by Taylor's hypothesis can be found. These are listed below:*

$$\overline{\left(\frac{du_1}{dt}\right)^2_m} = \overline{\left(\frac{du_1}{dt}\right)^2}\left[1 + \frac{\overline{u_1^2} + 2\overline{u_2^2} + 2\overline{u_3^2}}{U^2}\right] \quad (2.29)$$

$$\overline{\left(\frac{du_2}{dt}\right)^2_m} = \overline{\left(\frac{du_2}{dt}\right)^2}\left[1 + \frac{\overline{u_1^2} + \tfrac{1}{2}\overline{u_2^2} + \overline{u_3^2}}{U^2}\right] \quad (2.30)$$

$$\overline{\left(\frac{dT}{dt}\right)^2_m} = \overline{\left(\frac{dT}{dt}\right)^2}\left[1 + \frac{\overline{u_1^2} + \overline{u_2^2} + \overline{u_3^2}}{U^2}\right] \quad (2.31)$$

where m denotes the measured value determined from equation (2.22). These corrections will be used on all derivative measurements in this investigation.

* George and Beuther (1979) were able to show this equation to be

5. Isotropy of Velocity Fluctuations. Although not related to the applicability of Taylor's hypothesis, Lumley also developed a criterion to determine the degree of isotropy of the velocity fluctuations. The fluctuations of a particular wavenumber will be isotropic if

$$F_{11}^1(k_1) > \frac{4\pi^2}{k^3}(\nabla\bar{u})^2 \tag{2.32}$$

None of the above criteria are satisfied for the largest scales of any turbulent flow, only for the small scales. By non-dimensionalizing relations 2.24 a-c in terms of the Kolmogorov length scale, approximating the mean velocity gradient with u/ℓ, and utilizing the isotropic spectral relationships, the following relations result.

$$2\pi \frac{u}{U} R_\ell^{-3/4} \frac{1}{k\eta} \ll 1 \quad ; \; R_\ell = \frac{u\ell}{\nu} \tag{2.33a}$$

$$3\pi^2 \frac{u^2}{U} R_\ell^{-1.5} \left(\frac{1}{k\eta}\right)^2 \ll 1 \tag{2.33b}$$

$$\frac{F_{11}^1(k_1)}{(\epsilon\nu^5)^{1/4}} \left(\equiv \phi_{11}(k\eta)\right) \lll \frac{U^2}{u^2} R_\ell^{1/2} \frac{1}{k\eta} \tag{2.33c}$$

$$\frac{F_{11}^1(k_1)}{(\epsilon\nu^5)^{1/4}} > \frac{4\pi^2}{(k\eta)^3} R_\ell^{-1} \tag{2.33d}$$

When all four of the above relations are valid, the flow can be described adequately as isotropic frozen regions convected by a spatially uniform fluctuating convection velocity. If in addition, Lumley's model is used to correct for the fluctuating convection velocity, accurate values of the spectral functions and the streamwise spatial derivatives (and thus the dissipation) can be computed. These four criteria will be compared to the present data in section 5.2.

Chapter 3. Description of the Experiment

3.1 Introduction

The goal of this investigation was to measure the turbulent kinetic energy budget in a turbulent plume. To accomplish this, two main design criteria needed to be satisfied in the final development of the experimental program. The first was to have a large enough Reynolds number to assure the negligibility of various terms in the governing equations (such as the viscous terms). It should also be large enough to assure the existence of an inertial subrange in the spectrum of the velocity fluctuations. The second was to have a microlength at least twice as large as the probe size. The turbulent microlength is equal to $2\pi\eta$ where η is the kolmogorov microscale defined by:

$$\eta = \left(\frac{\nu^3}{\epsilon}\right)^{1/4} \tag{3.1a}$$

where $\epsilon (\equiv \frac{u^3}{\ell})$ is the total dissipation/mass of the flow. Thus:

$$\eta = \frac{\nu^{3/4}\ell}{u^{3/4}} \tag{3.1b}$$

The Kolmogorov microscale is a measure of the smallest size fluctuation that exists in a turbulent flow. Fluctuations smaller than this are quickly dissipated by viscosity.

As can easily be seen, the only way to increase both the Reynolds number and the microscale simultaneously is to increase the length scale ℓ. This generally means making a larger plume and moving farther away from the source, which presents problems with probe sensitivity to diminishing velocity and temperature signals. This is particularly troublesome with the temperature in a plume, since it decays so rapidly with height. All these constraints were considered in the design of the experiment.

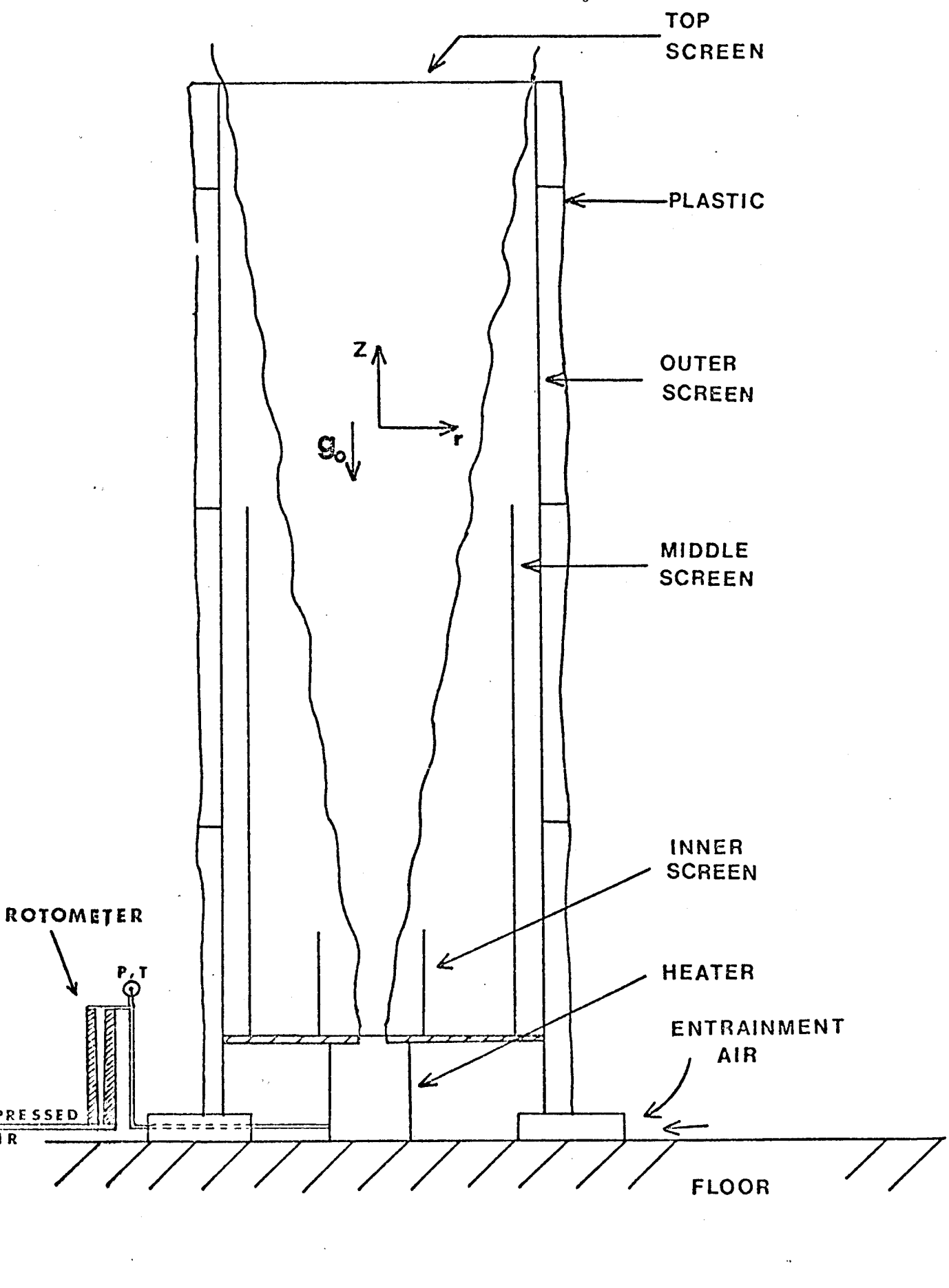
TOP
SCREEN
PLASTIC
z
r
a_o
OUTER
SCREEN
MIDDLE
SCREEN
INNER
SCREEN
ROTOMETER
P, T
HEATER
ENTRAINMENT
AIR
PRESSED
FLOOR

3.2 Description of the Plume Facility

The plume facility is located in a large room (5000 sq. ft.) with a ceiling height of 24 ft. The facility consists of a large, square, steel structure (6' x 6' x 20') which is wrapped in 4 mil plastic to prevent crossdrafts. The interior of this enclosure has three sections of window screening to prevent unwanted circulation - each two or three layers in thickness. A sketch of the entire facility is presented in Figure 2.

The plume is generated by passing compressed air through an insulated electric heater placed at the base of the steel structure. This heater is described in detail in Figure 3. Before entering the heater the air is filtered and the mass flow rate is measured with a calibrated rotometer. The air enters at the base of the heater and passes through a section of sintered bronze containing resistance heating elements. The air then passes through two screens and a 15:1 contraction ratio to exit into the ambient air. The exit temperature can be raised in excess of 300°C and maintained at a constant temperature with an Electromax controller connected to an SCR power supply. The exit profiles of velocity and temperature were flat to within 2%. Since both the mass flow rate and the heat flux are variable, it is possible to create exit conditions with a densimetric Froude number of unity. This enables the flow to become fully developed sooner than if a pure heat source were used. The heater has an output capability of 3000 watts, but normally is operated at less than 500 watts. This provides a center-line mean velocity of 0.75 meters per second at 1 meter above the exit.

Air for entrainment is fed to the base of the heater, rises between the plastic and outer layers of screening, and is entrained radially inward through the screens. The distance between the plastic and the outer screen is roughly 6 to 8 inches. This distance is too small to adequately provide

Figure 3 - Plume Heater

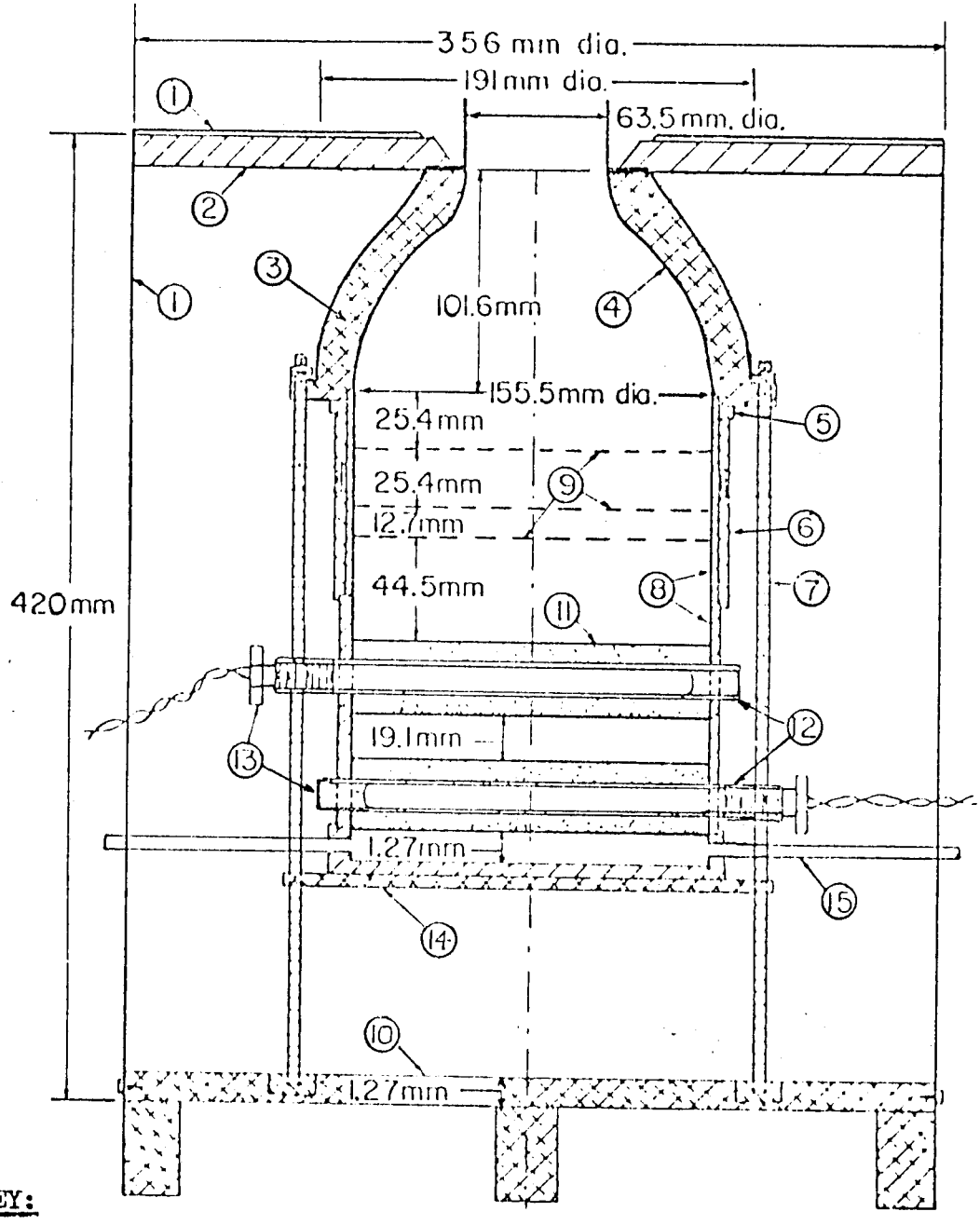

KEY:

(1) Container for silica aerogel insulation, sheet steel. (2) Cerafelt insulation. (3) Aluminum exit nozzle. (4) inner surface; Radius (mm.) = $31.75 + 2.42E{-}08\ x^5 - 6.1E{-}06\ x^4 + 4.36E{-}04\ x^3$. (5) Gasket. (6) Bronze sleeve. (7) Three threaded rods spaced 120° apart. (8) Copper spacer. (9) Stainless steel screens; 1.18 wires/mm.,0.305 mm. dia. (10) Aluminum base plate. (11) Two sintered bronze castings; density 5 g/cm^3, smallest passage 150 um. (12) Eight copper pipes; top four positioned perpendicular to bottom four. (13) Eight electric heaters; Watlow Firerod C6A81, 400 W. each. (14) Bronze base plate. (15) Four air inlet pipes, 90° apart.

recirculation of air. Along with some baffles to hold the plastic away from the screens, this is the prime cause of stratification in the plume. This outer screen is two to three layers thick and rises the full height of 20 ft. The middle layer of screening is octagonally shaped (and thus more closely tailored to the shape of the plume), has a diameter of roughly 5 ft., and extends only 8 ft. in height. Most of the measurements are taken in this section. The innermost layer of screening is circular in shape, 1-1/2 ft in height, has a 2 ft. diameter.

The screening is also important for the plume to keep it from swirling. Without screening the entrainment air would be acted upon by Coriolos accelerations and just like a bathtub drain, the plume would begin to swirl in a circular motion after several hours of running. This is because the time scale for the total experiment in an infinite environment is the length of time the plume is running. When this time scale approaches the time scale of the Coriolos acceleration (10^4 seconds) the induced vorticity will be amplified into a large vortex. The screens prevent this from happening, and no evidence of swirl has been noticed in this plume.

The plume was found to be extremely sensitive to the conditions of the room environment. The most sensitive area was at the exit from the heater - any slight draft would push the entire plume to one side and it would tend to stay there instead of returning to the center. The small circular screen was found to be very helpful in correcting this situation by stabilizing the plume. However, due to the sensitivity to drafts, the measurements were always carried out during the night when no one was in the room. The maximum deviation of the measured plume centerline was never greater than 1 degree from vertical at a height of 2 meters after these procedures were implemented.

3.3 Measurement Technique

The measurements of velocity and temperature are taken with a specially designed three wire probe (figure 4) having two velocity sensors in an x-array and one temperature sensor. All three wires are spaced within a sphere of radius 1.25 mm, which assured resolution of scales as small as the Komogorov microscale. The two velocity sensors are gold plated wires of 2.5 μm. in diameter and have a length to diameter ratio of 250. They are operated in a constant temperature mode with an overheat of 0.3 to 0.4. This low overheat is necessary to minimize the contamination of the temperature sensor by the wakes of the hot-wires when measuring the outer, high intensity regions of the plume. The temperature sensor is a 1 μm. tungsten wire operated in a constant current mode with a current of 150 micro-amps to minimize velocity contamination. This wire has a length to diameter ratio of 400.

The velocity anemometers used in this investigation were commercial units manufactured by DISA Electronics (Models 55M01 and 55D01). These units are also capable of operating a temperature wire in a low overheat, constant current mode suitable for temperature measurements, but an amplifier drift of about 1° per day made them inadequate for this particular investigation. Instead, homemade temperature anemometers, similar to those described by Wlezien and Way (1977) were built. These anemometers, like their DISA counterparts, provide adequate frequency response and a linear response to temperature over a wide range. The difference is that the internal amplifier is operated in a closed loop feedback system, which reduced our drift from over 1° per day down to less than 1/10° per day. Appendix A2 contains a detailed description of these anemometers.

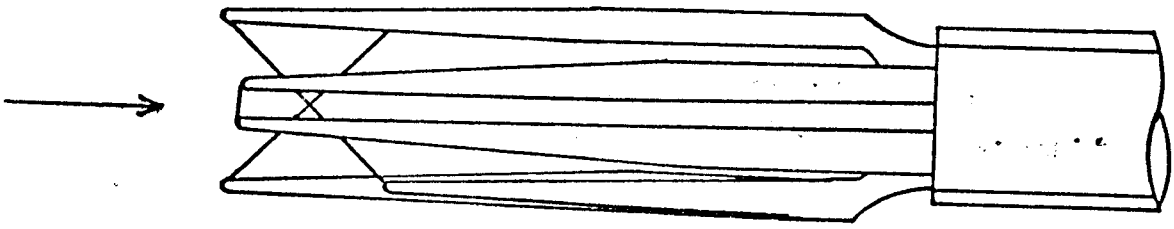

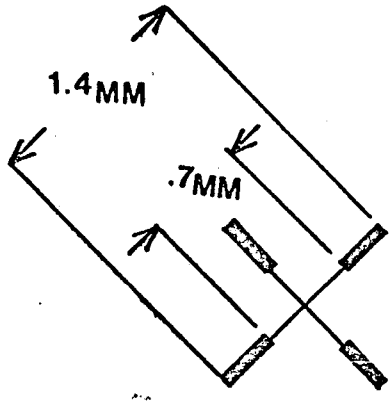
1.4MM
.7MM

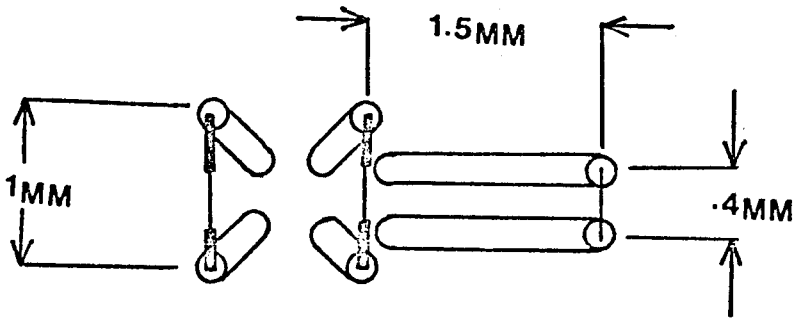
1MM
1.5MM
.4MM

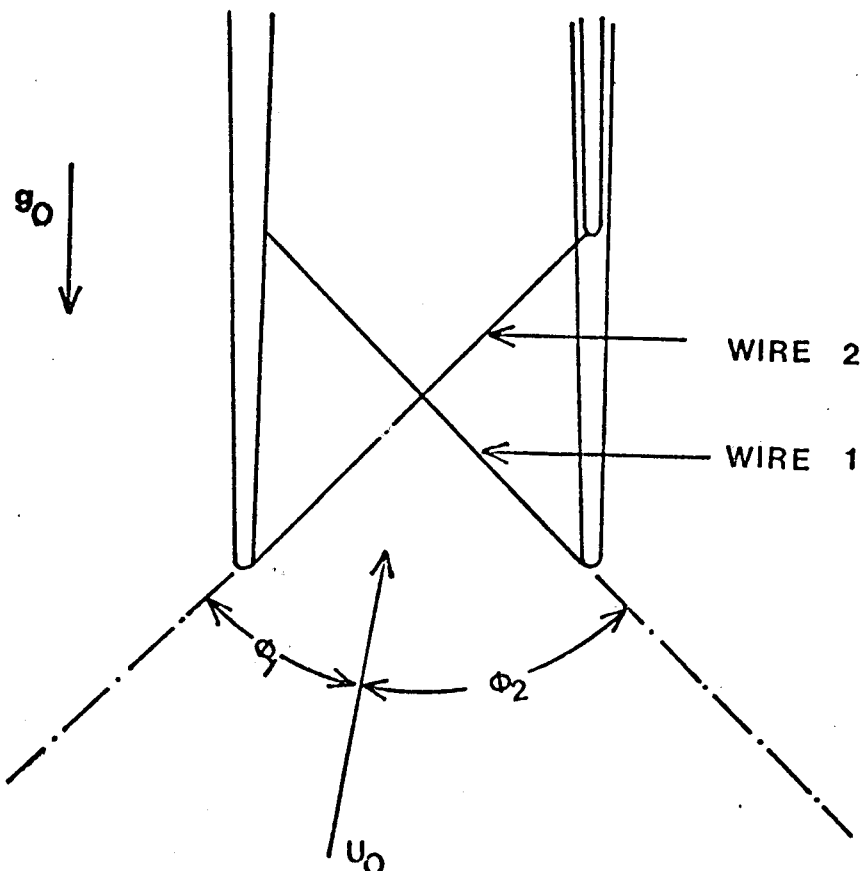
g_o
WIRE 2
WIRE 1
Φ_1
Φ_2
U_o

The anemometer outputs were amplified, differentiated, and filtered before being digitized by a DEC AR11 A/D Converter. This signal processing can be seen graphically in Figure 5 . The A/D converter had 16 channels with 10 bit resolution over a range of -2.5 to +2.5 volts (effective resolution approximately 5 mv.). To adequately sample the velocity anemometer output, two "buck and gain" amplifiers were built to subtract off a DC voltage and amplify the resultant signal. The temperature anemometers were built with internal adjustable gain and DC offset controls.

Analog differentiators are needed to measure the dissipation of the velocity and temperature fluctuations, since the time derivatives can not conveniently be calculated digitally with only 10 bits resolution.*

The two amplifiers and all three differentiators were low-pass filtered at 500 hz. to eliminate any unwanted high frequency noise. These are described in detail in Appendix A2.

Because of the higher levels of broadband noise in the temperature signals the temperature derivative had to be filtered again with a four pole Kronhite filter. This is the only filter that acted as an anti-aliasing filter (low-pass filters with a cut-off frequency of one half the sample frequency to prevent spectral aliasing). There are several reasons for the lack of additional filters, the primary one being that they were not necessary. For the velocity and temperature the signal strength at the cutoff frequency was already down to the bit resolution of the A/D. The electronic noise levels were down to that limit, and additional filters would have had little effect. This is due to the limiting nature of the digitizer quantization noise. Since the digitizer can only resolve down to 5 mv, signals of lower fluctuation levels cannot be resolved. Thus, low-level electronic noise is actually filtered out. In its place, the

* The high data rate required would result in a sample size much larger than that needed for statistical convergence with a corresponding increase in processing time.

Figure 5 - Block Diagram of Data Acquisition

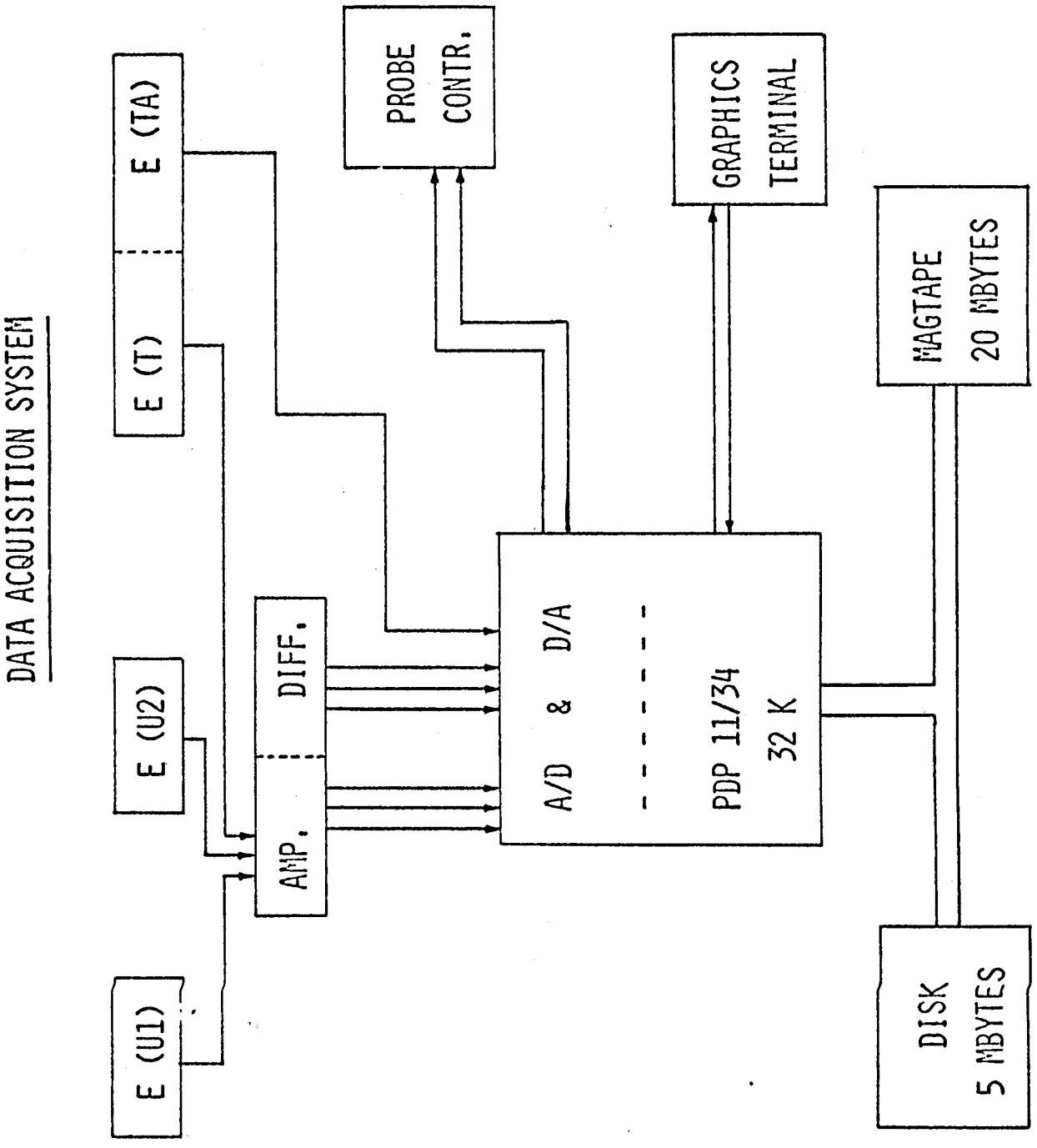

measured signal has the digitizer error imposed on it, which has a mean square value of:

$$\frac{c^2}{12} \tag{3.2}$$

where c is the bit resolution. This corresponds to an rms fluctuation of 2 mv. In terms of velocity and temperature, the 2 mv fluctuation is roughly 0.75 cm/s and 0.05°C respectively. The measured velocity and temperature spectra will also be affected, having a constant noise level given by equation 3.3 added to the true spectra

$$S_n(f) = \frac{c^2}{12 \cdot f_n} \tag{3.3}$$

f_n is the sampling frequency.

The derivative signal did have some measureable electronic noise, but it was felt that the noise level (2-3 mv. rms) would add far less error to the derivative measurements than the pass band attentuation and phase shift of the filters that were available. The exception to this was in the case of the temperature derivatives, but the tremendous phase lag introduced by the filter ruined the chance to calculate the cross moments of the temperature-velocity derivatives. Unfortunately, this was not realized until after most of the measurements were taken.

The AR11 also has two D/A outputs and several logic outputs to control relays. These are used to automate the control of a two dimensional traverser which moves a probe. This traverser has a vertical range of 1 meter and a horizontal range of 35 cm, but the traverser mount can be manually positioned on any one of the six supports 75 cm apart, thus extending the vertical range from floor to ceiling. The radial range can be manipulated in a similar fashion by adding or subtracting extension segments from the horizontal traversing rod.

The traverser is controlled by the analog control circuit described in Appendix A2. This controller compares an input voltage with the position voltage as determined by a potentiometer, and supplies $\pm$ 20 volts to the DC motor until the two voltages coincide. Noise on the long input lines from the potentiometer can cause a slight oscillation and vibration of the probe after the proper position is reached. To prevent this a relay is included so that the motor can be turned off completely by the computer. The input voltage can be supplied internally by turning a position knob on the controller box (Manual operation) or by the D/A of the AR11 (computer operation). Software exists in the form of a stand-alone program that accepts input from a terminal, subroutines which move the traverser to the next location in an array, and a calibration routine that allows a computer to reference the actual physical location of the probe. Although the traverser has proved quite reliable, programmers have not, and many safety shut off switches have been added to prevent the traverser from moving past its limit or striking one of the support beams. Since the computer gets no return signal from the controller telling it when the probe is in position, the subroutine calculates the time needed for the probe movement and waits an adequate period of time before releasing control back to the calling program.

3.4 Calibration

The velocity and temperature wires are calibrated at the exit of the plume source at several velocities and temperatures. The temperature reference is obtained from a copper-constantin thermocouple placed near the sensor and the velocity reference is determined by applying mass conservation to the reading of the upstream rotometer. Since the air temperature changes as it passes through the heater, its upstream properties must be measured. This is accomplished with a manometer and a thermometer placed

at the exit of the rotometer as was illustrated in figure 2. The rotometer was calibrated by measuring the output velocity of the plume source with a laser Doppler anemometer.

The velocity sensor calibration is accomplished by converting the anemometer voltage and flow velocity to Nusselt number and Reynolds number as defined by equations (3.4a) and (3.4b).

$$R_d = \frac{U_o d}{\nu} \tag{3.4a}$$

$$Nu = \frac{I^2 R_w}{\pi L K (T_w - T_g)} \tag{3.4b}$$

where T_w is the wire temperature, T_g is the gas temperature, d is the wire diameter, L is the wire length, R_w is the wire resistance, and κ is the thermal conductivity of the gas. A polynominal of the form of equation (3.5) is then fitted to this data.

$$R_d = A_0 + A_1 Nu^{1/2} + A_2 Nu + A_3 Nu^{3/2} + A_4 Nu^2 \tag{3.5}$$

This is illustrated in figure 6. The calibration for the two wires does not coincide because of slight differences in the length and diameter of the wires. These parameters were not measured and there was undoubtedly some slight variation between the actual values and the manufacturers standard values. Since both wires were calibrated individually, this was not important. One parameter that was difficult to measure was the sensor resistance. Because there was no way of shorting the probe across the sensor without fear of breakage, this parameter was adjusted after the calibration to give the best collapse of the data for all temperatures.

Evaluating Reynolds number at the local gas temperature and Nusselt number at the film temperature ($T_{film} \equiv \frac{T_{gas} + T_{wire}}{2}$) gives good collapse of the data for a Reynolds number range of .02-.25. This differs from the

VELOCITY CALIBRATION DATA

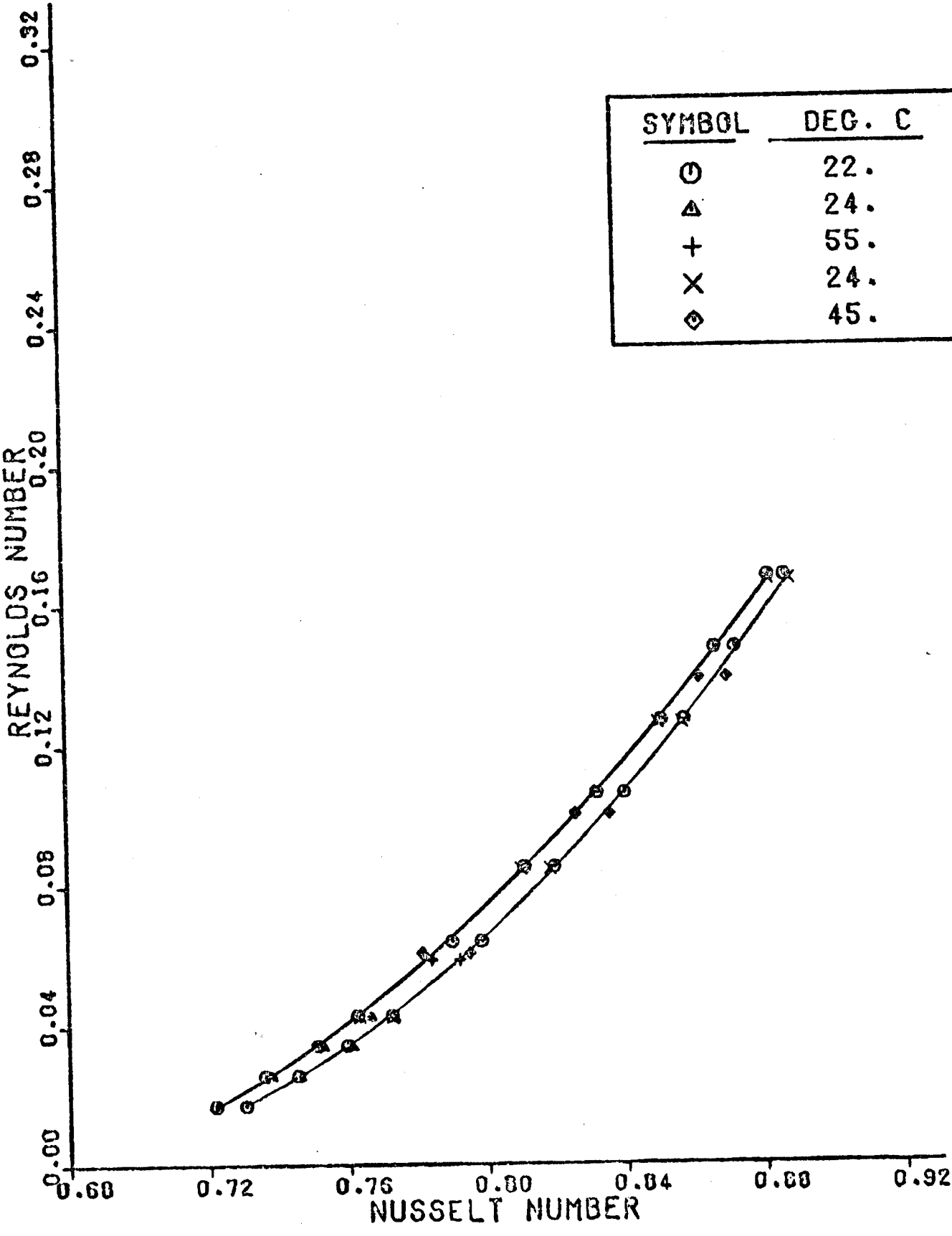

methods of Collis and Williams (1959) who evaluated both these parameters at the film temperature and used a temperature loading factor of the form shown in the equation (3.6).

$$R_d = f\left(Nu \cdot \left(\frac{T_g}{T_f}\right)^{0.17}\right) \qquad (3.6)$$

McAdams(1954) suggested a similar method except he evaluated the viscosity at the film temperature and only the density at the gas temperature. Over the range of temperatures this investigation covered, the present method seemed to give a slightly better collapse. The polynominal-type equation used to fit this data was chosen for ease of calculation by a computer. It should be noted that the standard method of writing this type of equation (Nu = f(Re)) is incorrect when fitting a curve by a method of least squared error. Although the fitted curve will be nearly identical if the scatter in the data is small, the problems involved with inverting the equation make it unsuitable for use in this type of data processing system.

Since the heater has such a long thermal time constant (estimated at 1 hour because of its high heat capacity and the low cooling velocities), calibration at many different temperatures is impossible to complete in the course of one day. This is particularly a problem for low velocity/high temperature calibration, as the heater time constant is inversely proportional to the mass flux. A typical procedure is to obtain a set of velocities at several different ranges of temperature during the day, take measurements during the night, and obtain two more temperature ranges of calibration the following day. This provides more than adequate data for a good calibration and serves as a check against drift in the anemometers.

The temperature sensors are calibrated at the same time as the velocity sensors. The current through the temperature wire is low enough (150 μA)

that the velocity sensitivity of the wire is negligible*, and the calibration reduces to a linear expression as shown in equation (3.7).

$$T = C_1 + C_2 \cdot E_t \tag{3.7}$$

The entire calibration procedure is carried out using the on-line minicomputer and a calibration program named "WIRECAL". All anemometer signals are sampled directly through the A/D channel they are eventually measured on, thus eliminating the possibility of a calibration error arising from a different gain between various voltmeters and the A/D.

The reference temperature and flow rate are entered manually at a remote terminal and written out to a data file on the disk along with the mean of the sampled voltage. The data files for each wire contain a preamble of the physical properties of the wire (length, diameter, resistance, etc.) and can have calibration data added or deleted to them any number of times. The calibration program can handle many different wires at once, but to facilitate calibrating both of the x-wires simultaneously the program will pause momentarily and then take a second pass on any specified wire. A bell is rung during this slight pause (2 sec.) to allow the operator to rotate the probe 90° so that the second wire is held perpendicular to the flow. A specially designed mount for the x-wire probe makes this a simple task and assures that all wires are calibrated under identical conditions. The coefficients of the least squares fit and a plot of the data along with the fitted curve can be obtained at anytime during the calibration procedure.

The wires also have to be calibrated for angle dependence. This also is a computer controlled operation, and is performed in a similar fashion as described above. The mount which holds the x-wire is marked with one degree graduations. A special program is run which instructs the operator

*The effect of a 0-1.0 m/s velocity change is of the order of 0.1 C°.

to position the x-probe at an angle of 50° from the vertical and rotate it 5 degrees each time the bell on the terminal is rung by the computer. By sampling both wires at once, both calibrations can be obtained at the same time. It should be noted that ideally one would want to rotate the flow and keep the probe in a vertical position, as this is the position it would be in when actually measuring the plume. However, angle calibrations at velocities as low as 25 cm/s were performed with the entire unit inclined 45° and no significant difference could be noticed.

Fitting an analytical expression to the angle calibration was a much more difficult task than originally thought. This was particularly true for the low Reynolds number range of calibrations. Previous investigations have used empirical curves such as the cosine law, Champagne law and even more sophisticated models as those put forth by Drubka, Nagib & Tan-Atichat (1977) These are given below along with a schematic diagram in figure 7.

$$U_{EFF} = U_o \cos\phi \tag{3.8}$$

$$U_{EFF} = U_o \left(\cos^2\phi + K\sin^2\phi\right)^{1/2} \tag{3.9}$$

$$U_{EFF} = U_o \left(1 - b\left(1 - \cos^m\phi\right)\right) \tag{3.10}$$

where U_0 is the total velocity and ϕ is the angle between U_0 and the wire normal. Due to the low Reynolds number, the angle calibration in this investigation turned out to be extremely sensitive to the velocity. This is due, in part, to a wake effect from the prongs and in part to the natural convection limit of the wires as the wire approaches 90° to the horizontal.

The final form of the angle calibration used is given in equation (3.11).

Figure 7 - Angle Calibration Geometry

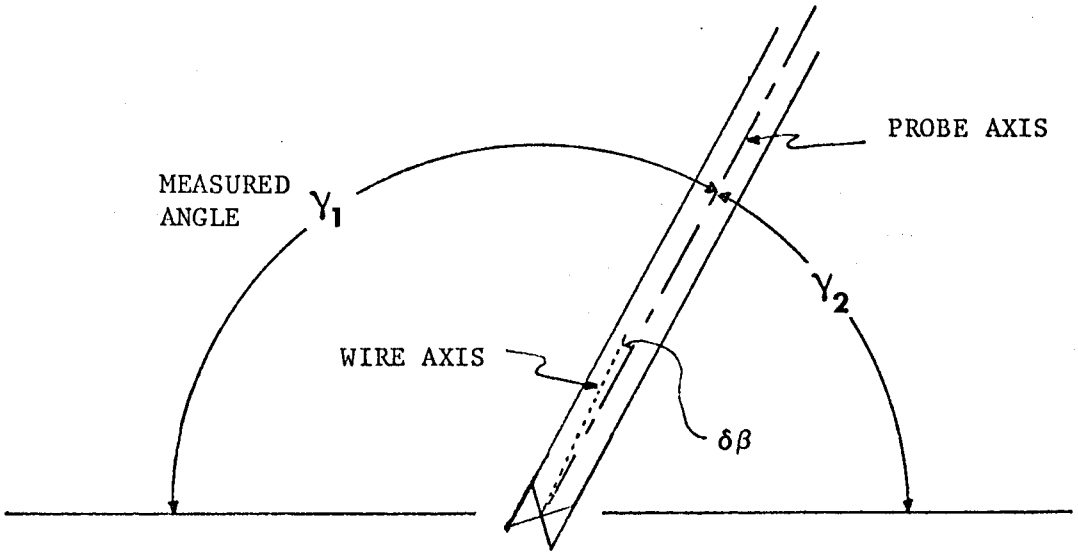

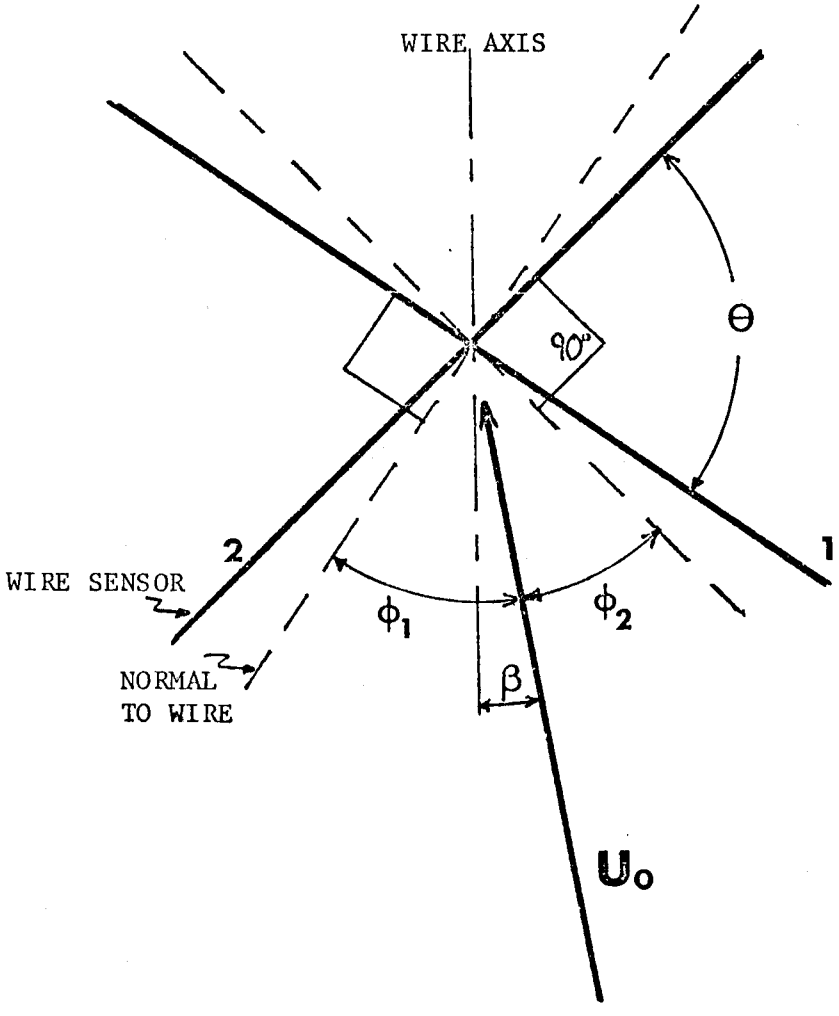

$$U_{EFF} = U_o\left[\cos^2(\phi-\phi_o(U_o)) + K(U_o)\sin^2(\phi-\phi_o(U_o))\right]^n \quad (3.11)$$

This must be solved by an iterative technique because of the velocity dependence of the coefficients. The technique is discussed in more detail in Appendix A3. Figure 8 shows an example of the angle dependence at at three different mean velocities. As the velocity approaches zero, the wire response is nearly constant regardless of the orientation. This creates a serious problem in interpreting low velocity signals.

Figure 9 shows graphically the mapping of the measured effective velocities of each wire onto the cone-shaped region of actual velocity vectors. Assuming an ideal x-wire (no prong support interference, symmetric sensitivity), no data can fall outside this cone. The dashed and dotted lines correspond to a cosine law and the Champagne law. At high velocities, all three will perform adequately as long as the relative cross-stream velocity is not large. At low velocities they deviate considerably - the Champagne Law only working over a narrow range of velocities and the cosine law failing entirely.

In practice, the x-wire is not ideal, and data will occur that falls outside the cone shown previously in Figure 9. This affects all calibration relations except the cosine law, and must be minimized if useful information is to be obtained. It is usually caused by a high turbulence intensity in the v or w components, and is especially troublesome when the mean velocity is low. This is because the wires are fairly insensitive to direction at low velocities, and any small measurement error (electronic noise, velocity component perpendicular to plane of x-wire, wake of one wire on the other, or a velocity or temperature gradient

ANGLE CALIBRATION DATA

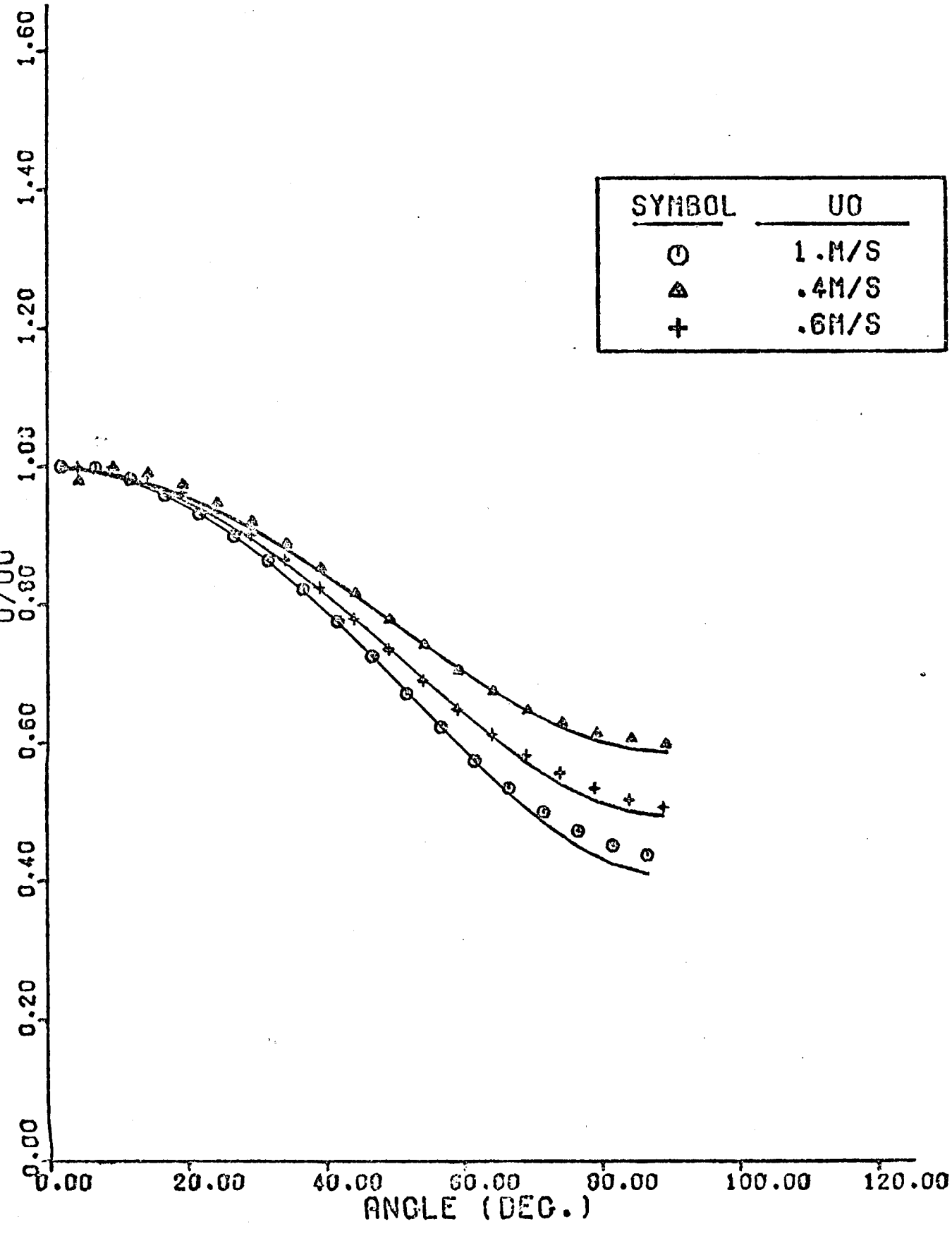

ANGLE CALIBRATION OF X-WIRE

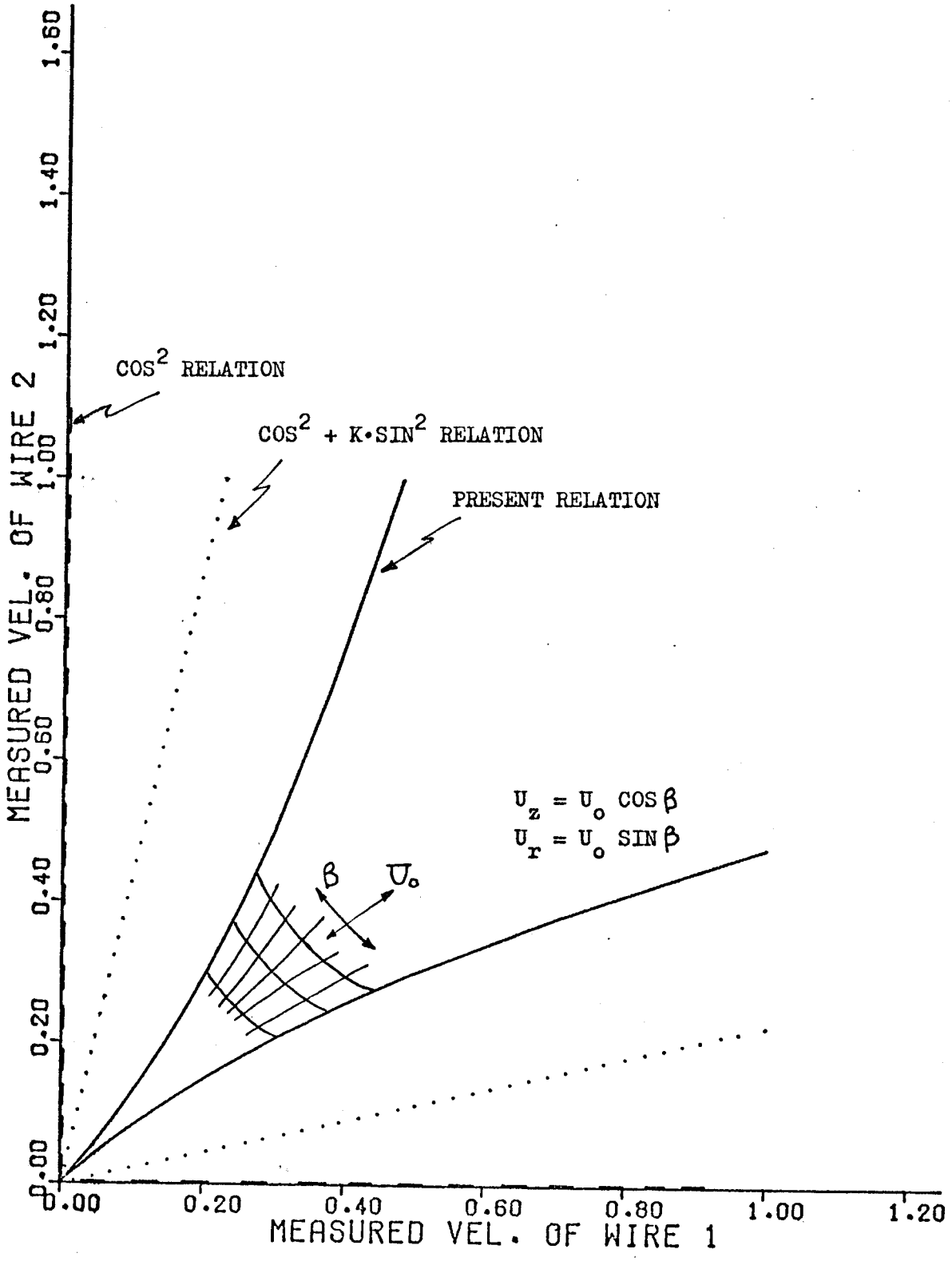

between the wires) can create a large error in the output and even to cause the data point to lie outside the calibration region. This problem, called drop-out, can be considerable in flows such as a plume. Further discussion of how to analyze this data is found in Chapter 5.

Chapter 4. Description of Signal Processing/Data Analysis

4.1 Data Acquisition

The main variables of interest in this investigation are the vertical and radial components of velocity, the temperature difference and the derivatives of all three of these. As described in the previous section, these six signals are electronically conditioned to have a mean value near zero volts and an rms voltage fluctuation of 1/2 volt. This provided for an adequate resolution by the 10 bit digitizer (-2.5 to +2.5 volts range) and insures against clipping which would bias the higher moments. The electronic noise level is held to 2-3 mv rms on all signals except the temperature derivative, where it is nearly twice this value. Since the digitizer resolution is 5 mv, this noise has little effect on the higher moments and actually improves the accuracy of the mean values by "whitening" the signal. This is particularly important in the calibration where the input signal is steady. The effective resolution in calibration is estimated to be 1 mv.

Two main types of data acquisition need to be used in this investigation: low-speed sampling of data for moments, and high speed sampling for spectral data. These are both handled by the same program which will be described later in this section. The sampling rates are determined by the integ scale and the Kolmogorov microscale respectively. The integral scale is approximately .25 second which means that to obtain independent samples, the data should be sampled no faster than twice every second (two time scales For 2048 independent samples, which results in a $\pm$ 0.6% relative spread of the measured mean value, the time required is nearly 20 minutes. The error bounds increase considerably for the higher moments (see Section 5.1).

The fast sampling rate is determined by the Kolmogorov microscale which for this flow is approximately 0.5 mm. To prevent spectral aliasing, a sample frequency at least twice as large as the highest frequency in the flow must be chosen (c.f. Jenkins & Watts (1968)). In the experiments the sample frequency was set at 250 Hz since:

$$f \geq \frac{U}{2\pi\eta} \simeq 200 \qquad (4.1)$$

By taking 1024 points in each block, and block averaging several spectra, a relatively smooth spectrum can be measured having a frequency span from 0.25 Hz to 125 Hz. Typically only 16 blocks of spectral data were averaged together due to the long processing time required for the Fast Fourier Transform. The resulting average was then filtered over 1/10 or 1/3 octaves for smoothing.

All this data is taken automatically by a PDP11-34 computer as described in Section 3.3.The program "PLUME" runs the data acquisition and stores the data on disk and tape. The program itself is run automatically by the RSX-11M operating system at a prescribed time. A flow chart of this operation is given in Figure 10a. When the program is started automatically late in the evening (usually after 11 PM to ensure an undisturbed environment) it reads three data files to obtain all the necessary information needed to run the experiment. This includes such things as the output file names, sample rates, number of samples, measuring locations (usually about 24, which will take 8 hours) and traverser calibration data. It then writes much of this out to the mag tape to create a preamble file. The traverser is then moved to the first position, the data sampled and stored in sequentially numbered files on the tape, and the average ambient temperature (averaged over the 20 min. sampling period) is written out to a separate disk file. If spectral data is to be taken also, the above steps are repeated using the faster sampling rate and different number of points. The program then moves the probe to the next location and repeats the sampling until all positions have been sampled.

The sign of the z-coordinate is used as a code to determine whether or not to take spectral data. If the current position read in from the data file is negative, spectral data is taken; if positive, it is not. In either case the traverser is sent to the absolute value of the z-location. This provides an easy way of taking spectral data at only a selected number of locations.

Figure 10a - "Plume" Flow Chart for Data Acquisition

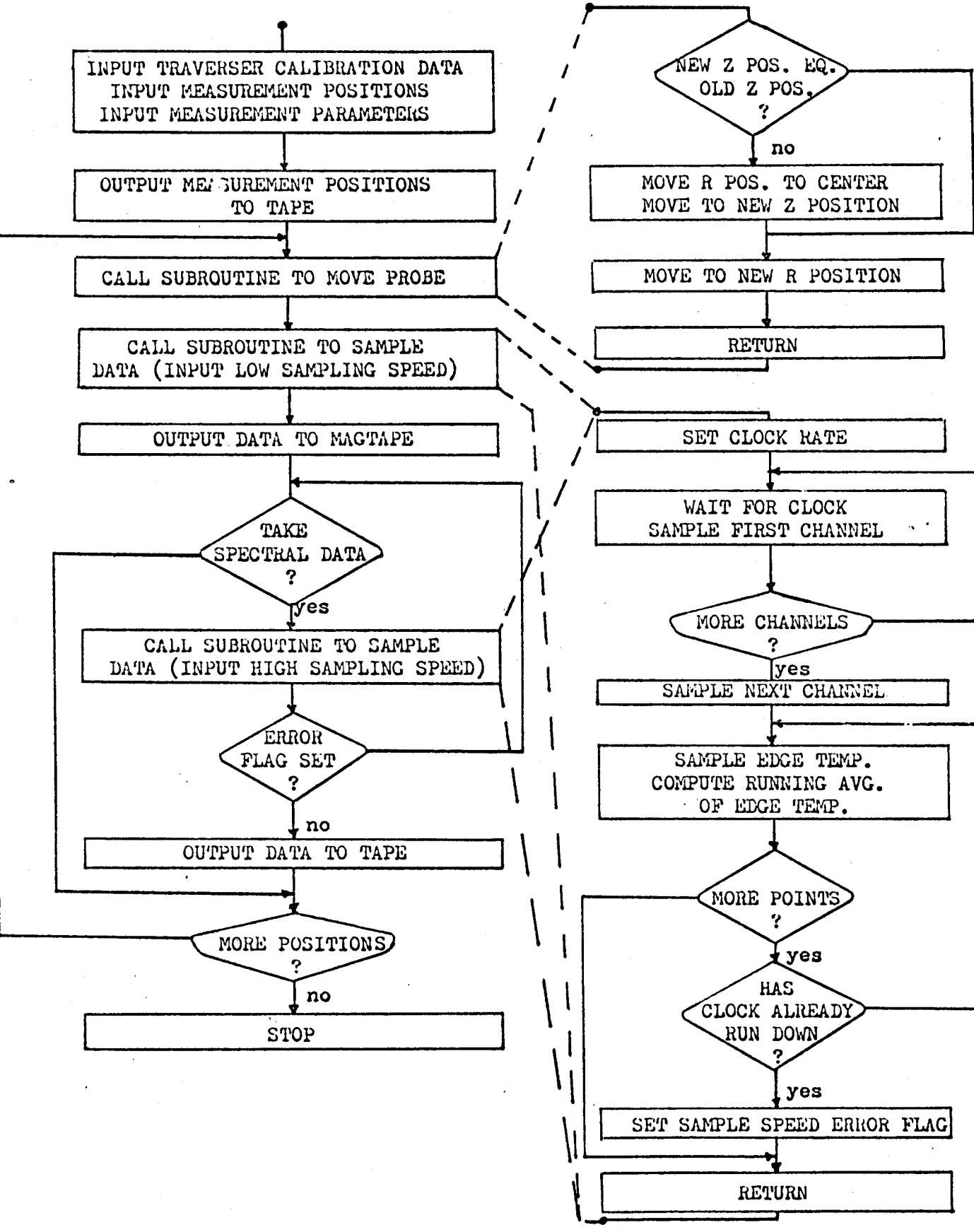

Since the computer system is dedicated to this project, the sampling program used is a rather crude one which continually checks the done bit of the A/D clock to time the samples. Originally it was hoped to convert the voltages to velocity and temperature before dumping them on tape, but the time required to do this was longer than the time between samples. Had this been possible, the sampling program would have used program interrupts to enable the computer to do something other than check the done bit between samples(which it did an estimated one billion times during each experiment!).

The data pertaining to the plume source conditions is recorded manually both before and after the running of the "PLUME" program. This data consists of the mass flow rate read from a rotometer and the exit temperature monitored by a thermocouple. The rotometer has a thermometer inside of it to record the inlet temperature. Since the inlet air line has a pressure regulator and the plume exit temperature is controlled by an electronic controller, these two conditions do not vary significantly during the course of the experiment. Of the two the air flow is the least stable, changing by 3-4%. This is believed due to an oil build-up in the rotometer from the air line since the reading is consistently lower at the end of the experiment. This oil coming from the air compressor mandates regular cleaning of the rotometer after 12 hours of continuous running at 100 SCFM.

4.2 Data Conversion

The data stored on mag tape consists of only the raw voltages measured by the A/D converter. This data needs to be converted back to physical variables using the calibration results discussed earlier. Since the conversio is such a lengthy and time consuming process for a small lab computer, it is desirable to do it only once. Unfortunately the computer used in this

Figure 10b - "Deriv" Flow Chart for Data Conversion

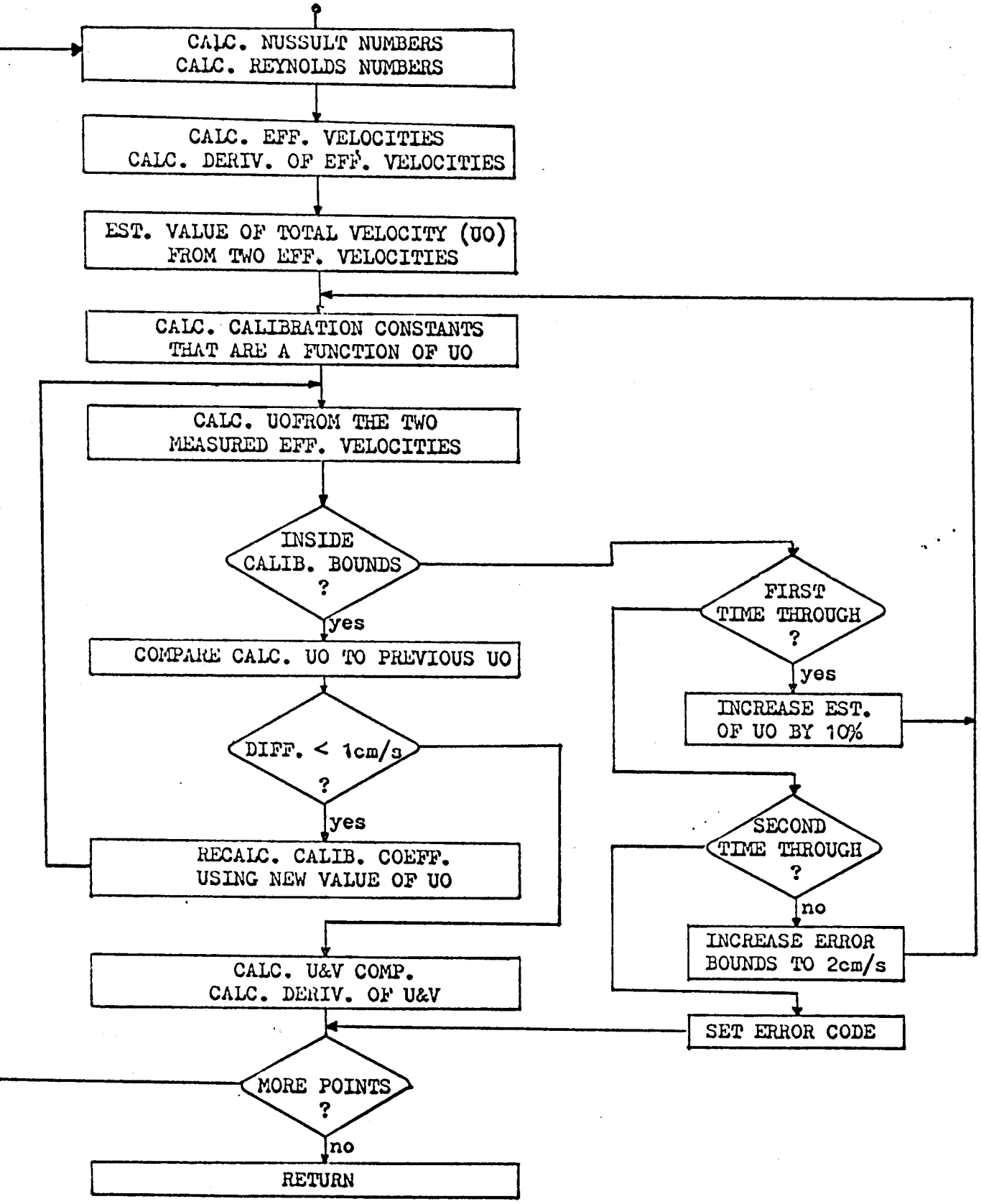

investigation had only one tape drive, which meant that the raw data had to be overwritten as the process went on. This was accomplished by adding one extra block of blank data to each data file when the data was taken with the program "PLUME". This formed a buffer region on the tape between each data file so that a second program "CONVERT" could read a file, convert the voltages to physical variables, rewind the tape one file, and rewrite the data on top of the old. This buffer zone is necessary because the tape is not a formatted device and the physical location of a file on the tape can vary somewhat.

The convert program reads in all the necessary calibration data for the velocity and temperature sensors plus the transfer characteristics of the amplifiers and differentiators. The temperature is the easiest signal to unravel, since it is entirely linear. The temperature derivative is also fairly simple since the transfer characteristic of the differentiators is simply:

$$e_o = C_1 + C_2 \frac{de_i}{dt} \qquad (4.2)$$

where C_1 is small (ideally zero).

The amplifiers are also linear, making it simple to determine the actual anemometer output voltages and their time derivatives. The final conversion from this point to the actual velocity components is done in subroutine "DERIV", whose flow chart is outlined in Figure 10b. Detailed analysis of this can also be found in Appendix A3. The first section of this subprogram uses the calibration relations found in Equations 3.4 and 3.5 to calculate the effective cooling velocity of each wire. The time derivative of these expressions is also obtained. Then using an iterative procedure, the angle calibration (Equation (3.11))is solved for the u and v velocity components. Once these have been determined, it is straightforward (although rather involved) t

2-D PROBABILITY CONTOURS

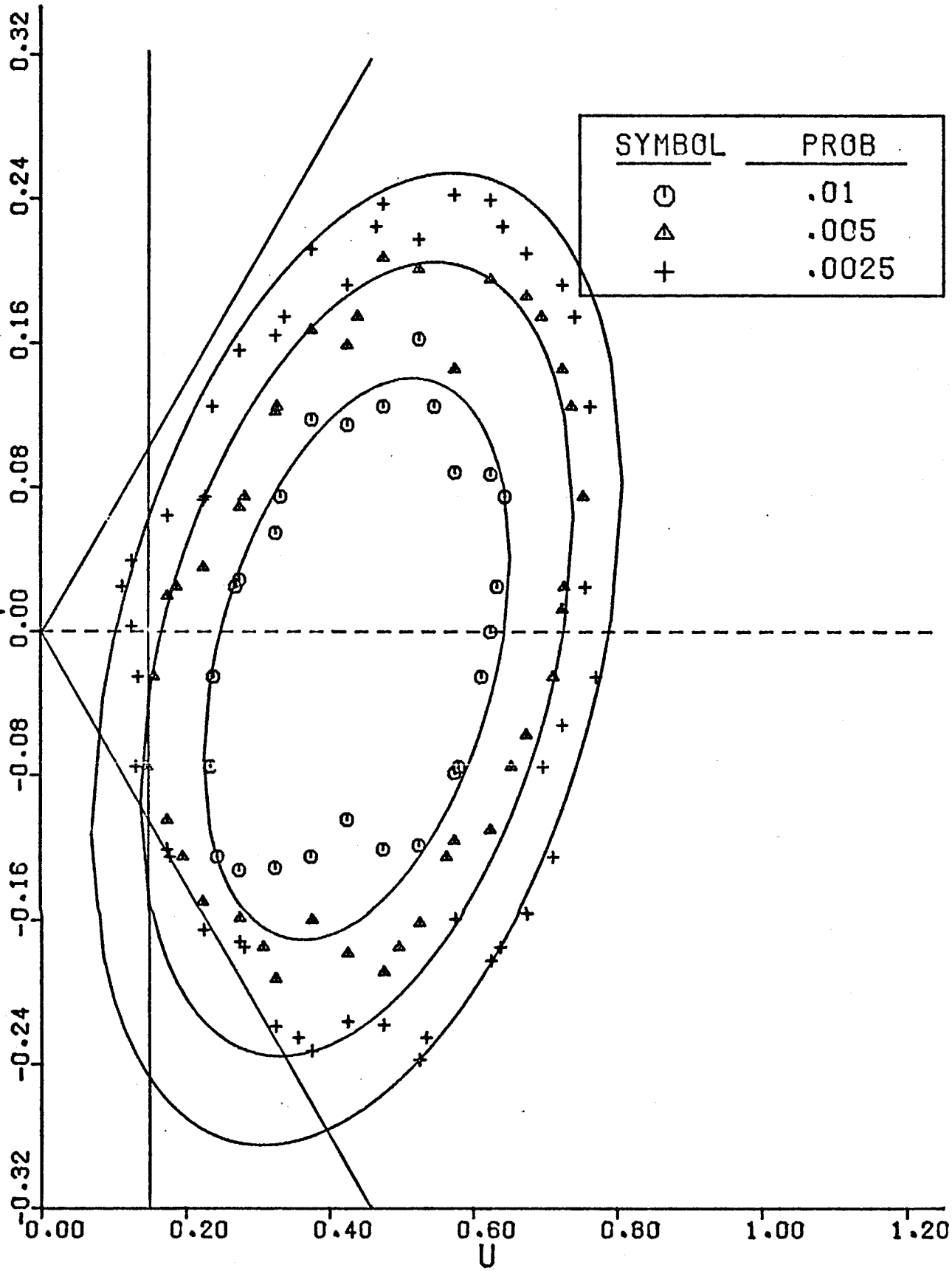

differentiate the angle calibration expression to obtain $\frac{du}{dt}$ and $\frac{dv}{dt}$.

Unfortunately, the data points are not all well behaved, and some of the pairs of input voltages do not correspond to real velocity components. When this occurs the data point is generally discarded. The possible causes for this drop-out were discussed in Section 3.4. If the drop-out is caused by noise, the point can sometimes be saved by widening the error bounds of the iterative solution method. However this can only be increased slightly because the derivative values are strongly linked to the velocity. By increasing the error acceptance until a non-imaginary solution is found, reasonable values for the u and v components of velocity can be obtained but the values of $\frac{du}{dt}$ and $\frac{dv}{dt}$ can become extremely large. In fact, this is such a problem that the measured velocity vector had to be limited to within 35° of vertical. If not, the error due to the flatness of the angle dependence at these angles will be too large to permit accurate determination of the derivatives. In effect, there is a singularity in the derivative solution when the flow is parallel to either of the wires that makes the error become infinite.

The consequences of this are large at the outer regions of the plume (η>0.1), where the drop-out rate can exceed 50%. Since much of it is caused by large excursions of the v velocity component, the effects on the higher moments can be significant. Figure 11 shows a 2-D probability plot of the u and v velocity components at η = .05 with a drop-out rate of 9%. The two slanted lines represent a cutoff of all velocity vectors exceeding $\pm$ 35°. The vertical lines represents the lower limit of the hot-wire calibration (15 cm/s As can be seen, the lower left corner of the probability contour is dramatically compressed. The lower velocity limit is just beginning to be of importance, although it will be much more significant at larger radial

MBIENT TEMP. AS A FUNCTION OF TIME

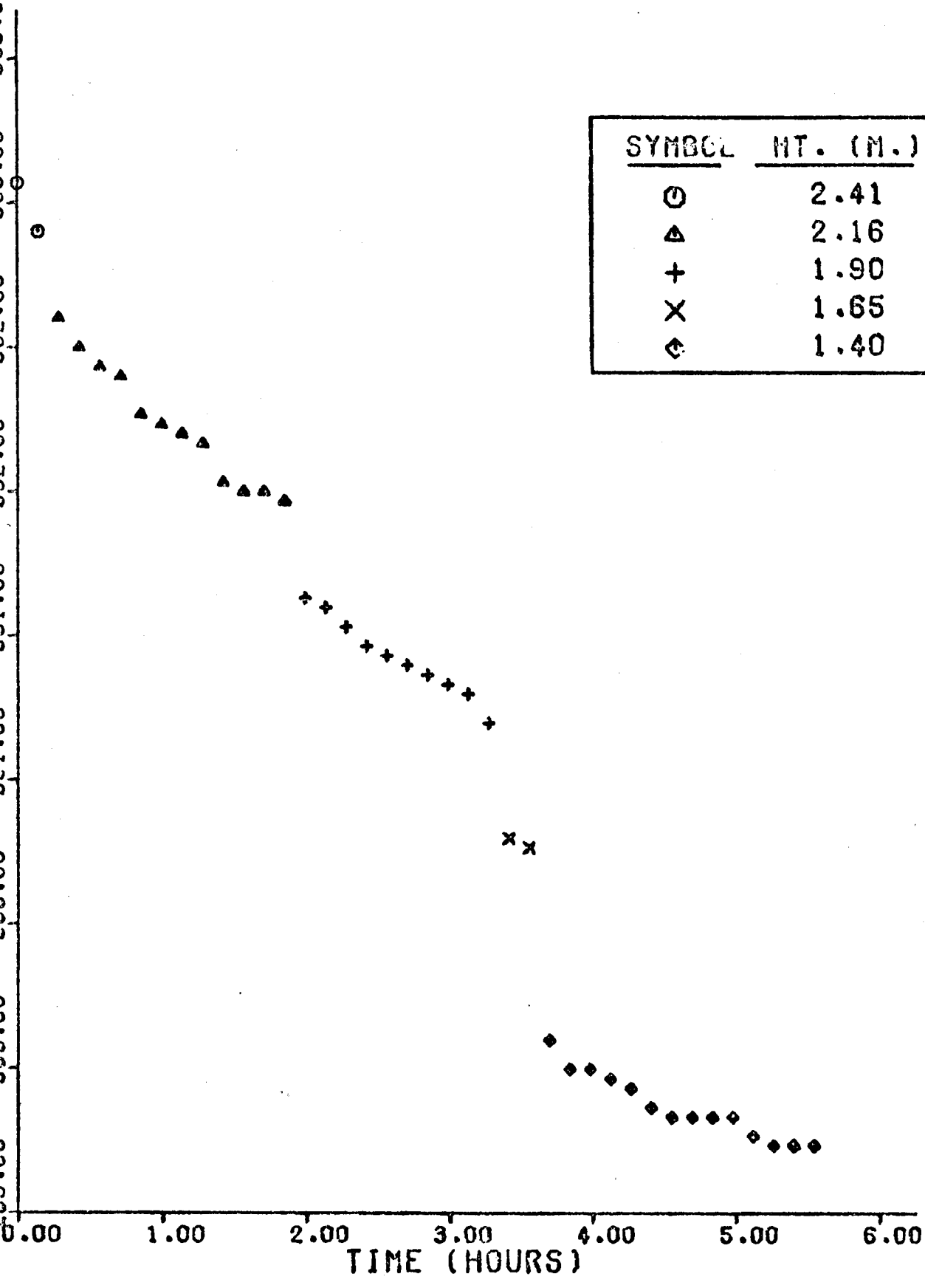

distances where the mean velocity is lower. (There is no actual cutoff in the program for velocities which are too low, but the accuracy of the calibration worsens to the point that the velocity pairs are often incompatable with the angle calibration and give imaginary solutions.) The problems associated with correcting for drop-out will be discussed in Chapter 5.

One further problem remains to be solved - that of the value of the buoyancy flux, F_o. This is measured directly at the plume source, and in a uniform environment it is constant at all heights. However, in a stably stratified environment the buoyancy flux is a decreasing function of height. Its z-dependence can be determined one of two ways. First, the measured velocity and temperature profiles can be integrated radially at each vertical position. Second, and the primary method used in this investigation, the z-dependence can be determined from the ambient temperature gradient. Since the ambient temperature is measured at various heights, as shown in Figure 12 , the temperature gradient can be calculated (Fig.13). For this calculation, it is assumed that the temperature gradient does not change over the course of the experiment. The curve fit to the temperature gradient is of power law form and given by

$$\frac{dT_\infty}{dz} = 8.5\, z^{-3} \qquad (4.3)$$

Since the vertical gradient of F_o is proportional to the momentum flux and the ambient temperature gradient, as shown by Morton, Taylor and Turner (1956 the differential equation shown below.

$$\frac{dF_o}{dz} = -M\, g_o \beta \frac{dT_\infty}{dz} \qquad (4.4)$$

can be solved for $\frac{dF_o}{dz}$. Using the above fit to the ambient temperature gradient, one finds that $\frac{dF_o}{dz} \propto \frac{1}{\sqrt{z}}$. The value of the buoyant flux as a function of height is shown in Figure 14. This will be important later for normalizin the profiles of the moments at various heights.

Z DEPEND. OF AMBIENT TEMP. GRADIENT

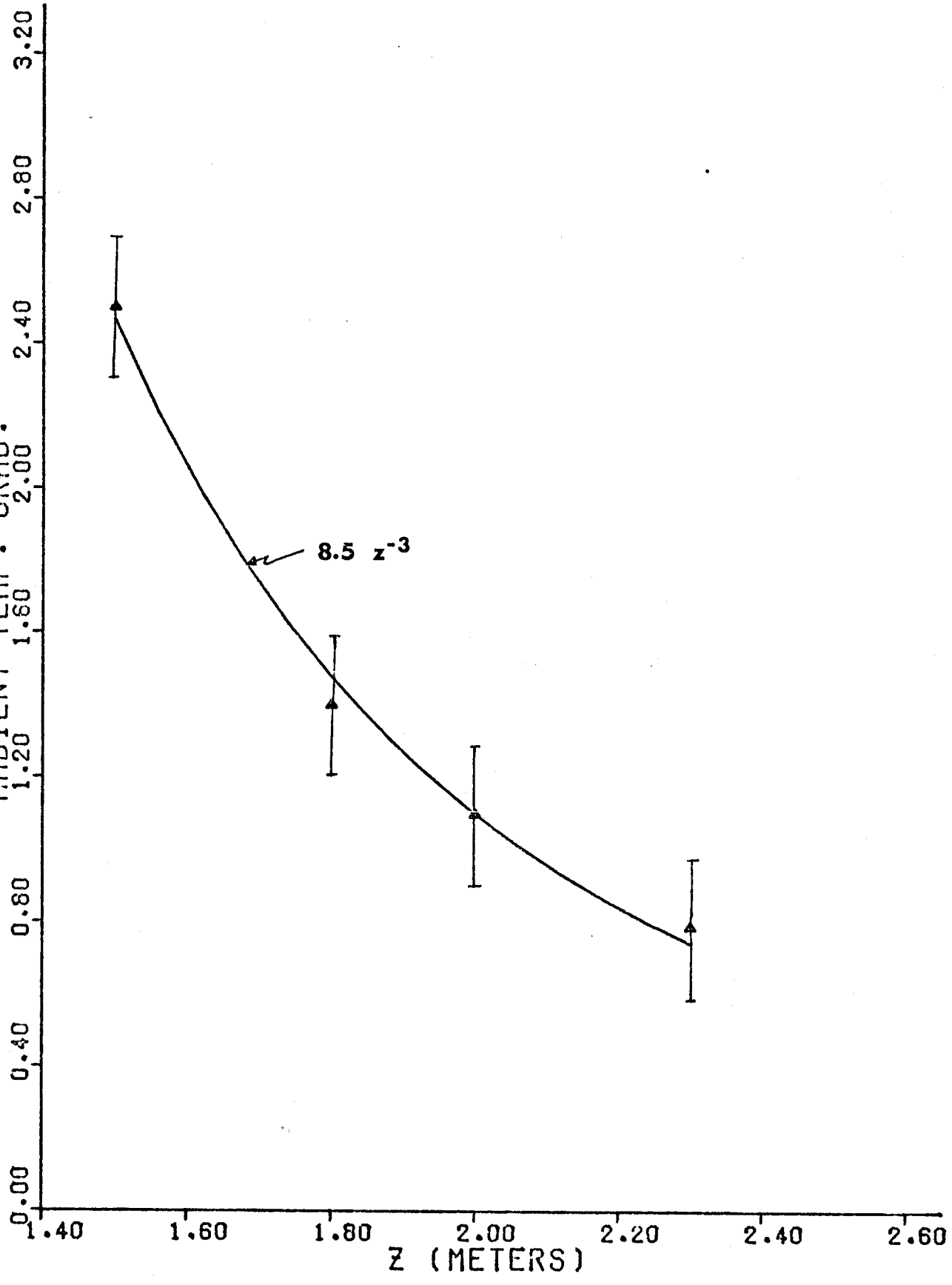

Figure 11

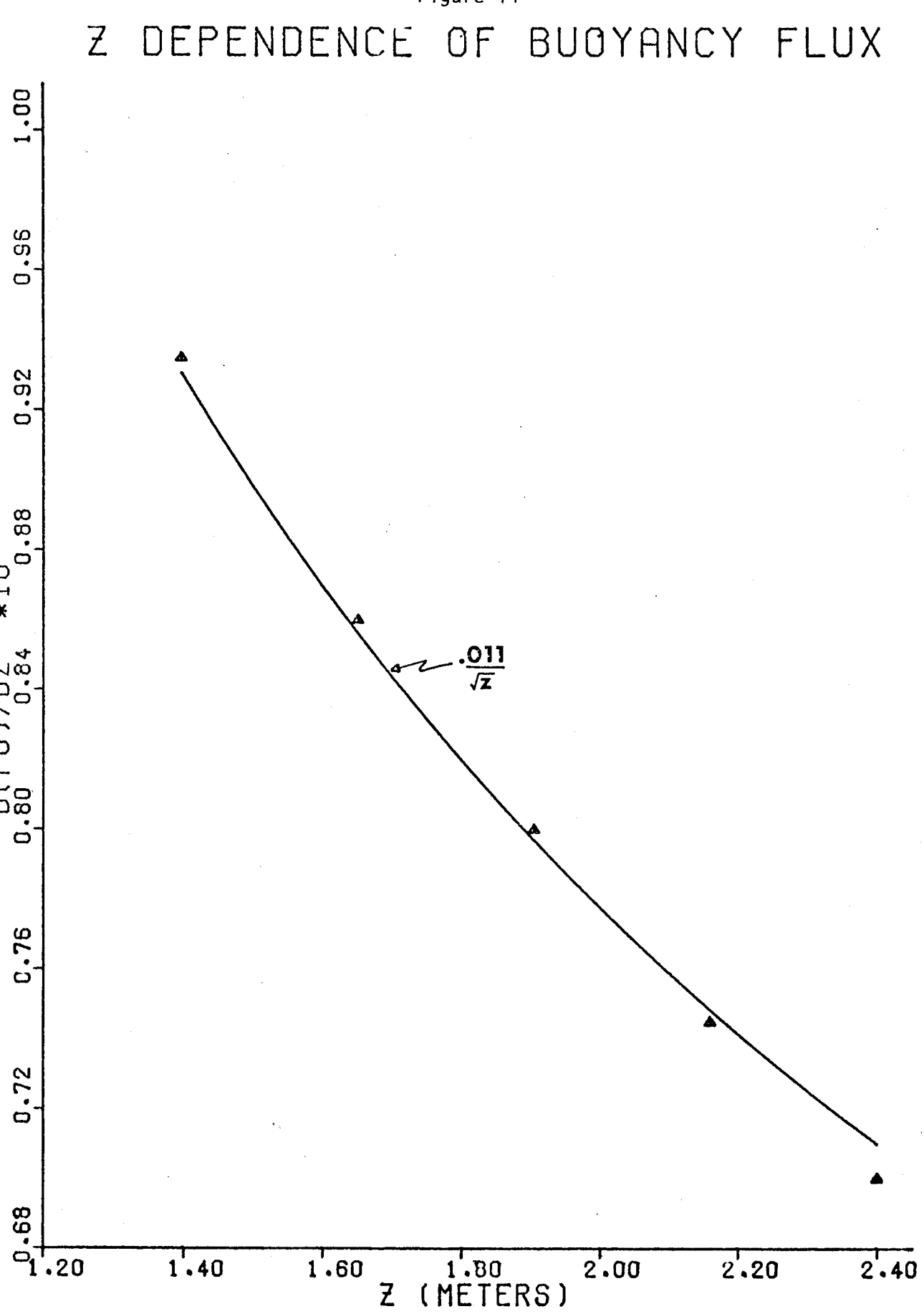
Z DEPENDENCE OF BUOYANCY FLUX
1.00
0.96
0.92
0.88
0.84
0.80
0.76
0.72
0.68
.011/√z
1.20
1.40
1.60
1.80
2.00
2.20
2.40
Z (METERS)

Chapter 5. Presentation and Discussion of Results

5.1 Moments of Velocity and Temperature

One of the main results of this investigation is the evaluation of the first, second and third moments of the velocity and temperature distributions. These include not only the means and standard deviation, but also cross terms such as the Reynolds stress ($\overline{uv}$) and third order terms that play an important role in the turbulent energy balance. These are defined by the following general relations.

$$\overline{u^n} = \frac{1}{N-1} \sum_{I=1}^{N} (u(I)-\bar{u})^n \tag{5.1}$$

$$\overline{u^n v^m} = \frac{1}{N-1} \sum_{I=1}^{N} (u(I)-\bar{u})^n (v(I)-\bar{v})^m \tag{5.2}$$

A computer program appropriately named "MOMENT" is used to read all the velocities and temperatures from the mag tape and calculate all first, second and third moments, plus the fourth moments of u and v, and all second moments of derivatives. These are then stored on the disk for future analysis.

Just as the variable u(t) is a random variable, so is its n^{th} moment. If N is the number of independent samples taken, it is easy to show that the variance of the n^{th} moment can be written as

$$VAR[\overline{u^n}] = \frac{\overline{u^{2n}}}{N} \tag{5.3}$$

Since in turbulence $\overline{u^{2n}}$ tends to be greater than $\overline{u^2}^n$ and this ratio increases with n, many more samples are needed to obtain reasonable statistics for the fourth moments than for the mean. As mentioned earlier, N for this investigation is 2048. For a Gaussian distribution, the relative errors of the second, third and fourth moments are 4%, 9% and 23% respectfully. For turbulence that is not Gaussian, these values might be considerably higher (Tennekes and Wyngaard (1972)).

In addition to these problems with the statistical variance of the higher moments, there is still the bias due to the drop-out affecting them. Several attempts have been made to correct the deficiencies in the higher moments by fitting curves to the unaffected parts of the probability density functions, but not nearly enough data points were taken at each location to accomplish this since the statistical fluctuation in the tails of the probability distributions is considerably higher than the fluctuation of the integrated distributions and their moments (VAR $[P(u)] = \frac{1}{NP(u)}$). The only correction possible was for the Reynolds stress, which was determined from a joint Gaussian distribution (see Figure 11). The first moments of u and v are used as measured and the correlation was adjusted to give the minimum mean square error over three quadrants (ignoring the bottom left). These corrections are generally about 20%, but are sometimes almost 100% when the uv correlation is high. Figure 11 is such an example. Although the dropout is only 9%, nearly all of it is in the extreme portion of the uv distribution. The measured correlation is 0.28, whereas the fitted curve is 0.55.

Originally the second moments of u and v were also calculated by fitting a Gaussian curve to the probability function, but the results were often heavily biased. This bias is due to a somewhat arbitrary cutoff point for low velocities. By rejecting points in the lower left quadrant (high negative v, low u) the distribution of v is biased in the lower half. By rejecting all values with v less than the mean, a slight error in estimating the mean leads to a large bias in the variance. Since the corrections are usually small, the measured values of $\overline{u^2}$ and $\overline{v^2}$ are presented without correction.

This problem also extends to higher moments of u and v when they are

highly correlated. Several schemes were tried to correct these moments, such as fitting the probability density with a Gram-Charlier Expansion. However, due to the statistical uncertainty of the measured probability density, these methods failed to provide dependable results. Thus, the measurements of $\overline{u^2v}$, $\overline{uv^2}$ and $\overline{u^2v^2}$ will have significant error around $\eta = 0.05 - 0.1$.

One way to minimize this problem in future measurements is to misalign the x-wire so that it sees more of the large u-v excursions. This is contrary to the present philosophy of most investigators of aligning the probe with the flow. In regions of high uv correlations, a misalignment shift of 5° can reduce the $\overline{uv}$ error by as much as 50%.

Since the data taken in this investigation were taken at different heights with different values of F_o, the moments are normalized by the dimensional similarity discussed in Equations (2.3) and (2.4). Although this normalization is only valid for a uniform environment (F_o is constant), it can be extended to slightly stratified environments as long as the local value of the buoyancy flux is used. The higher moments can be expressed in terms of correlation coefficients. For example, $\overline{u_z^2 u_r} \Big/ \left[\overline{u_z^2}\left(\overline{u_r^2}\right)^{1/2}\right]$ equals ρ_{112}, the correlation coefficient.

In the past, most investigators of turbulent plumes used a Gaussian profile to fit the mean temperature and velocity data. However, there is no physical argument to justify this profile. A more appropriate choice is to use as empirical fits the forms obtained by Yih with an eddy viscosity solution for turbulent Prandtl number equal to 1.1. As mentioned earlier in Section 2.2, these forms are not expected to fit well at the outer region of the plume due to the use of a constant eddy viscosity across the flow. However, in the central core region, they should work well. These expressions are

$$f(\eta) = \frac{f_1}{(1+A\eta^2)^2} \tag{5.4}$$

and

$$g(\eta) = \frac{g_1}{(1+A\eta^2)^3} \tag{5.5}$$

where in our case f_1, g_1 and A are determined from the data by using a method of least squares. By substituting $f(\eta)$ into the continuity equation one can obtain an expression for the radial velocity,

$$k(\eta) = (1/6\eta - 5/6A\eta^3) \cdot f(\eta) \tag{5.6}$$

For a uniform environment, for which these forms were derived, the constant A is the same for all profiles. However, for a stratified environment there is a definite trend which narrows the width of the velocity profile. Figures 15 and 16 present the mean profiles of velocity and temperature for a moderately stratified plume in similarity variables. The data was taken at heights of 22-38 diameters above the plume source, and the exit Froude number of the plume source was near unity. The values

Figure 46 f

MEAN TEMPERATURE

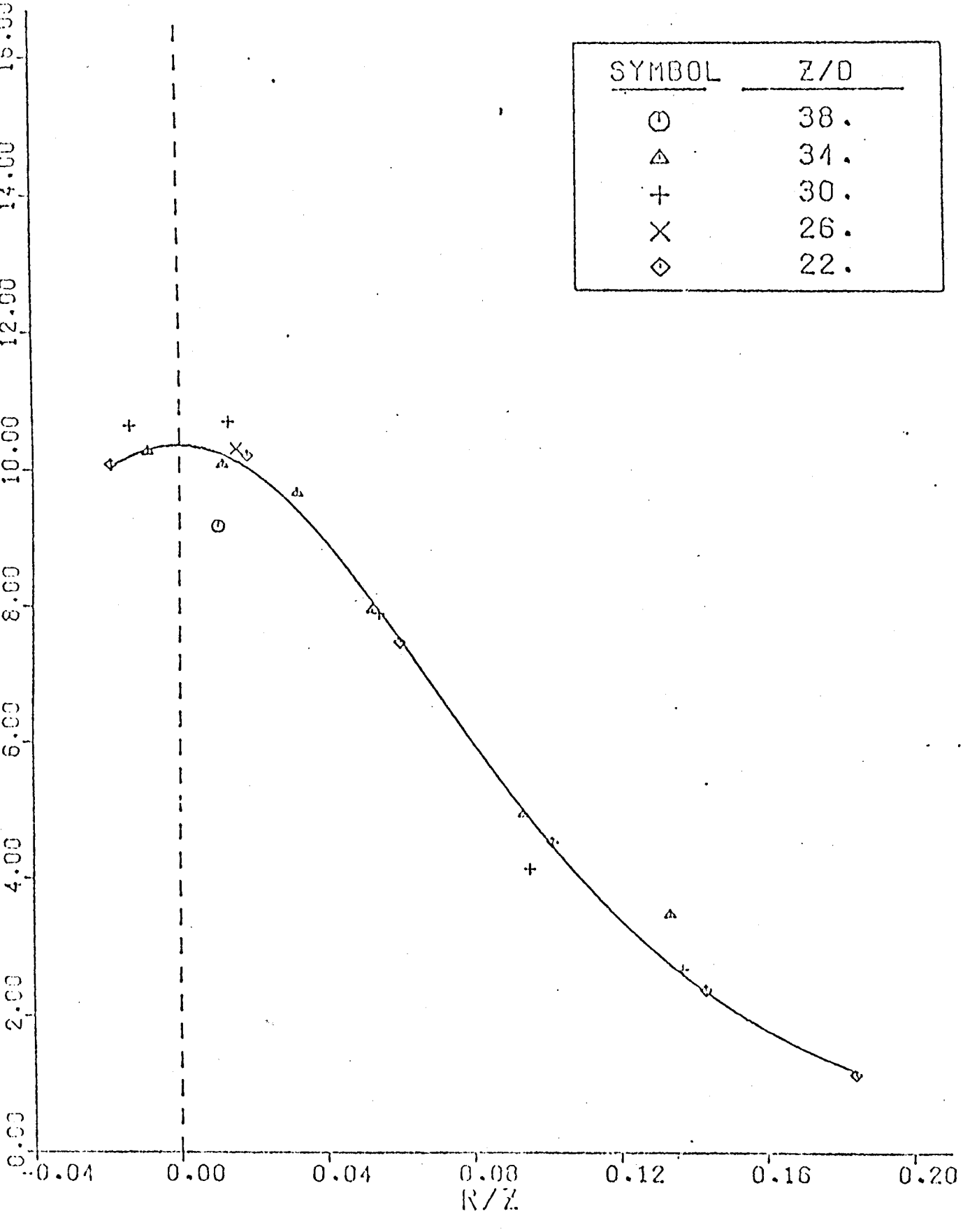

Figure 13 -

MEAN VELOCITY PROFILES

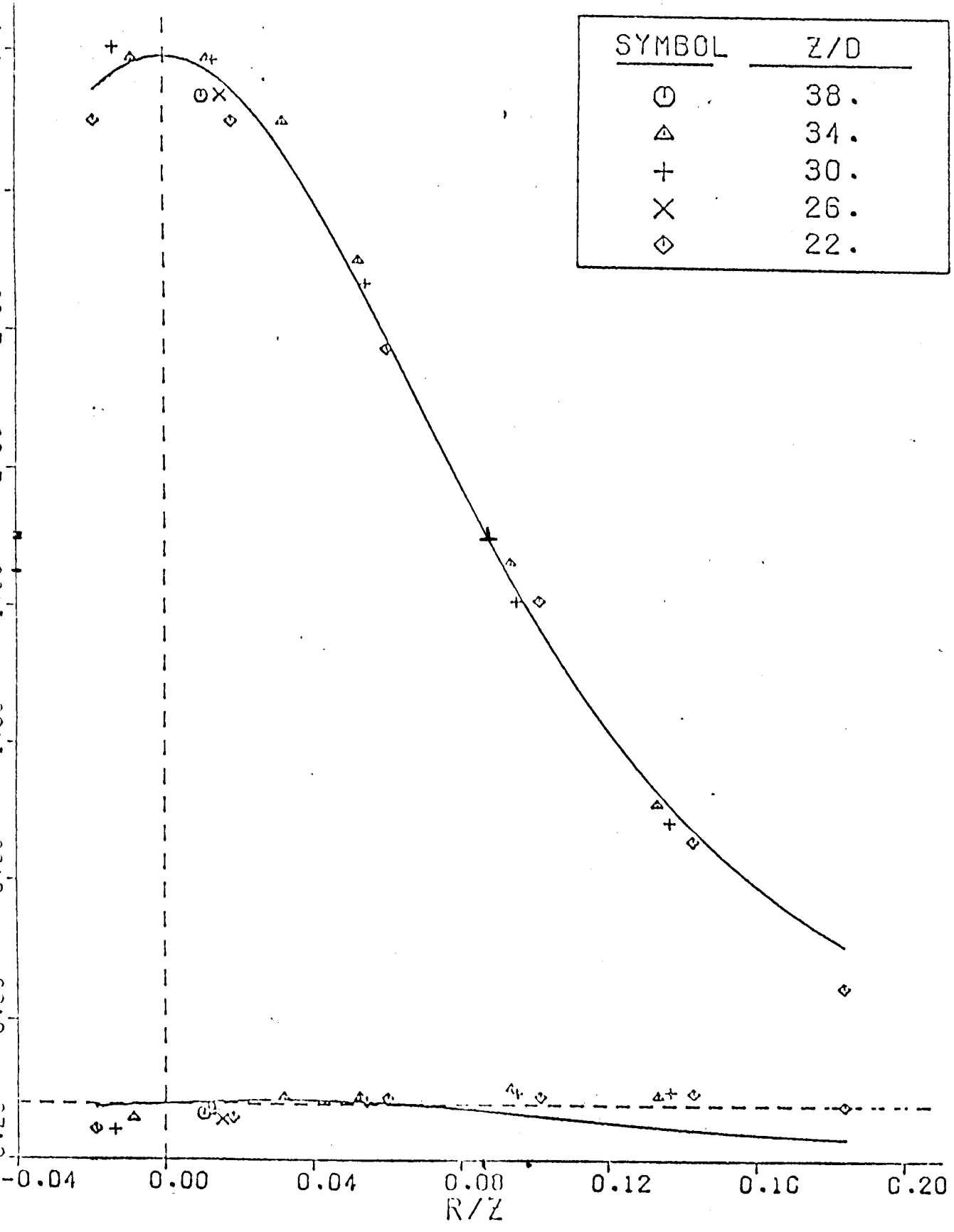

of f_1, g_1 and the plume width are summarized in Table 1, along with previous data from more uniform environments.

The velocity profile is much narrower than that measured previously under less stratified conditions (A=46 vs. 33, Beuther, Capp and George (1979)), and peaks at a higher level (F=3.8 vs. 3.6). The temperature profile peaks higher(g_1= 10.4 vs. 9.5), but retains approximately the same shape. The value of 33 for the width of the temperature profile from the second set of data was chosen as a compromise to agree with the width of the velocity profile. If these two coefficients had been chosen separately, they would have been closer to 30 and 35 for the temperature and velocity respectively. This fits the trend of the narrowing velocity profile with increased stratification. In fact, for the present set of data, the velocity and temperature profiles have nearly the same shape.

TABLE I

Ambient Environment	F_1	A	g_1	A
Uniform (George et al. 1977)	3.4	28	9.1	28
Slightly Stratified (Beuther et al. 1979)	3.6	33	9.5	33
Moderately Stratified (Present data)	3.8	46	10.4	31
Original data of Rouse, et al (1952)	4.7	55*	11.0	30*

The discrepancies of the data of Rouse, et al. with other investigations have often been explained as due to poor measurement equipment (wind vane anemometers), but as can be seen from Table I, part of this effect could be due to a stratification in the ambient environment. Although this is not evident in their raw data, little of their data appears to be taken at

*These values are approximate fits of this form of the equation to the data of Rouse, et al. The original data was given with a Gaussian curve fit.

different heights with a constant buoyancy flux, which makes it difficult to spot this trend.

Figures 17 and 18 show the velocity and temperature fluctuation data (again normalized to similarity variables). In agreement with George et al. (1977), Nakagome and Hirata (1977) and Beuther, Capp and George (1979), the centerline vertical velocity fluctuations were 26% of the mean centerline value, and showed little change under differing amounts of stratification. The radial velocity fluctuations also remained the same as before at 16% of the mean centerline vertical velocity. The temperature fluctuations were only 30% of the centerline temperature difference, a value considerably lower than that of George et al. and Nakagome and Hirata who obtained values of 38% and 35% respectively. The earlier work in this investigation obtained a value of 30-33% for the temperature fluctuation intensity. (This last result is not found in reference of Beuther, Capp & George, which presents temperature fluctuations that are a factor of 25% too high.) The off-axis peak in the $\overline{u^2}$ profile was not observed by other investigators, but this discrepancy is perhaps due to their single wire probes, which mix the u and v fluctuations together. The peak was noted in all profiles measured as part of this investigation, and is also predicted by the computational model of Tamanini (1977).

The Reynolds stress, $\overline{u_z u_r}$, is presented in Figure 19. The shape of this profile follows very closely the derivative of the mean velocity profile in the core region of the plume, explaining why an eddy viscosity model seems to work so well in this flow (v. Baker et al.(1979)). The $\overline{u_z u_r}$ correlation coefficient has a maximum value of 0.5 near $\eta = 0.1$ The turbulent Reynolds number, defined from the eddy viscosity model by

Figure VI 10

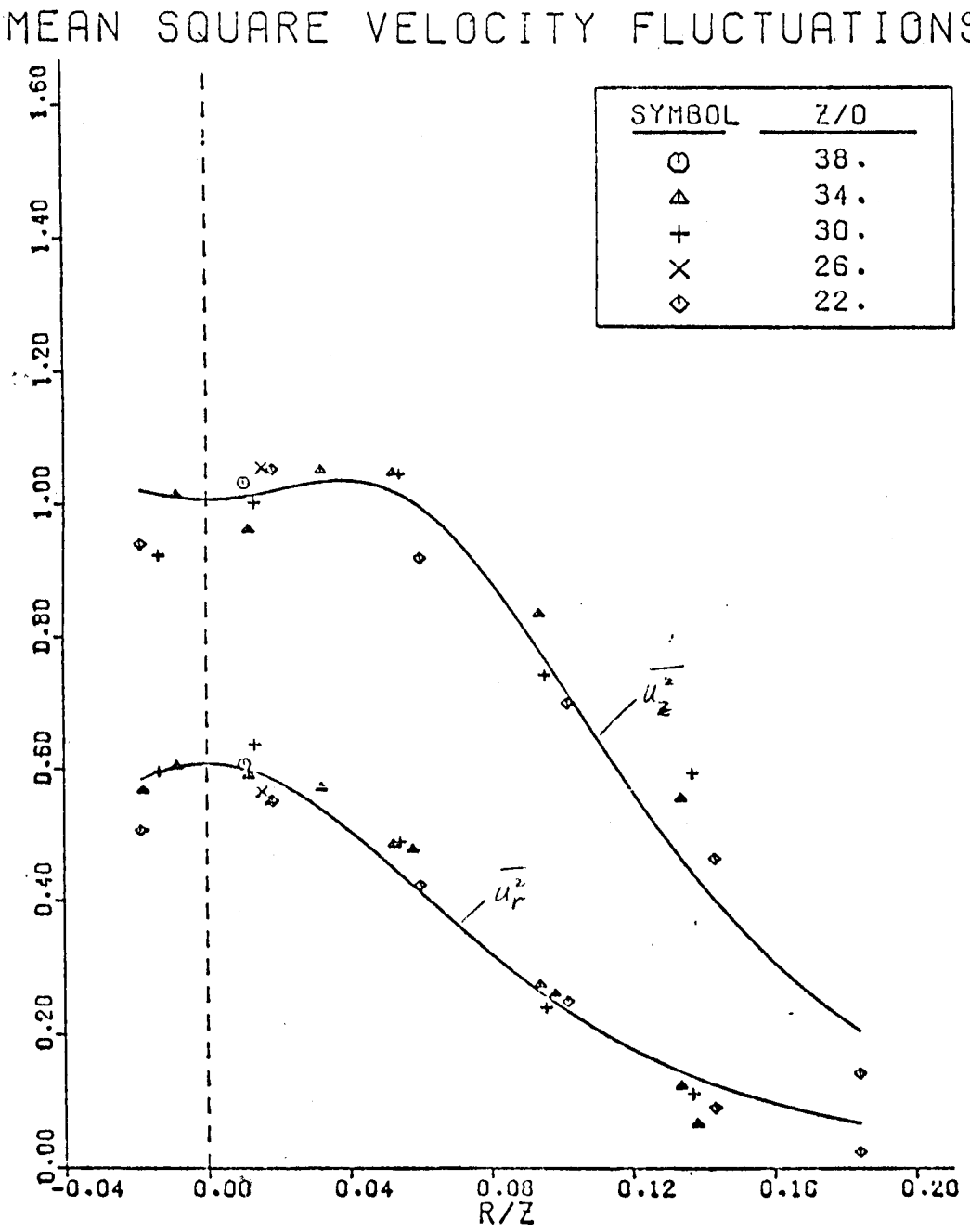
MEAN SQUARE VELOCITY FLUCTUATIONS
SYMBOL
Z/D
38.
34.
30.
26.
22.
$\overline{u_z^2}$
$\overline{u_r^2}$
1.60
1.40
1.20
1.00
0.80
0.60
0.40
0.20
0.00
-0.04
0.00
0.04
0.08
0.12
0.16
0.20
R/Z

Figure 18

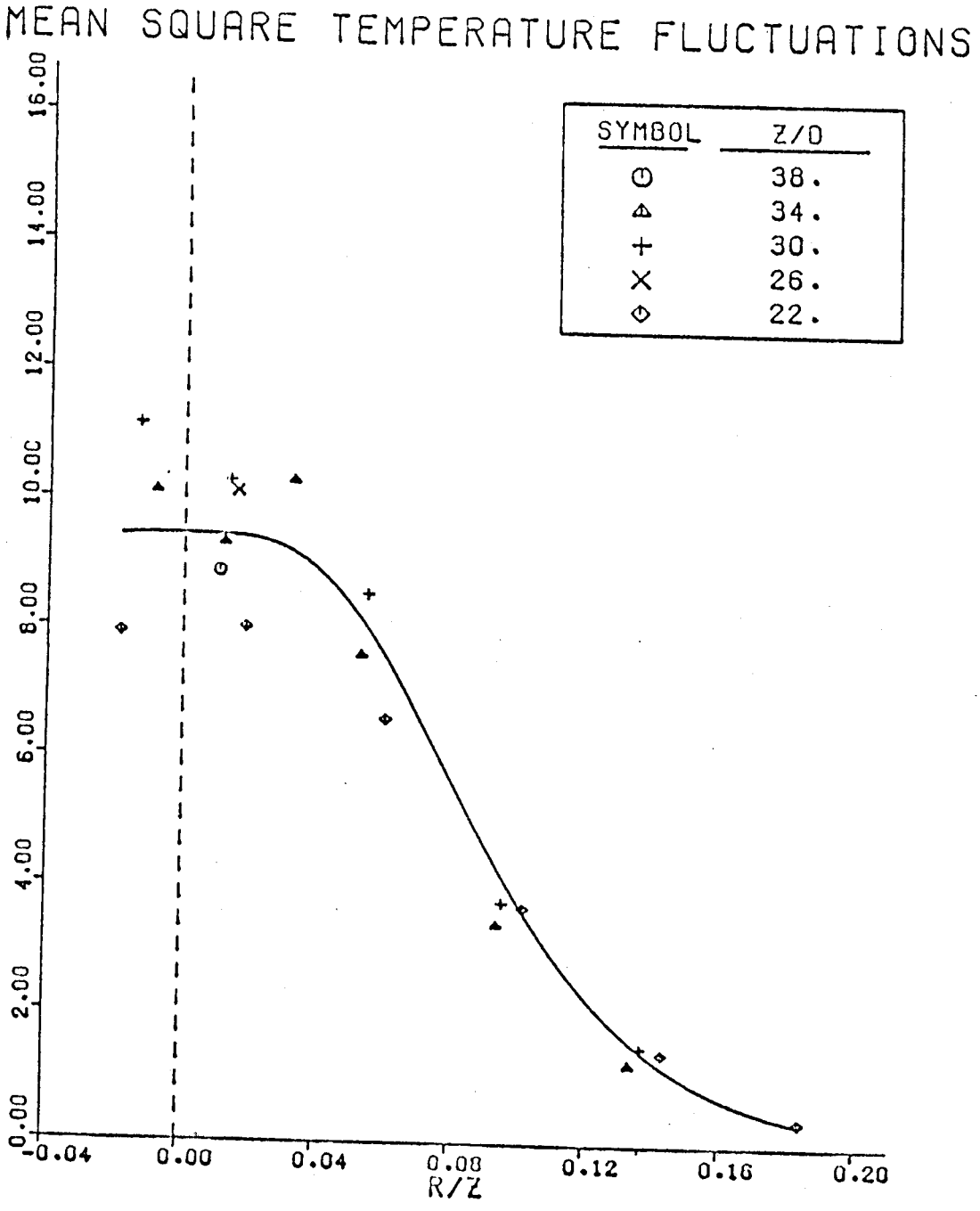
MEAN SQUARE TEMPERATURE FLUCTUATIONS
SYMBOL
Z/D
38.
34.
30.
26.
22.
16.00
14.00
12.00
10.00
8.00
6.00
4.00
2.00
0.00
-0.04
0.00
0.04
0.08
0.12
0.16
0.20
R/Z

Figure 29 17

REYNOLDS STRESS

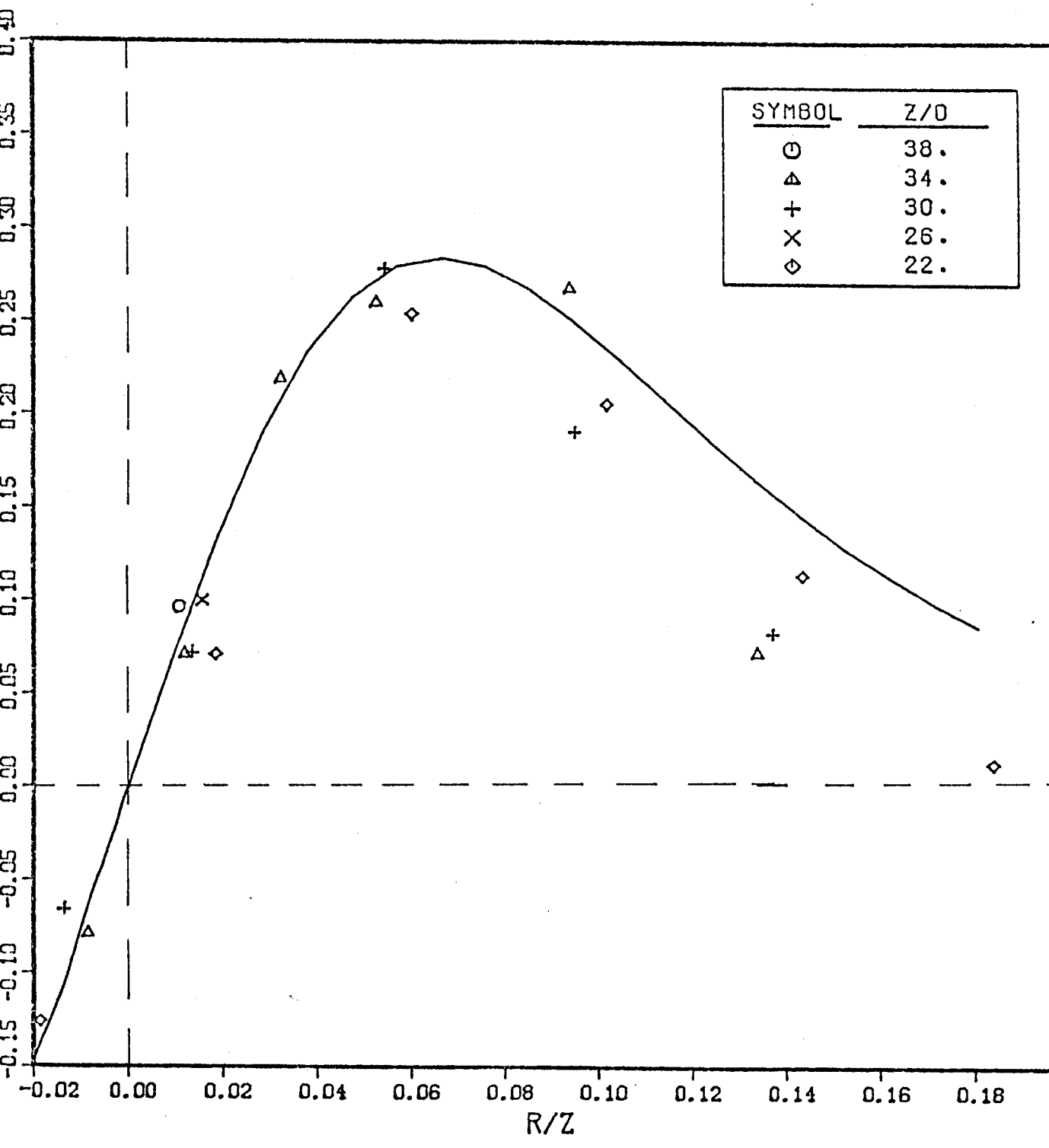

$$R_T = \frac{F_o^{1/3} z^{2/3}}{\nu_T} \tag{5.7}$$

can be determined from the curvature of the velocity profile at the origin and the slope of the Reynolds stress. In dimensionless form

$$R_T = \frac{f''(o)}{h'(o)} \tag{5.8}$$

where F and h are the non-dimensional vertical velocity and Reynolds stress terms, respectively, and the primes denote differentiation with respect to η. From this data it appears that $R_T = 93$. This is considerably larger than the value of 60 cited by George, et al. and the value of 68 presented earlier by this author. The difference is due to the narrowing of the velocity profile by the stratification.

The vertical and radial turbulent heat flux are presented in Figure 20. The vertical component has a slight off-axis peak at $\eta = 0.05$ (also not observed by other investigations, but predicted by Tamanini's computer model), and remains relatively constant out to $\eta = 0.1$. Because the mean vertical heat flux ($\overline{U}_z \overline{\Delta T}$) drops off much faster, the turbulent vertical heat flux can be quite significant in the outer regions of the plume. George, et al. estimated the overall contribution of $\overline{u_z t}$ can be as high as 15%, although the data presented here indicates a contribution closer to 10%. This lower value is also associated with a lower correlation coefficient of .59 - .60 vs. .67 for George et al. No explanation for this difference is known. Nakagome and Hirata measured a very low value of 0.45 for the correlation. This unusually low value could be due to a velocity contamination of the temperature sensor, caused by too high of a current through the wire. The velocity dependence of the temperature wire used in this investigation was practically unmeasurable due to the low current through the wire (150 μA).

Shown with the radial turbulent heat flux, $\overline{u_r t}$, is a curve proportioned to the radial gradient of the mean temperature. By analogy with

TURBULENT HEAT FLUX

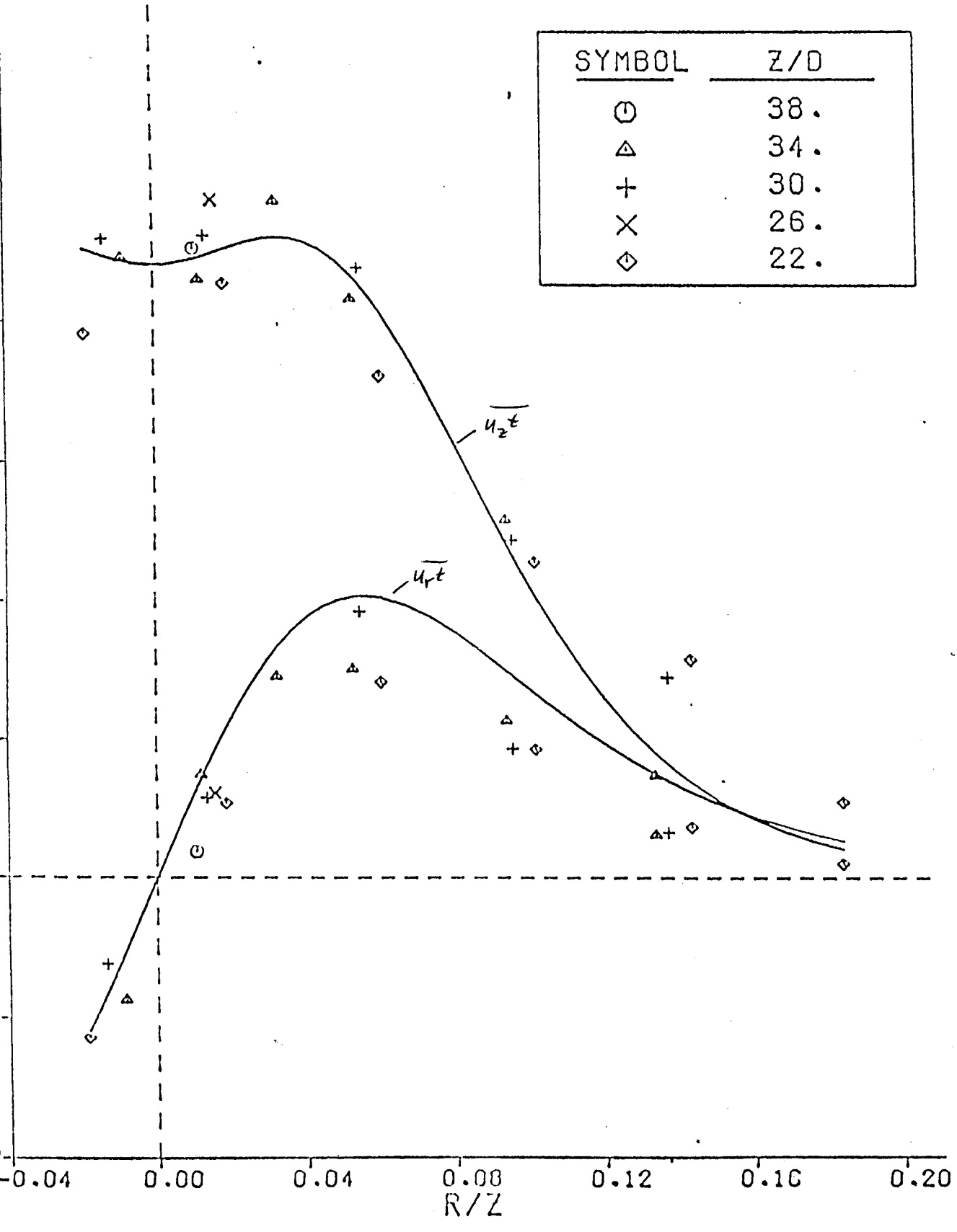

the velocity, one can define a turbulent Prandtl number by

$$P_T R_T = \frac{F_o^{1/3} z^{2/3}}{\gamma_T} = \frac{g''(o)}{w'(o)} \qquad (5.9)$$

where g and w are the non-dimensional buoyancy and radial heat flux, respectively P_T is approximately unity (1.2), which is in agreement with other investigations (c.f. Baker 1980).

By using the fitted curves in Figures 15 through 20, it is possibl to plot all the significant terms of the mean momentum and temperature balance equations (equations(2.14) and (2.16). The analytical expressions the curve fitting of the first and second moments are given in Table II. These curves are still in similarity variables. The reconstructed mean momentum balance is shown in Figure 21. The temperature balance is in Figure 22.

Since the plume is not in a uniform environment, the calculation of the z derivatives involves the z-dependence of the buoyancy flux as found from Figure 14. It is obvious that all the terms do not balance perfectly especially in the temperature balance. This is because of the choice of curve fitting. The profiles are not really similar - it's just that the deviation from similarity is small enough that the fitted curves agree well with the data. However, when combined to form the balances, these slight errors are more noticeable, especially in the outer regions. Term 2 of the temperature balance is an example of this problem. The term $(\overline{U}_z \frac{dTo}{dz})$ is due entirely to the stratification of the ambient air. In a uniform environment it is absent. This term decays like the $\overline{U}_z$ velocity component across the flow, since $\frac{dTo}{dz}$ is a constant. However, every other term in the balance decays at a much faster rate (at least like $\overline{U}_z^2$). Unless another function is chosen to fit the data in these outer regions,

Figure 21

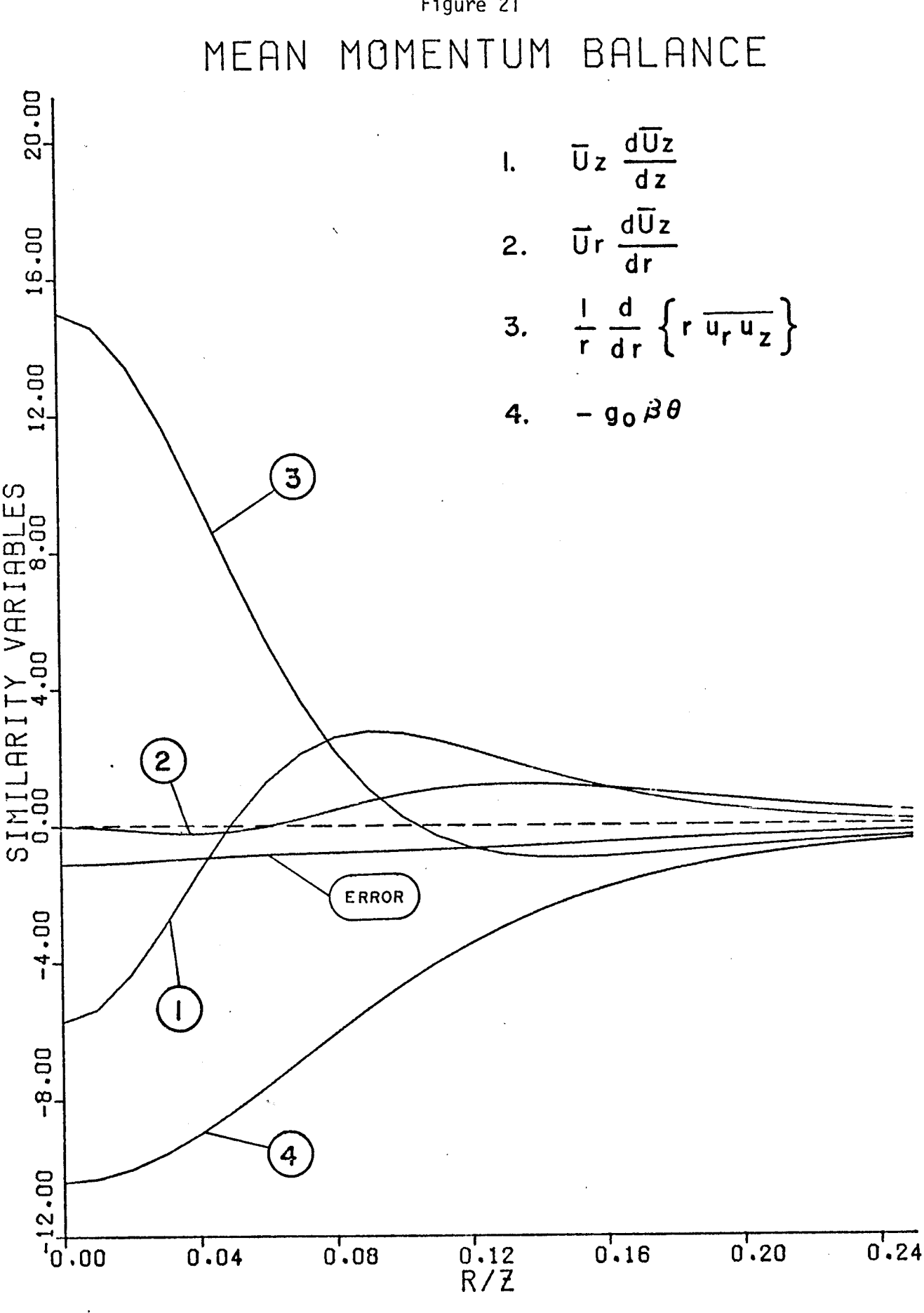
MEAN MOMENTUM BALANCE
1. $\bar{U}_z \frac{d\bar{U}_z}{dz}$
2. $\bar{U}_r \frac{d\bar{U}_z}{dr}$
3. $\frac{1}{r}\frac{d}{dr}\left\{r\,\overline{u_r u_z}\right\}$
4. $-g_o \beta\theta$
SIMILARITY VARIABLES
20.00
16.00
12.00
8.00
4.00
0.00
-4.00
-8.00
-12.00
0.00
0.04
0.08
0.12
0.16
0.20
0.24
R/Z
1
2
3
4
ERROR

MEAN TEMPERATURE BALANCE

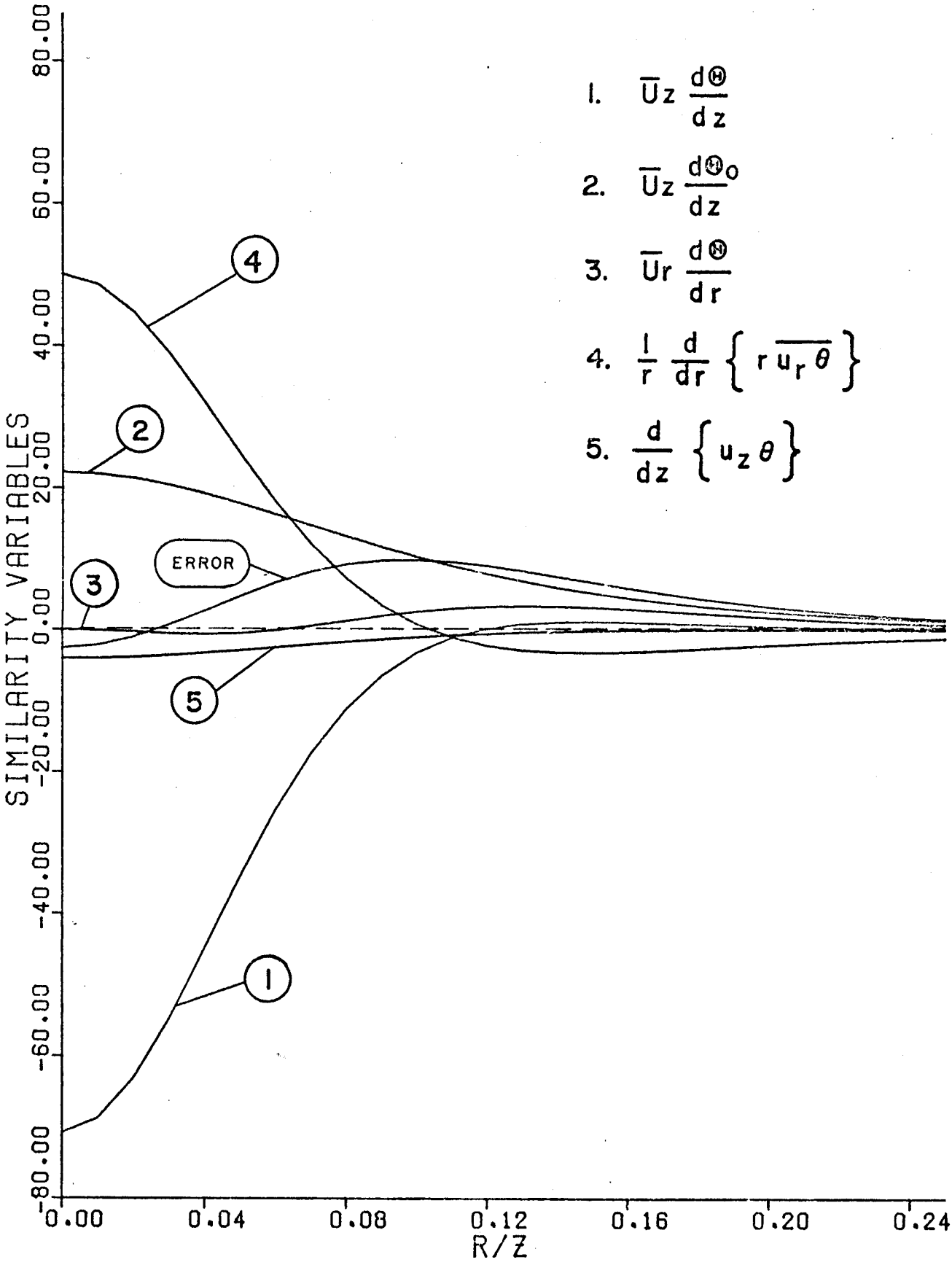

TABLE II

Fitted Curves for 1st & 2nd Moments

Variable	Similarity Function	Fitted Curve
$\overline{U}_z$	$f(\eta)$	$\frac{3.8}{[1+46\eta^2]^2}$
$\overline{U}_r$	$k(\eta)$	As defined by Equation (2.1
$g_o\beta\Delta T$	$g(\eta)$	$\frac{10.4}{[1+31\eta^2]^3}$ OR $\frac{10.4}{[1+46\eta^2]^2}$
$\overline{u_z^2}$	$h_{11}(\eta)$	$\frac{1+230\eta^2}{[1+46\eta^2]^4}$
$\overline{u_r^2}$ $(=\overline{u_\phi^2})$	$h_{22}(\eta)$	$\frac{.61}{[1+59\eta^2]^2}$
$(g_o\beta)^2\,\overline{t^2}$	$h_{33}(\eta)$	$\frac{.95+2550\eta^2}{[1+45\eta^2]^6}$
$\overline{u_z u_r}$	$h_{12}(\eta)$	$\frac{7.45\eta}{[1+46\eta^2]^3}$
$g_o\beta\overline{u_z t}$	$h_{13}(\eta)$	$\frac{1.77+650\eta^2}{[1+46\eta^2]^6}$
$g_o\beta\overline{u_r t}$	$h_{23}(\eta)$	$\frac{17.25\eta}{[1+46\eta^2]^3}$

TABLE III

Fitted Curves for 3rd Moments

Variable	Fitted Curve to Correlation Coefficient
$\overline{u_z^3}$	$\rho_{111}(\eta) = .23 + 13.5\eta^2 + 2575\eta^4 - 35000\eta^6$
$\overline{u_r^3}$	$\rho_{222}(\eta) = -.49\eta + 10.9\eta^2 + 1200\eta^3 - 7400\eta^4 + 11630\eta^5$
$\overline{u_z t^2}$	$\rho_{123}(\eta) = .3 + 35\eta^2 - 5000\eta^6$
$\overline{u_r t^2}$	$\rho_{233}(\eta) = 60\eta^2 - 200\eta^3$
$\overline{u_z u_r^2}$ $(=\overline{u_z u_\phi^2})$	$\rho_{122}(\eta) = -.05 + 65\eta^2 - 7000\eta^6$
$\overline{u_z^2 u_r}$	$\rho_{112}(\eta) = (-3.1\eta + 1540\eta^3)\ \mathrm{EXP}\ [-15\eta]$

an error term as shown is unavoidable. Unfortunately, the amount of data in these outer regions is small, and its accuracy is poor because of the high turbulence intensities and the resulting directional ambiguities of the wires and the drop-out problems mentioned earlier. Thus, no attempt was made to choose profiles which minimize this error since a complicated non-linear regression was already used to minimize the error in each profile. To minimize the error in the momentum and temperature balance is not impossible, but it would not be worth the effort required. The 5-10% error that is typical of these balances is not deemed extremely significant.

Very few investigators compare all the terms in the momentum balance to validate their data. The few that do generally publish only the integrated results (across the flow). Such an analysis is always a worthwhile exercise, and would undoubtably shed light on differences between different sets of data. Even long standing experimental references have been found to contain serious errors when analyzed in this manner (Baker (1980)).

Table III contains fitted polynomial curves for 6 of the 9 third moment correlation coefficients. These 6 all play an important part in the turbulent energy budgets, which will be discussed at the end of this chpater. These 6 moments, along with the remaining three third moments and three fourth moments are plotted in Figures 23 through 34. All these collapsed quite well at various heights except the $\overline{u_r^2 t}$ correlation The reason this one moment is out of line with the rest is not understood. This moment is not important to the flow dynamics of interest.

Figure 23

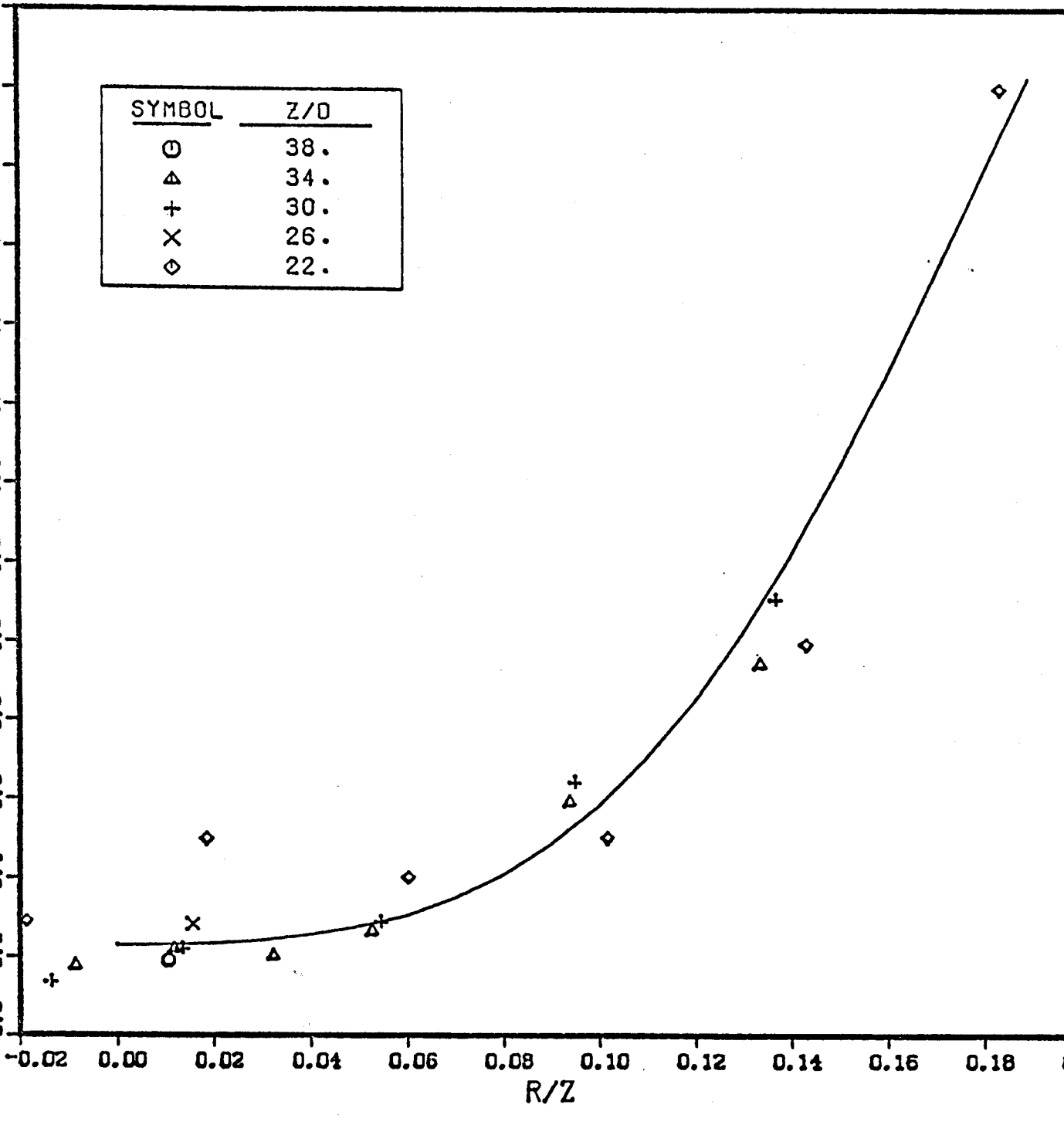
UUU CORRELATION
SYMBOL
Z/D
38.
34.
30.
26.
22.
-0.02
0.00
0.02
0.04
0.06
0.08
0.10
0.12
0.14
0.16
0.18
R/Z

Figure 24

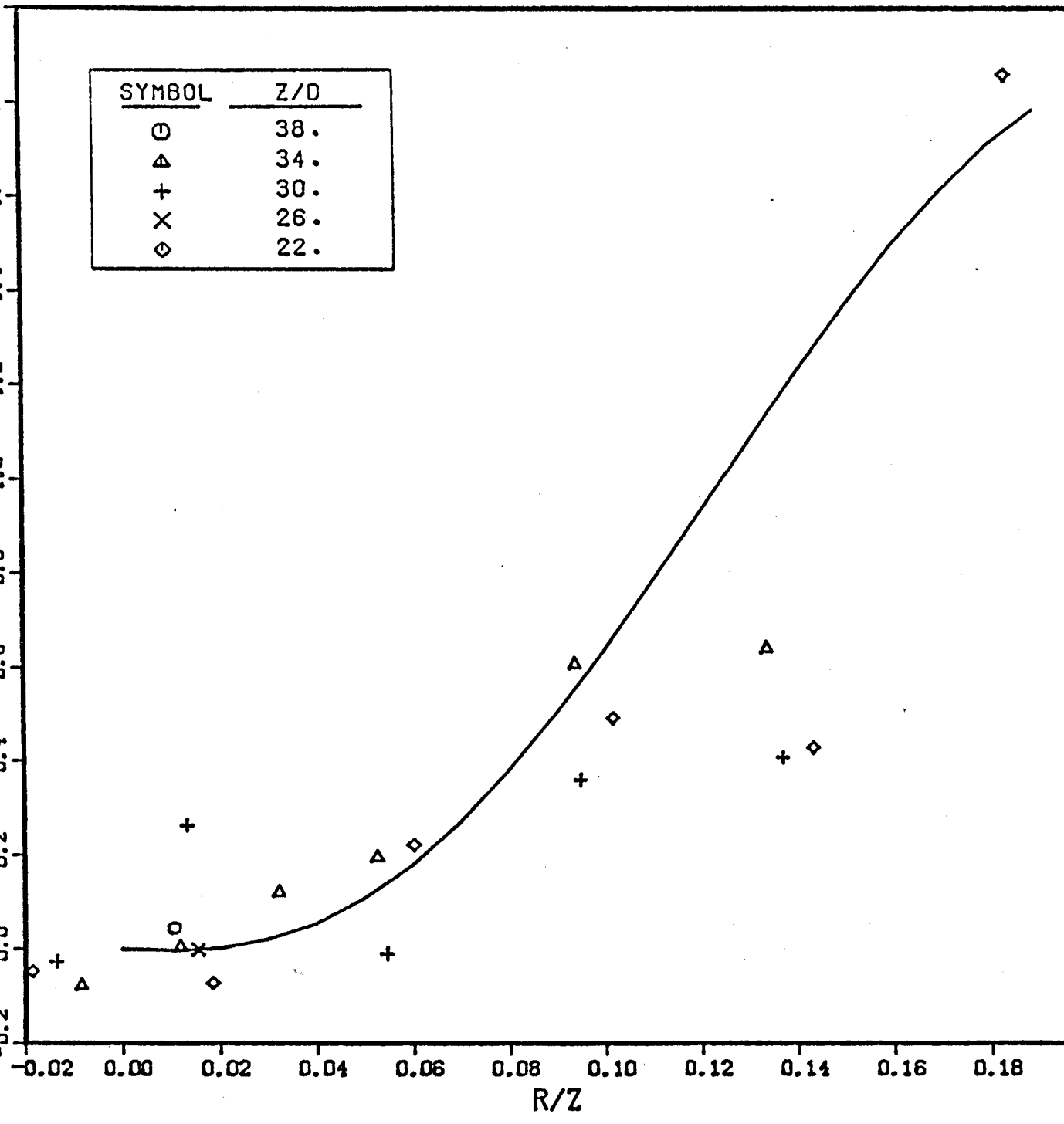
VVV CORRELATION
SYMBOL
Z/D
38.
34.
30.
26.
22.
-0.02
0.00
0.02
0.04
0.06
0.08
0.10
0.12
0.14
0.16
0.18
R/Z

Figure 25

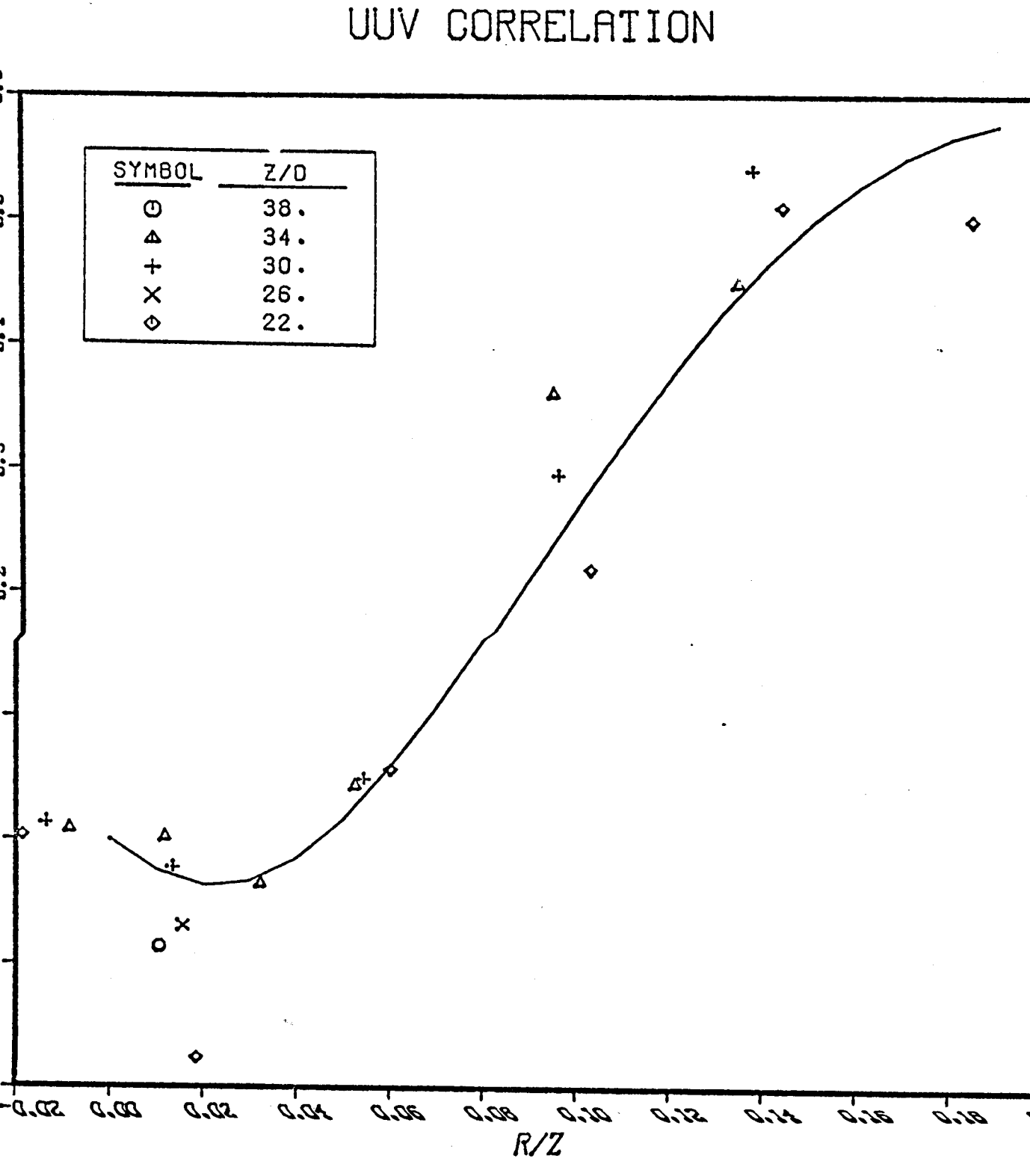
UUV CORRELATION
SYMBOL
Z/D
38.
34.
30.
26.
22.
0.02
0.04
0.06
0.08
0.10
0.12
0.14
0.16
0.18
R/Z

Figure 26

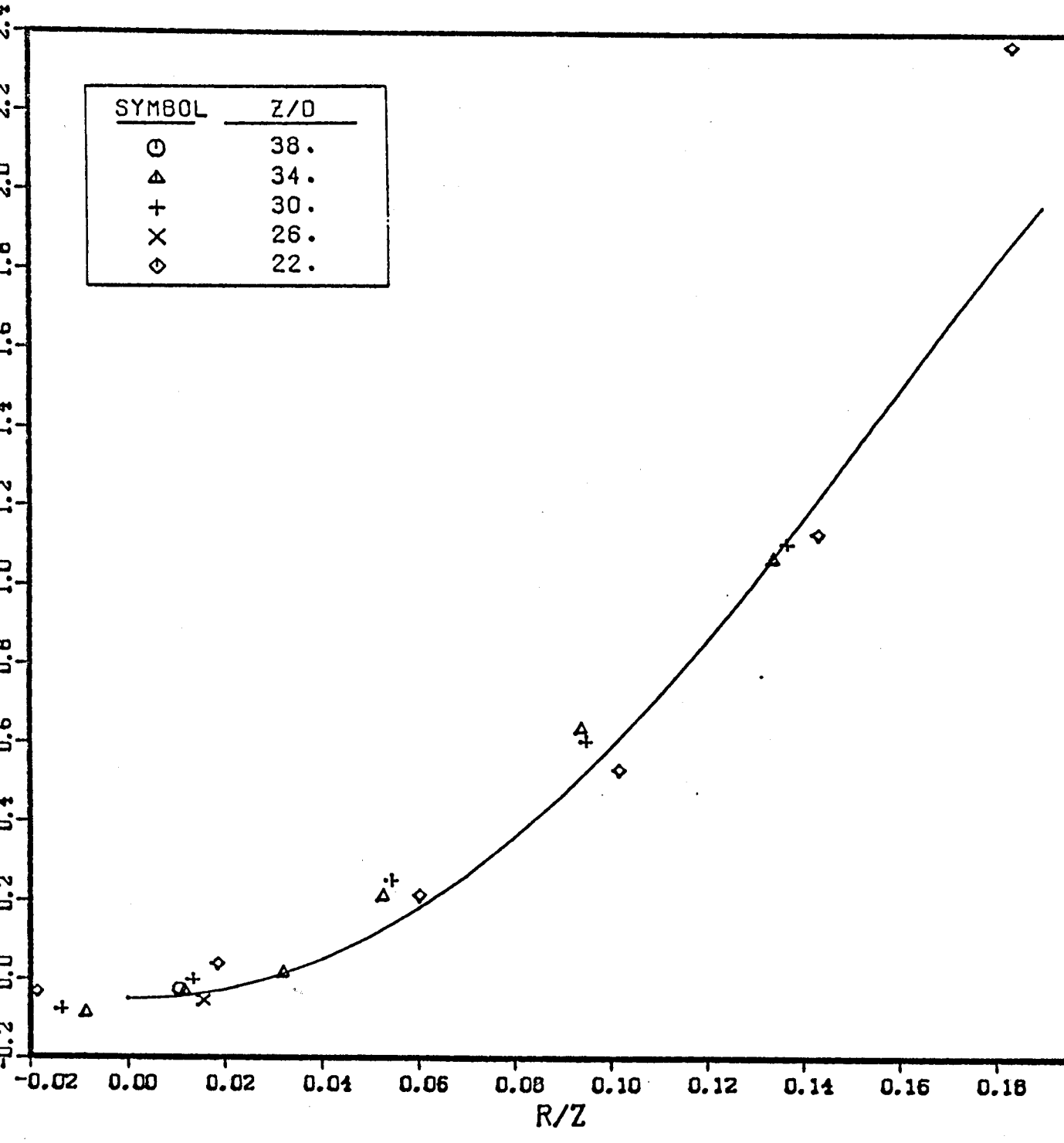
UVV CORRELATION
SYMBOL
Z/D
38.
34.
30.
26.
22.
-0.02
0.00
0.02
0.04
0.06
0.08
0.10
0.12
0.14
0.16
0.18
R/Z

Figure 27

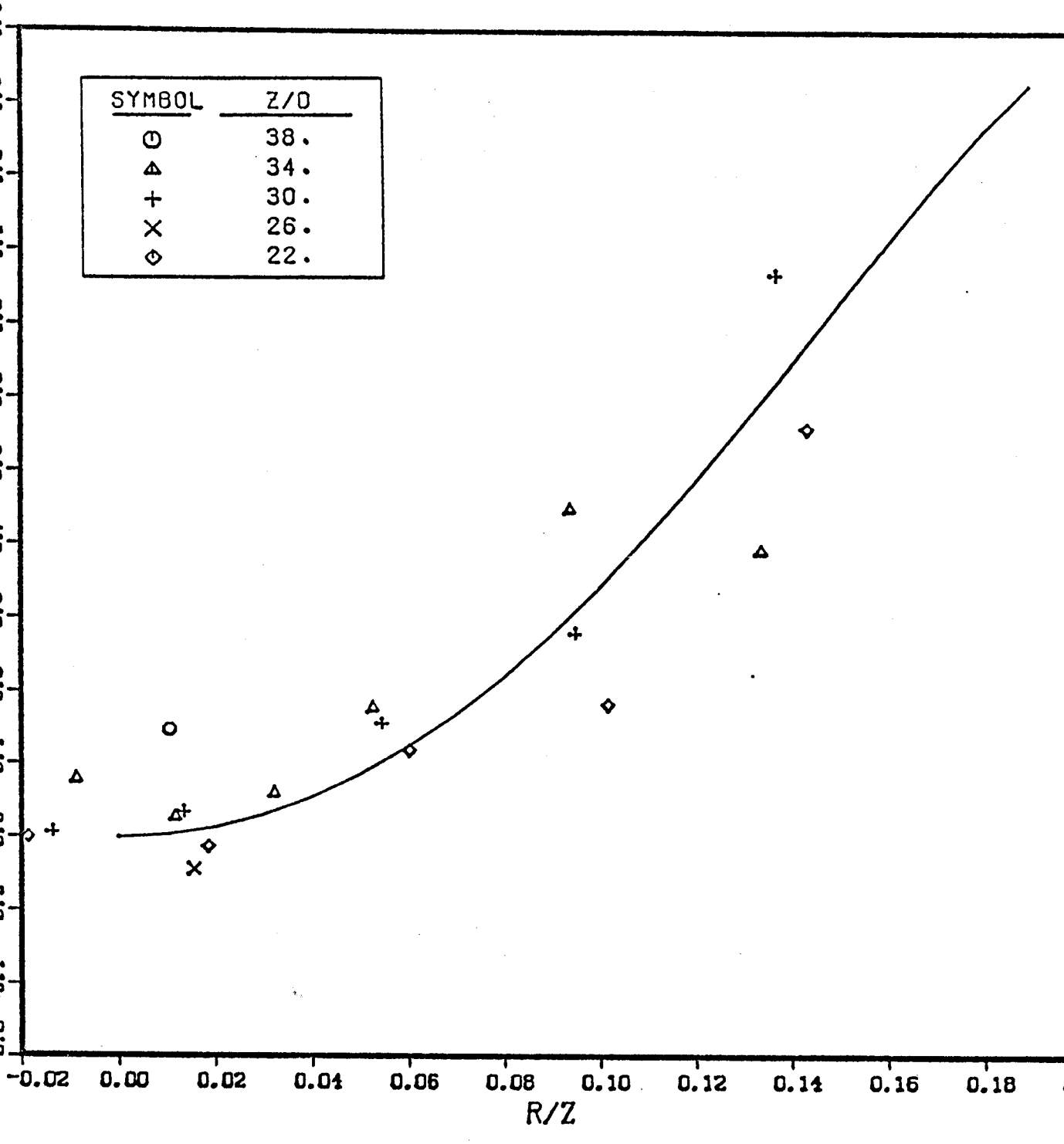
UTT CORRELATION
SYMBOL
Z/D
38.
34.
30.
26.
22.
-0.02
0.00
0.02
0.04
0.06
0.08
0.10
0.12
0.14
0.16
0.18
R/Z

VTT CORRELATION

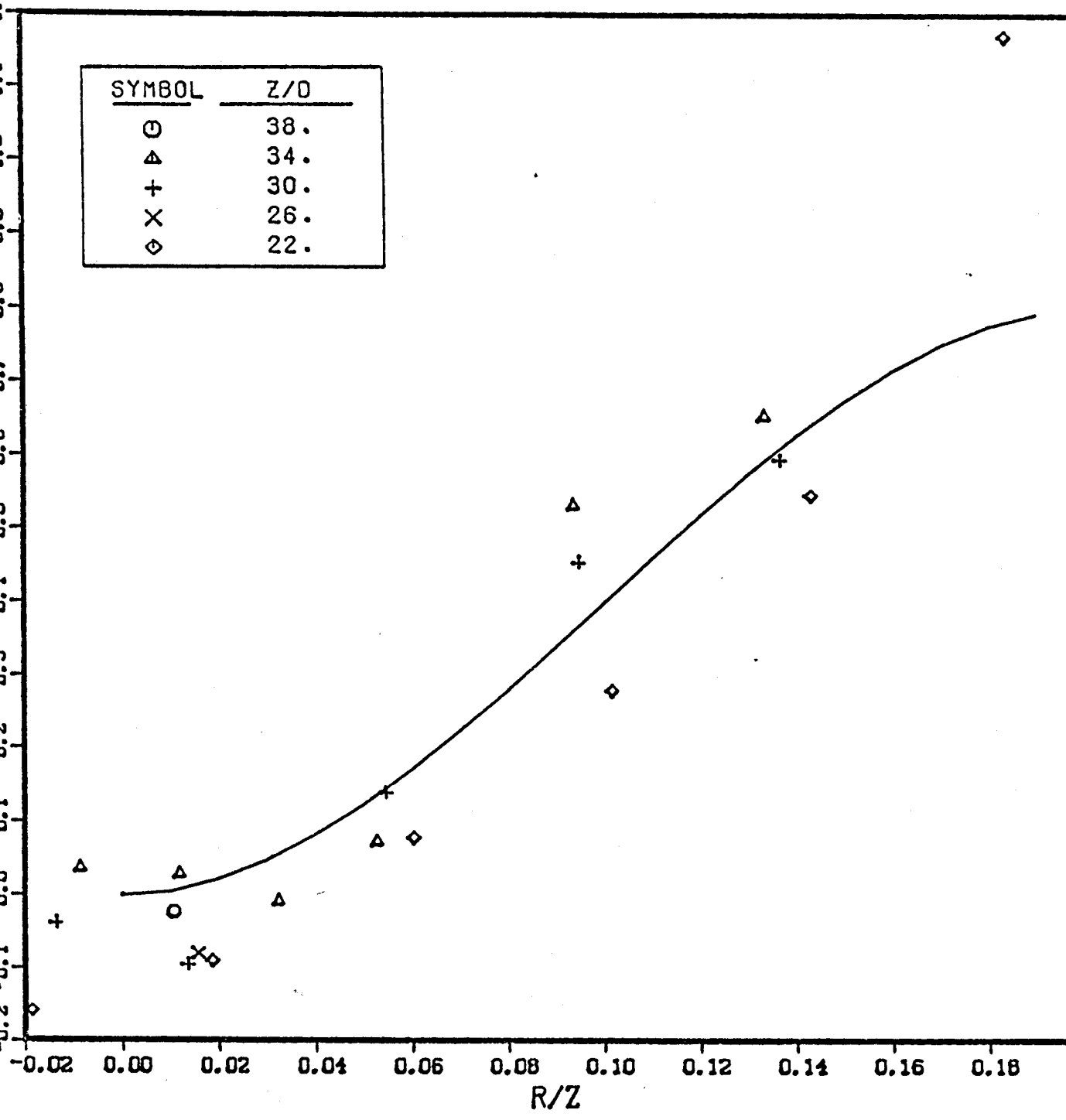

Figure 29

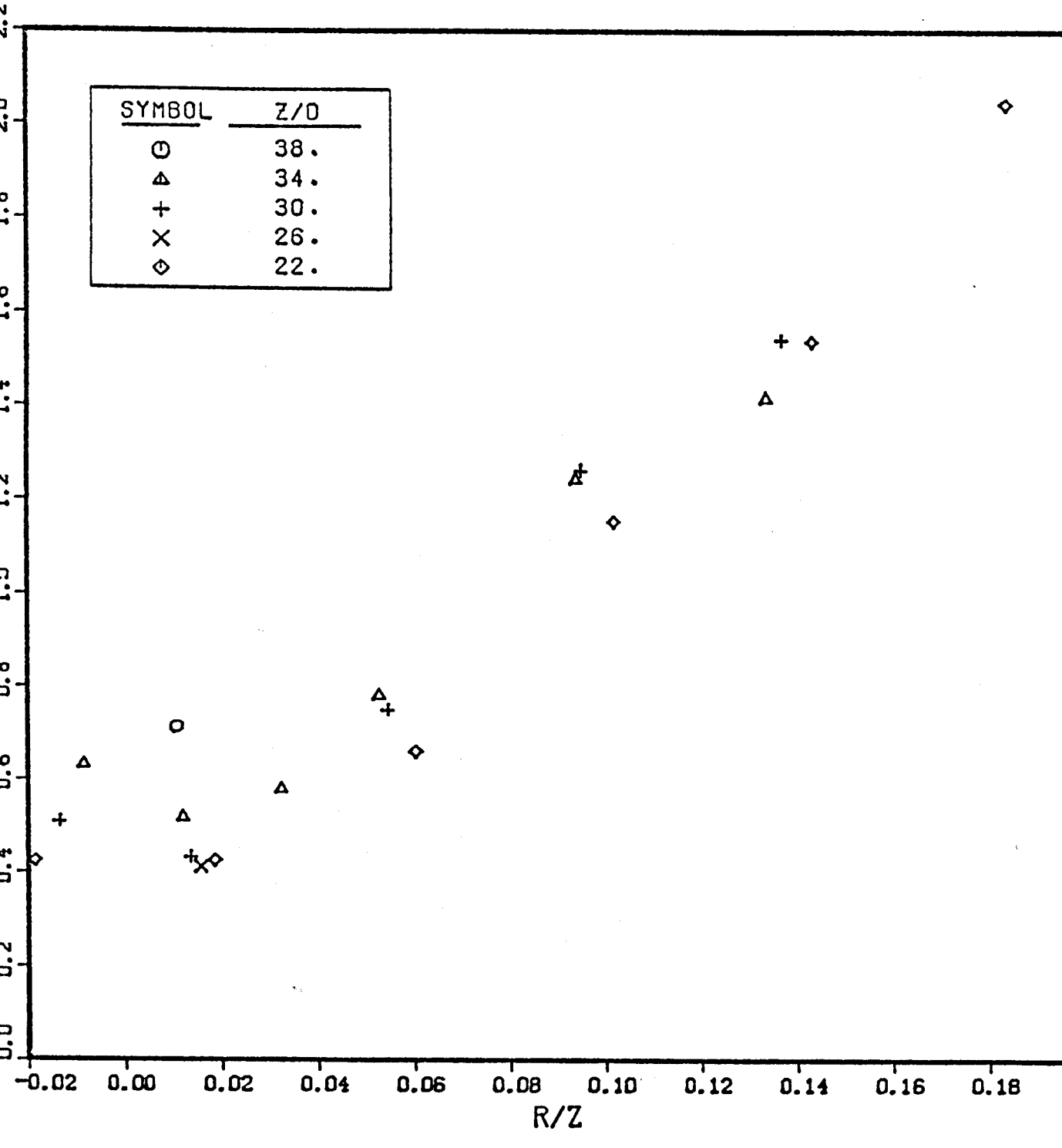
TTT CORRELATION
SYMBOL
Z/D
38.
34.
30.
26.
22.
-0.02
0.00
0.02
0.04
0.06
0.08
0.10
0.12
0.14
0.16
0.18
R/Z

UUT CORRELATION

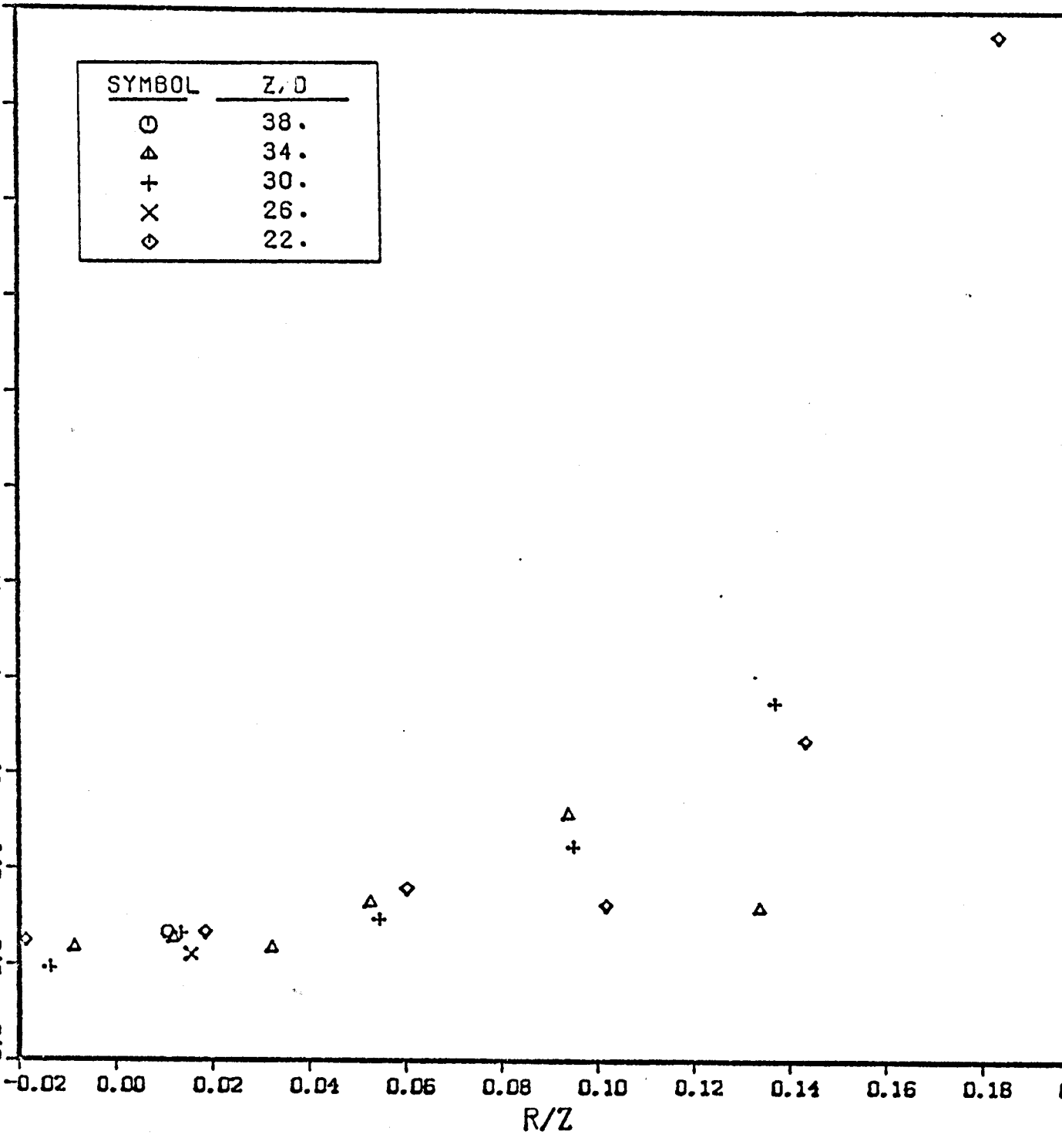

VVT CORRELATION

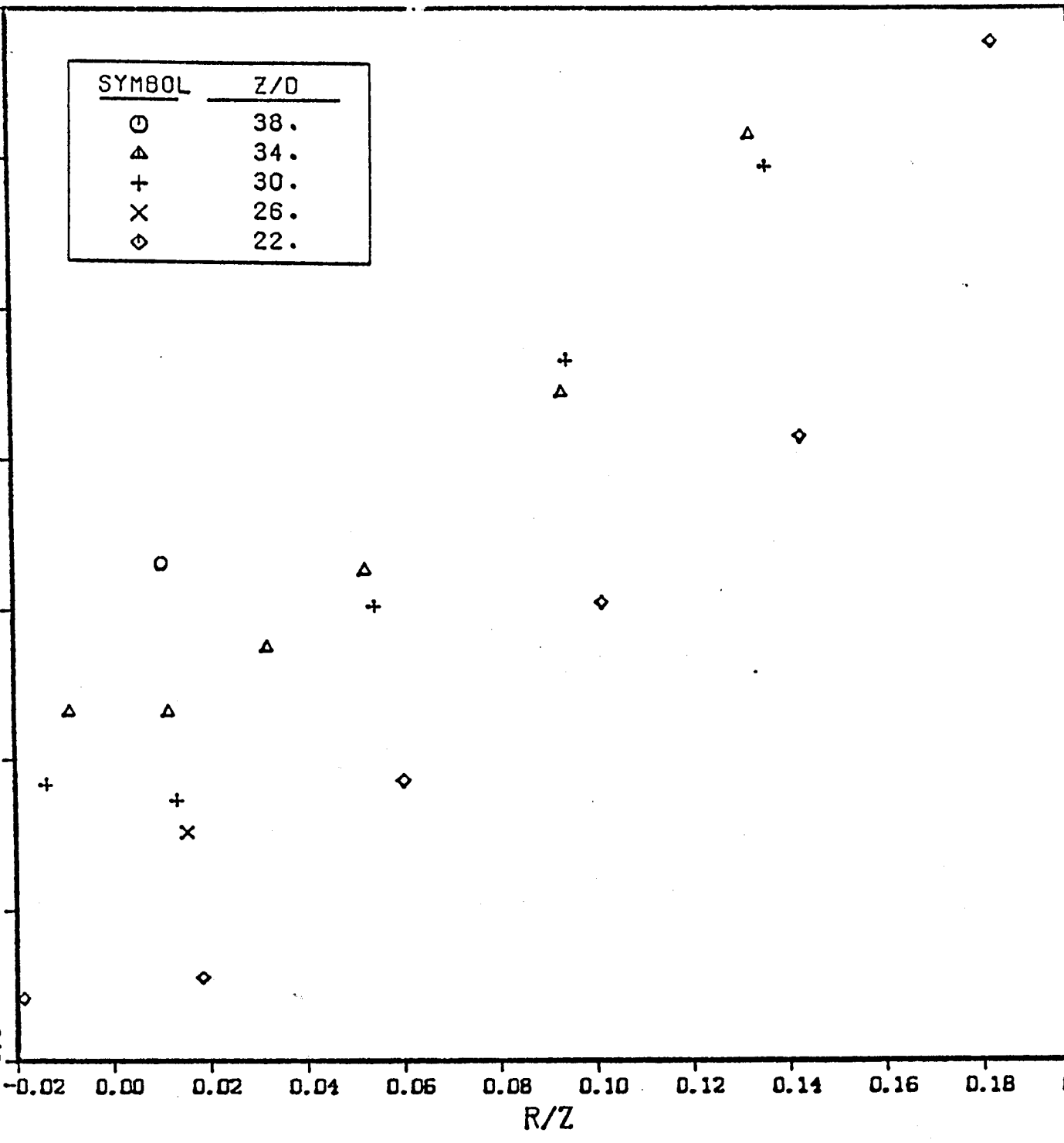

Figure 32

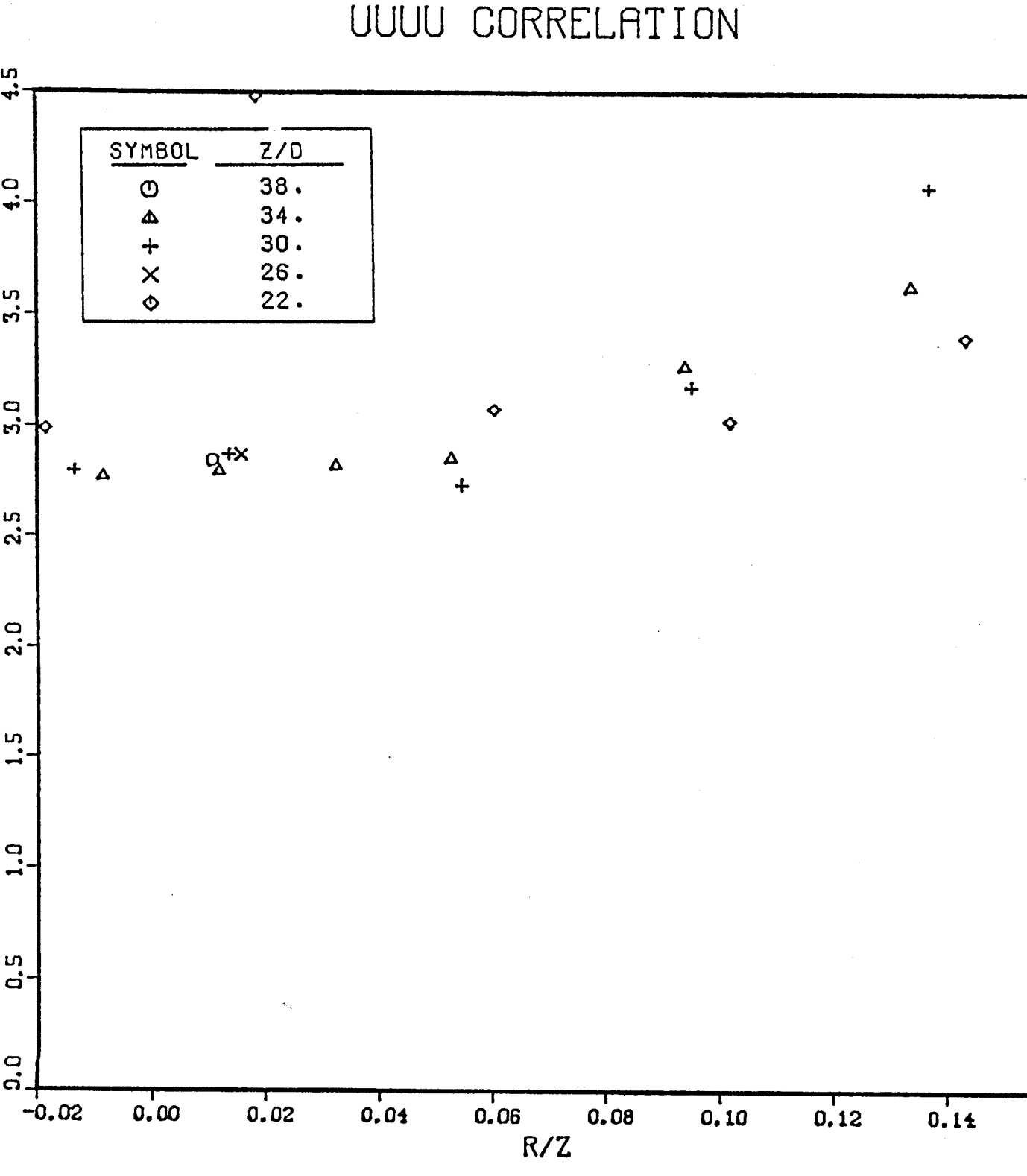
UUUU CORRELATION
SYMBOL
Z/D
38.
34.
30.
26.
22.
4.5
4.0
3.5
3.0
2.5
2.0
1.5
1.0
0.5
0.0
-0.02
0.00
0.02
0.04
0.06
0.08
0.10
0.12
0.14
R/Z

Figure 33

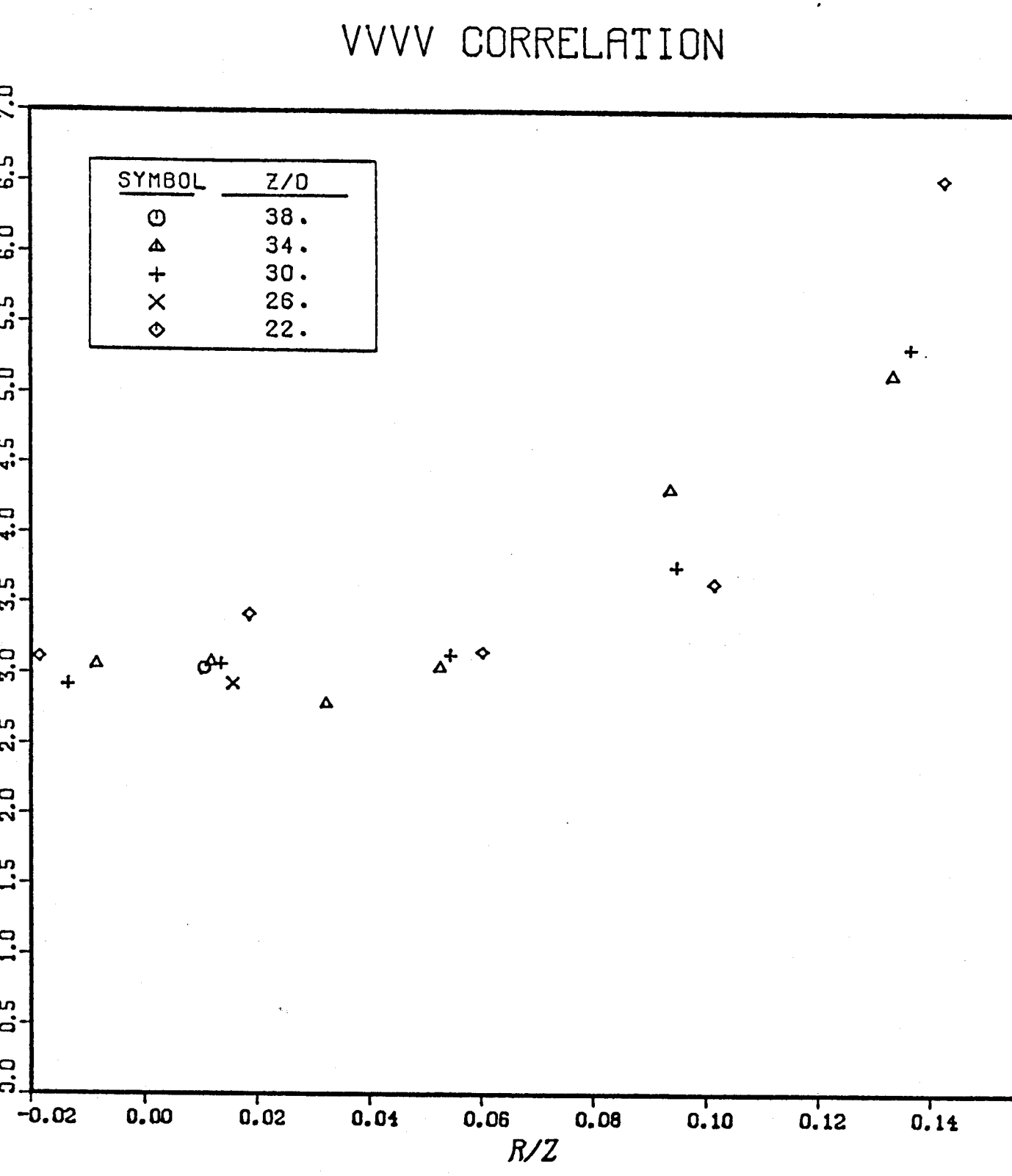
VVVV CORRELATION
SYMBOL
Z/D
38.
34.
30.
26.
22.
7.0
6.5
6.0
5.5
5.0
4.5
4.0
3.5
3.0
2.5
2.0
1.5
1.0
0.5
0.0
-0.02
0.00
0.02
0.04
0.06
0.08
0.10
0.12
0.14
R/Z

Figure 34

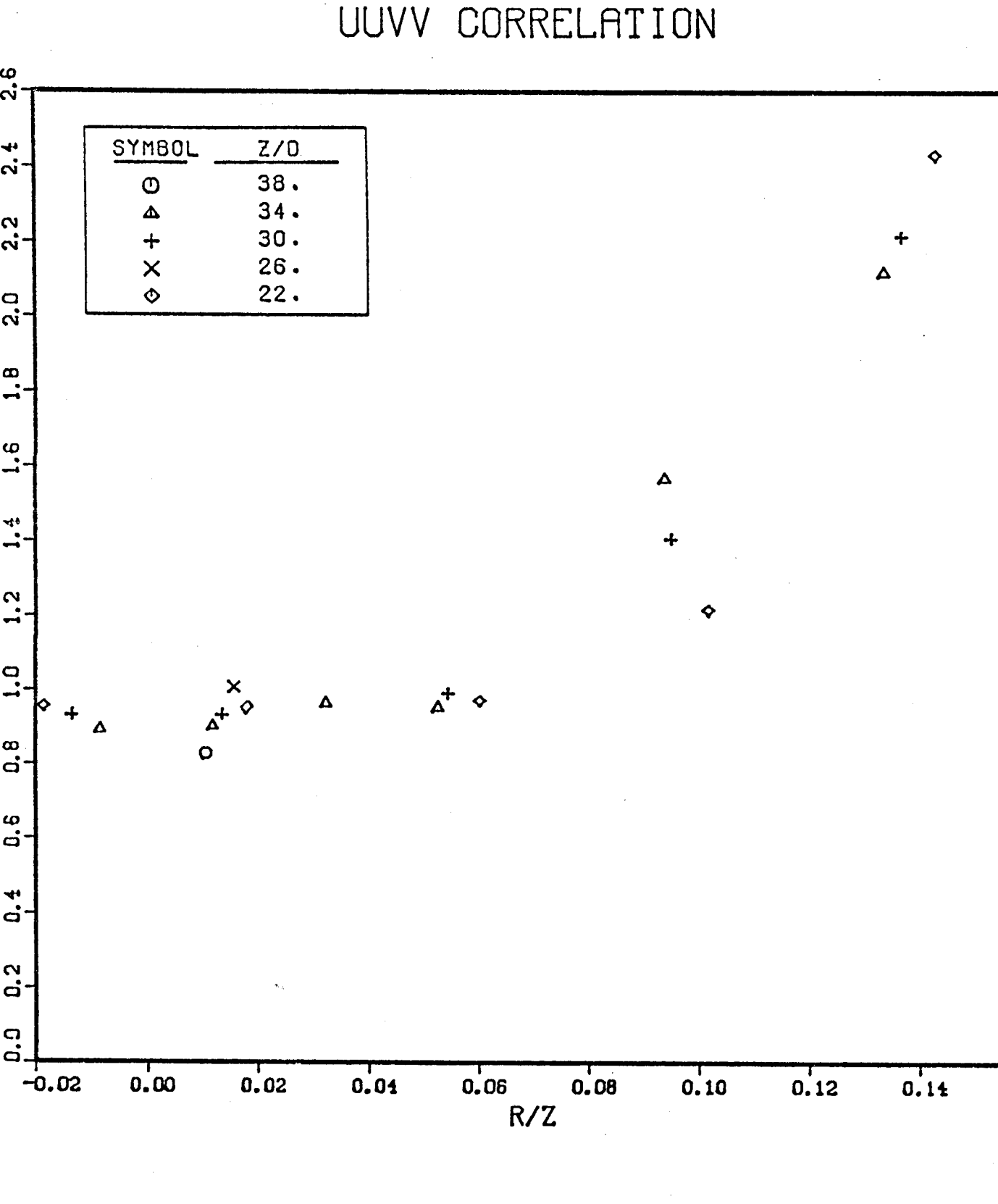
UUVV CORRELATION
SYMBOL
Z/D
38.
34.
30.
26.
22.
2.6
2.4
2.2
2.0
1.8
1.6
1.4
1.2
1.0
0.8
0.6
0.4
0.2
0.0
-0.02
0.00
0.02
0.04
0.06
0.08
0.10
0.12
0.14
R/Z

The fourth moments follow the Gaussian shape quite well in the interior of the plume, but deviate substantially at large values of r/z. For the correlation coefficient of $\overline{u^4}$ and $\overline{v^4}$, a Gaussian behavior would have a constant value of three. For the $\overline{u^2v^2}$ coefficient, the value depends upon the shape of the Reynolds stress, $\overline{uv}$. Considering the drop-out problems associated with $\overline{uv}$, the values for $\overline{u^2v^2}$ cannot be stated with much confidence. Figure 35 illustrates the comparison between $\overline{u^2v^2}$ and the corresponding correlation derived from the Reynolds stress by assuming a Gaussian distribution. The agreement is quite good, especially in the center portion of the plume. It is worst at the outer edge of the plume and in the center of the shear layer where the uv correlation is largest.

5.2 Moments of Velocity and Temperature Derivatives

Using the techniques described in Section 5.1, the moments of the velocity and temperature derivatives can be calculated. Derivative moments are important for studying the dynamics of turbulent flows, especially the dissipation of turbulent kinetic energy. By measuring second derivatives (the derivative of the derivative signal) one can study the dynamics of the turbulent vorticity. Since this investigation was concerned with the turbulent energy balances of kinetic energy and temperature fluctuations, only first derivatives were measured.

By applying Taylor's hypothesis (section 2.3) the measured time derivatives can be converted to spatial derivatives.

$$\frac{d}{dz} = \frac{1}{U}\frac{d}{dt} \qquad (5.10)$$

UUVV CORRELATION WITH GAUSSIAN PREDICTION

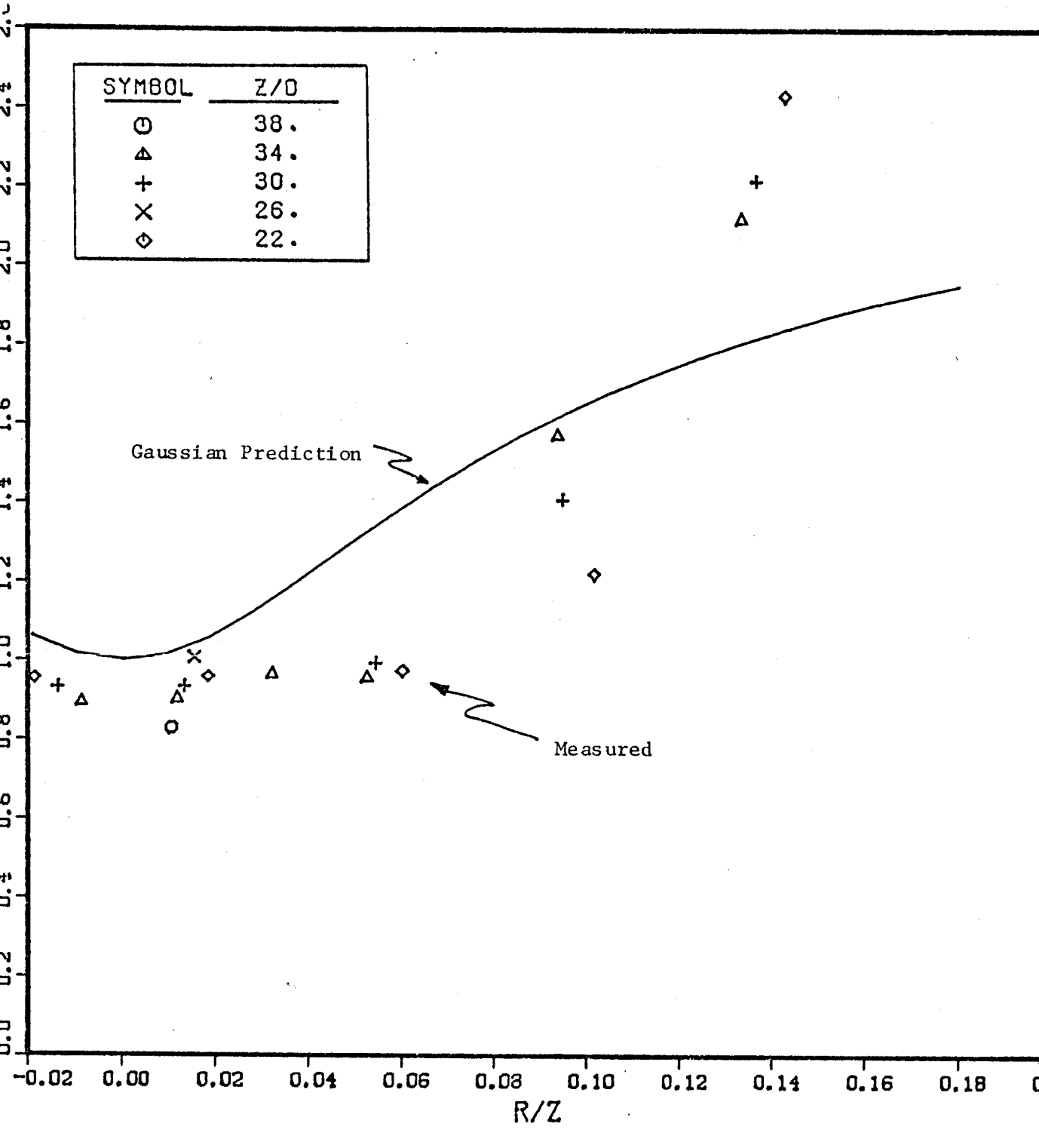

Because of the problems of applying Taylor's hypothesis in flows with large velocity fluctuations, the derivatives must be corrected by using the correction scheme of Lumley presented in equations (2.29) through (2.31). All data presented will have already been corrected in this manner. It should be noted how large the correction terms can get. At r/z of 0.13, the measured value of $(\overline{\frac{du}{dz}})^2$ is nearly a factor of two too large for this flow. This correction is often ignored in many investigations, even in strong shear flows. Since the calculated dissipation is proportional to this term, it also will be too large.

Derivative signals present special problems in data analysis because they do not have Gaussian probability density functions, but are distributed in a mean log-normal distribution. This fact was predicted by Oboukhov (1962) and Gurvich and Yaglom (1967) and is known as Kolmogorov's third hypothesis. Other investigators, such as Tennekes and Wyngaard (1972) suggest an exponential form for the probability density function, but the main effect is still that the derivative signal has a broad distribution with considerable weight in the tails of the distribution. This leads to much larger statistical fluctuation in the calculated moments than for simple velocity moments (assuming the same averaging time). For the second moment of the derivatives this relative error is estimated to be 2-3 times larger than the error in the second moment of velocity or temperature (assuming a kurtosis of the derivative signal of about 5-6). Thus the rms fluctuation for the derivative estimators is 8-10%.

Assuming the derivatives to be locally isotropic, the following relationships can be deduced (c.f. Hinze (1975), Tennekes and Lumley (1972)):

Dissipation of $\frac{\overline{u_z^2}+\overline{u_r^2}+\overline{u_\phi^2}}{2}$: $\epsilon = 15\nu\overline{\left(\frac{du_z}{dz}\right)^2}$ (5.11)

Dissipation of $\frac{\overline{t^2}}{2}$: $\epsilon_t = 3\gamma\overline{\left(\frac{dt}{dz}\right)^2}$ (5.12)

The Taylor microscales for velocity and temperature can be defined by:

$$\overline{\left(\frac{\partial u_z}{\partial z}\right)^2} = \frac{\overline{u_z^2}}{\lambda^2} \tag{5.13}$$

$$\overline{\left(\frac{\partial t}{\partial z}\right)^2} = \frac{\overline{t^2}}{\lambda_t^2} \tag{5.14}$$

For isotropic turbulence, Corrsin (1951) showed that

$$\frac{\lambda}{\lambda_t} = P_r^{1/2} \tag{5.15}$$

With the assumption of local isotropy, several relations between the derivatives can be formulated. The ones of interest to the measured values of this investigation are listed below.

$$\overline{\frac{\partial u_z}{\partial z}\frac{\partial u_r}{\partial z}} = 0 \tag{5.16}$$

$$\overline{\frac{\partial u_z}{\partial z}\frac{\partial t}{\partial z}} = 0 \tag{5.17}$$

$$\overline{\frac{\partial u_r}{\partial z}\frac{\partial t}{\partial z}} = 0 \tag{5.18}$$

$$\overline{\left(\frac{\partial u_z}{\partial z}\right)^2} = 1/2\,\overline{\left(\frac{\partial u_r}{\partial z}\right)^2} \tag{5.19}$$

$$\overline{\left(\frac{\partial u_z}{\partial z}\right)^2} = \frac{\overline{u_z^2}}{2\overline{t^2}}\,\frac{1}{P_r}\,\overline{\left(\frac{\partial t}{\partial z}\right)^2} \tag{5.20}$$

As mentioned in Section 3.3, the filter on the temperature derivative made it impossible to verify relations (5.17) and (5.18). However, earlier

preliminary measurements taken without the filter gave correlations around 0.05 for these two expressions. The present data is highly correlated (∿.25-.5), but this is due to the phase lag of the filter. Normally this correlation would imply a velocity dependence of the temperature sensor, a situation known to be extremely small in this experiment.

As shown in Equation (5.16), the $\overline{\frac{\partial u_z}{\partial z}\frac{\partial u_r}{\partial z}}$ cross term should also be zero, and the experimental values indicate that this is true. The correlation coefficient ranges from 0.01 to 0.1 on the centerline, but as high as 0.2 at large values of the radial coordinate. These high correlations might be due to a breakdown of the local isotropy assumption or a breakdown of Taylor's hypothesis (c.f. Section 2.4).

For the remaining isotropic relations, the agreement is not as good. Equation(5.20)is satisfied fairly well, but the ratio of the u velocity derivative variance to that of the v velocity (Equation(5.19))is far from 0.5. As seen in Table IV, both ratios vary considerably but average around one. At first, one might suspect an error in calculation for the u-v ratio since the trend is almost exactly a factor of two off. However, these numbers are consistent with the spectral measurements to be discussed in Section 5.3.

Since the u and v derivatives do not obey local isotropy, it is doubtful that accurate measurements of the dissipation can be obtained without direct measurement of all the derivative terms. However, for scaling purposes, the isotropic relations for the dissipation (equation 5.11) will be assumed valid. This question will be raised again in Chapter 6 in the discussion of the turbulent energy balance.

There are other serious problems surrounding these derivative measurements. Most noticable is their failure to collapse when scaled in similarity variables. Just as the regular velocity and temperature moments scaled with F_0 and z, so should the derivatives. This scaling is:

$$\nu\overline{\left(\frac{du_z}{dz}\right)^2} = d_1(\eta)\, F_0\, z^{-2} \tag{5.21}$$

$$\nu\overline{\left(\frac{du_r}{dz}\right)^2} = d_2(\eta)\, F_0\, z^{-2} \tag{5.22}$$

$$\gamma g_0^2 \beta^2 \overline{\left(\frac{dt}{dz}\right)^2} = d_3(\eta)\, F_0^{5/3} z^{-14/3} \tag{5.23}$$

However, as can be seen in Table V, the z-dependence is quite different from that given in Equations (5.21) - (5.23).

Part of this discrepancy lies in the stratification of the ambient environment. This is particularly true for the temperature derivatives, since the governing equations contain a term proportional to the local ambient temperature gradient. The variations of the velocity derivatives cannot be accounted for in this manner. Either the measurements are wrong, or else local isotropy is not valid in this region. Since there is no reason to suspect the data, especially in such a strongly biased manner (top to bottom), and since the u and v derivatives approach the isotropic relations as the height is increased, this probably indicates that the turbulent Reynolds number is not large enough at the lower positions to ensure local isotropy. However, to achieve larger Reynolds numbers the measuring height (or heat flux F_0) would have to be increased considerably.

The trends shown in Table V indicate a height of 3.5 - 4 meters would be sufficient (based on the ratio of $\overline{\left(\frac{\partial u_z}{\partial z}\right)^2}\Big/\overline{\left(\frac{\partial u_r}{\partial z}\right)^2}$. This height was originally planned for in the experimental design, but the resolution of the temperature difference was not large enough at these heights. The highest

TABLE IV

Derivative Measurements (Corrected for Taylor's Hypothesis)

TA	Correction Term from Lumley (1965)			Corrected Variances			Ratios		
	F(u)	F(v)	F(t)	$\overline{\left(\frac{\partial u_z}{\partial z}\right)^2}$	$\overline{\left(\frac{\partial u_r}{\partial z}\right)^2}$	$\overline{\left(\frac{\partial t}{\partial z}\right)^2}$	$\overline{\left(\frac{\partial u_z}{\partial z}\right)^2}\Big/\overline{\left(\frac{\partial u_r}{\partial z}\right)^2}$	$\frac{\overline{u_z^2}}{2\overline{t^2}}\,\frac{1}{Pr}$	$\overline{\left(\frac{\partial t}{\partial z}\right)^2}\Big/\overline{\left(\frac{\partial}{\partial z}\right.}$
005	1.21	1.12	1.14	250	222	18680	1.1	0.9	
01	1.24	1.13	1.15	240	214	15735	1.1	0.8	
03	1.26	1.15	1.17	252	245	16210	1.0	0.8	
05	1.32	1.19	1.22	207	242	13610	0.9	1.1	
09	1.50	1.32	1.36	143	180	5755	0.8	1.2	
3	1.88	1.62	1.67	130	307	2160	0.4	0.9	

TABLE V

n.)	$\nu z^2 F_o^{-1}\overline{\left(\frac{du_z}{dz}\right)^2}$	$\nu z^2 F_o^{-1}\overline{\left(\frac{du_r}{dz}\right)^2}$	$\gamma g_o^2 \beta^2 z^{11/3} F_o^{-5/3}\overline{\left(\frac{dt}{dz}\right)^2}$	R_ℓ
4	1.9	2.3	39.2	830
15	2.0	1.8	35.4	610
9	2.8	2.0	36.7	465
65	4.0	1.6	27.6	325
4	4.3	1.3	18.9	275

$R_\ell = \frac{u\ell}{\nu}$ where ℓ is defined by $\varepsilon = \frac{u^3}{\ell}$

measuring position used was 2.5 meters, and the resolution of ΔT at this height was adequate only for centerline values.

5.3 Spectra

The velocity and temperature fields, $T(\underset{\sim}{x},t)$ and $\underset{\sim}{u}(\underset{\sim}{x},t)$, can be decomposed from space-time domains (x,t) to wavenumber - frequency domains (k,ω) by means of Fourier transformations. However, the complexities involved in such transformations and the amount of data needed, make them difficult to perform. Fortunately, in many turbulent flows the velocity (and temperature) field is convected past the measuring probe at a high rate. If this rate is high enough the time required for a turbulent structure to be convected past the measuring volume is much shorter than the characteristic time of the turbulence itself. Thus, the measured function, $u_m(t)$, can be viewed as a response to a spatial variation being swept past the probe, and the time domain variations of the small spatial scales can be ignored. This is the frozen-field hypothesis of Taylor (1938). It's applicability and restrictions have been examined in detail in Section 2.4. The application of the criteria presented there will be discussed further later in this section.

Although Taylor's hypothesis is only valid for the small scales of turbulence, it is extremely useful. It provides a simple and fairly accurate method of relating the measured time fluctuations to the spatial variation of the flow. With this in hand, one can begin to write simple expressions relating the three-dimensional velocity spectrum (Equation (5.25)) to the measured time domain one-dimensional velocity spectrum (Equation(5.28))

$$R_{ij}(\underset{\sim}{r}) \equiv \overline{u_i(\underset{\sim}{x},t)\,u_j(\underset{\sim}{x}+\underset{\sim}{r},t)} \tag{5.24}$$

$$F_{ij}(\underset{\sim}{k}) \equiv \frac{1}{(2\pi)^3}\iiint_{-\infty}^{\infty} R_{ij}(\underset{\sim}{r})\,EXP\left[-i\,\underset{\sim}{k}\cdot\underset{\sim}{r}\right] d\underset{\sim}{r} \tag{5.25}$$

where $$\overline{R}_{ij}(0) = \overline{u_i u_j} = \iiint_{-\infty}^{\infty} F_{ij}(\underset{\sim}{k})\,d\underset{\sim}{k} \tag{5.26}$$

Similarly, $$R(\tau) = \overline{u_1(t)\,u_1(t+\tau)} \tag{5.27}$$

$$S_u(\omega) = \frac{1}{2\pi}\int_{-\infty}^{\infty} R(\tau)\,EXP\left[-i\omega\tau\right] d\tau \tag{5.28}$$

$$R(0) = \overline{u_1^2} = \int_{-\infty}^{\infty} S_u(\omega)\,d\omega \tag{5.29}$$

By using Taylor's hypothesis, equation (5.28) can be transformed into wavenumber space and related to the one-dimensional velocity spectrum defined by:

$$F_{11}^1(k_1) = \iint_{-\infty}^{\infty} F_{11}(\underset{\sim}{k})\,dk_2\,dk_3 \tag{5.30}$$

$$\overline{u_1^2} = \int_{-\infty}^{\infty} F_{11}^1(k_1)\,dk_1 \tag{5.31}$$

$$F_{11}^1(k_1) = \overline{U}_1 \cdot S_u(\omega) \tag{5.32}$$

where $k_1 = \frac{\omega}{\overline{U}_1}$

Similar expressions exist for scalar spectra, such as the temperature field.

$$S_t(\omega) = \frac{1}{2\pi}\int_{-\infty}^{\infty} R_t(\tau)\,EXP\left[-i\omega\tau\right] d\tau \tag{5.33}$$

$$\overline{t^2} = \int_{-\infty}^{\infty} F_t^1(k_1)\,dk_1 = \int_{-\infty}^{\infty} S_t(\omega)\,d\omega \tag{5.34}$$

$$F_t^1(k_1) = \iint_{-\infty}^{\infty} F_t(\underset{\sim}{k})\,dk_2\,dk_3 \tag{5.35}$$

Spectral functions can also be defined for the derivatives of the velocity and temperature fluctuations. These are outlined for both the frequency domain and wavenumber domain in equations (5.36)through(5.37).

$$\overline{\left(\frac{\partial u_z}{\partial t}\right)^2} = \int_{-\infty}^{\infty} S_{du}(\omega)\, d\omega = \int_{-\infty}^{\infty} \omega^2 S_u(\omega) d\omega \tag{5.36}$$

$$\overline{\left(\frac{\partial u_r}{\partial t}\right)^2} = \int_{-\infty}^{\infty} F^1_{du}(k_1) dk_1 = \int_{-\infty}^{\infty} k_1^2 F^1_{11}(k_1) dk_1 \tag{5.37}$$

$$\overline{\left(\frac{\partial u_z}{\partial z}\right)^2} = \frac{1}{U_z^2} \overline{\left(\frac{\partial u_z}{\partial t}\right)^2} \tag{5.38}$$

Another form of the three-dimensional velocity spectrum often referred to is the spectrum function, E(k). E(k) is the integration of $F_{ij}(\underset{\sim}{k})$ over spherical shells of radius $|\underset{\sim}{k}|$

$$E(K) = \tfrac{1}{2} \oint\!\!\oint F_{ij}(\underset{\sim}{k})\, d\sigma \tag{5.39}$$

where $d\sigma$ is the surface element of a shell of radius $|\underset{\sim}{k}|$. The factor 1/2 is due to the normalization of E(k):

$$\tfrac{1}{2} \overline{u_i u_i} = \frac{\overline{u_z^2} + \overline{u_r^2} + \overline{u_\phi^2}}{2} = \int_0^{\infty} E(k)\, dk \tag{5.40}$$

The interdependence of all these forms is greatly simplified if the flow can be considered locally isotropic, i.e. the orientation of the small scales is independent of the large scale structure of the flow. These inter-relations reduce to:

$$E(K) = K^3 \frac{d}{dK} \left(\frac{1}{k} \frac{d}{dK_1} F^1_{11}(k_1) \right) \tag{5.41}$$

$$\frac{d}{dk_1} F^1_{22}(k_1) = -\frac{k_1}{2} \frac{d^2}{dk_1^2} F^1_{11}(k_1) \tag{5.42}$$

$$E_t(k) = -k \frac{d}{dk} F^1_t(k_1)$$

In the inertial subrange, where $F_{11}^1(k_1)$ falls off as $k_1^{-5/3}$, it is easy to show from equation (5.42) that $E(k)$ and $F_{22}^1(k_1)$ also fall off as $k_1^{-5/3}$, and that $F_{22}^1(k_1) = 4/3\ F_{11}^1(k_1)$. This is a useful relationship for verification of the local isotropy assumption.

The existence of a universal equilibrium range in the energy spectrum was first proposed by Kolmogorov (1941). In it, Kolmogorov proposed that the motion associated with the small scales is statistically determined by only the dissipation, ε, and the kinematic viscosity ν. A transformation involving only these two parameters should reduce the spectra of small scale turbulence to universally similar forms. For the temperature field, the dissipation of temperature fluctuations, ε_t, is also important. For the one-dimensional spectra of velocity and temperature, the following universal functions can be defined:

$$\Phi_{11}(k,\eta) \equiv \frac{F_{11}^1(k_1)}{(\varepsilon\nu^5)^{1/4}} \tag{5.44}$$

$$\Phi_t(k,\eta) \equiv \frac{F_t^1(k_1)}{\varepsilon_t \varepsilon^{-3/4}\nu^{5/4}} \tag{5.45}$$

Also included in this hypothesis is the idea of a spectral region within the equilibrium range where the effects of viscosity are negligible. This region, called the inertial subrange, is the well known -5/3 region. The spectral forms for the inertial subrange of the velocity and temperature fluctuations are:

$$E(k) = \alpha \varepsilon^{2/3} k^{-5/3} \tag{5.46}$$

$$E_t(k) = \beta \varepsilon_t \varepsilon^{-1/3} k^{-5/3} \tag{5.47}$$

α and β are universal constants. Although the value of α is fairly well

agreed upon, the variance in measured values for β is large.

The corresponding one-dimensional spectral forms are:

$$F_{11}^{1}(k_1) = \alpha_1 \epsilon^{2/3} k_1^{-5/3} \tag{5.48}$$

$$F_{t}^{1}(k_1) = \beta_1 \epsilon_t \epsilon^{-1/3} k_1^{-5/3} \tag{5.49}$$

A summary of the experimental values for β and β_1 from a number of investigators is presented in Table VI.

TABLE VI

Comparison of Universal Constant of Temperature Spectra

Investigation	β	β_1
Grant, Hughes, Vogel, Moilliet (1968)	.52	.31
Gurvich and Zubkovskii (1966)	.56	.34
Gibson and Schwarz (1963)	.58	.35
Paquin and Pond (1971)	.63	.38
Champagne (1977)	.68	.41
Williams and Paulson (1977)	.83	.50
Lin and Lin (1973)	1.00	.60
Gibson, Stegen, Williams (1970)	1.93	1.16
Present Investigation	0.75	0.45 - 0.55
with calc. dissipation (c.f. Sect. 5-4)	0.5-0.65	0.3 - 0.4

$$E_t(k) = \beta\varepsilon_t\varepsilon^{-1/3}k^{-5/3}; F_t^1(k_1) = \beta_1\varepsilon_t\varepsilon^{-1/3}\, k^{-5/3}$$

As stated previously, the assumption of local isotropy and the frozen field hypothesis are deeply intertwined in the entire spectral theory. The results, however, are not totally dependent upon strict adherence to these assumptions. Indeed, any high-intensity shear flow fails to meet the criteria that the use of these assumptions demand at the large scales.

By applying the criteria of Lumley (c.f. section 2.4, equations 2.33 a-d) to a measured spectrum, one can see the scope of the problem. Figure 36 is such a plot, with three of the four criteria superimposed (the 1st and 2nd criteria reduce to nearly the same result, so the less stringent of the two is not plotted). The solid lines represent equalities, and the dashed lines and crosshatched areas represent the inequalities. The first two criteria (non-uniform convection velocities) eliminate the low frequency end and much of the central portion of the spectrum. The severity of these criteria is proportional to the turbulence intensity and inversely proportional to the three-fourths power of Reynolds number. Thus, for high Reynolds number flows with small turbulence intensities, these criteria become much less severe.

The third criterion (c) is for temporal variation of the eddy, and is not a major factor in this flow (or most other turbulent flows). This also becomes less severe with increasing Reynolds number of decreasing turbulent intensity.

The last criterion (d) is for isotropy of the small scales. As can be seen, the data fails to satisfy this inequality at any wavenumber. However, this is a dynamical relation and it is not certain how strong this inequality relation should be enforced (Lumley (1965a)). Unfortunately, in this flow most of the dissipation range is significantly below the inequality. This is in agreement with the derivative data presented in the last section where the data showed large deviations from isotropy.

Figure 36

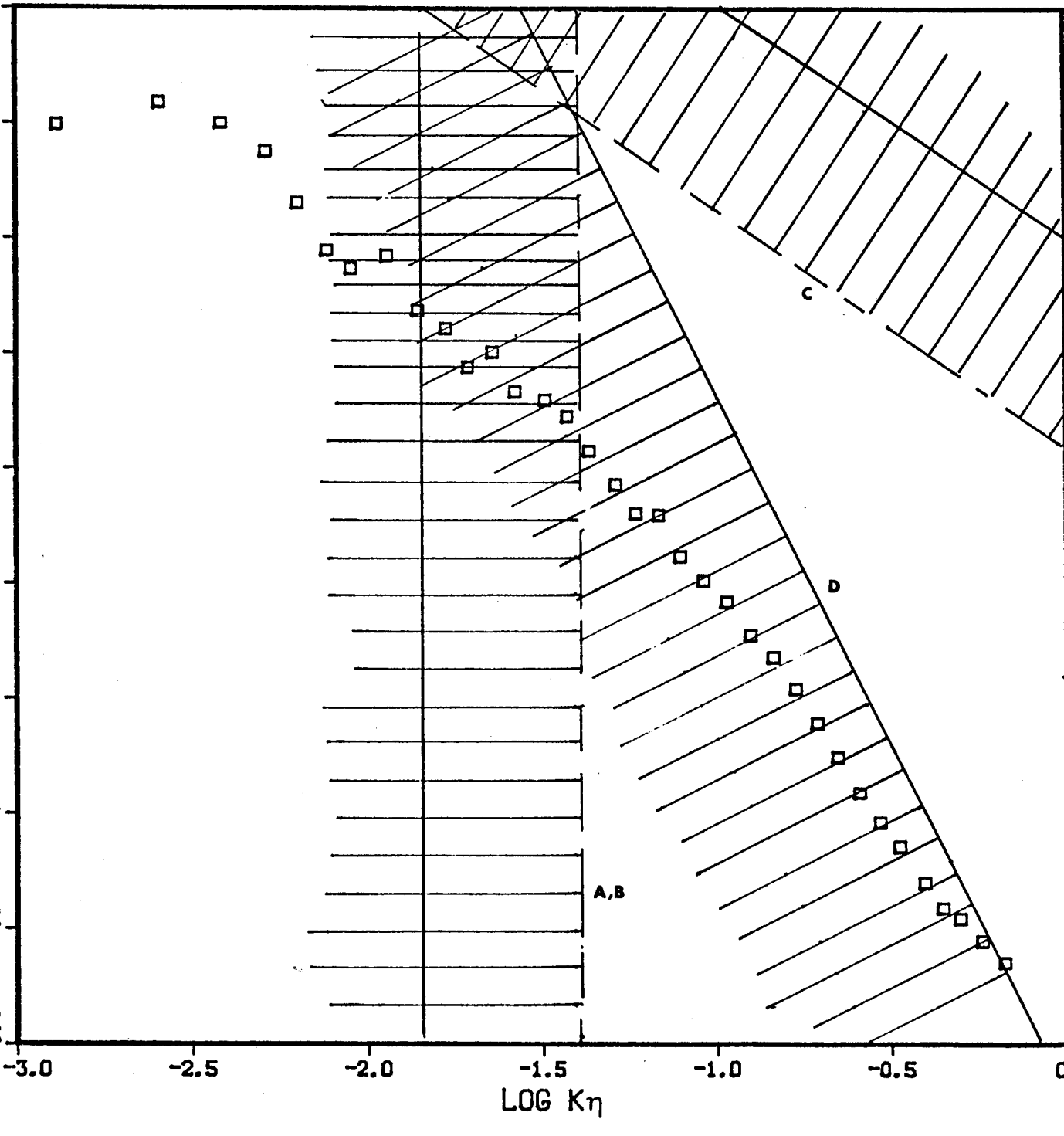

Another potential error in the spectral measurements is due to the drop-out discussed in Section 4.2. With sections of data points missing, the usual method of Fourier transforming the data must be modified. For data sets with just a few drop-out points the missing data can be set equal to the mean. However, this will bias the level of the spectrum to a lower value (since the overall mean-square is lower with the zero-points included). A more correct way to calculate the spectrum is to evaluate time-lag products and then Fourier transform the resulting covariance function. This method is much more time consuming to use, but it is necessary. As the drop-out rate increases, not only is the spectral level affected, but also the shape. Attempts to predict the filtering effect of drop-out on the straight FFT were unsuccessful. (Note: Since the drop-out did not affect the temperature signals, the temperature spectra were evaluated by using a fast Fourier transform routine to transform the data directly.)

The spectral results are presented in Figures 37 through 46. Figure 37 shows the vertical velocity spectrum at several positions normalized as in Equation (5.44). The curves are theoretical models; the upper one is corrected by Lumley's correction scheme for fluctuating convection velocities. The curve is an integrated form of the von-Karman spectrum coupled with a Pao-Saffman type spectrum at the small scales.

$$E(k) = \alpha \epsilon^{2/3} \left[\frac{k_o^{-17/3} k^4}{\left[1+\left(\frac{k}{k_o}\right)^2\right]^{17/3}} + \frac{2.25}{k\eta} \right] \exp\left[-1.5\alpha \left(k\eta^{4/3} + k\eta^2\right)\right] \qquad (5.50)$$

k_o is chosen so that E(k) integrates to 3/2 $\overline{u^2}$. By integrating this and utilizing the isotropic relations in Equations (5.41), the theoretical curves for the 1-D spectra can be obtained.

Due to the limited inertial subrange in this flow, it is difficult to

Figure 37

VERTICAL VELOCITY SPECTRA

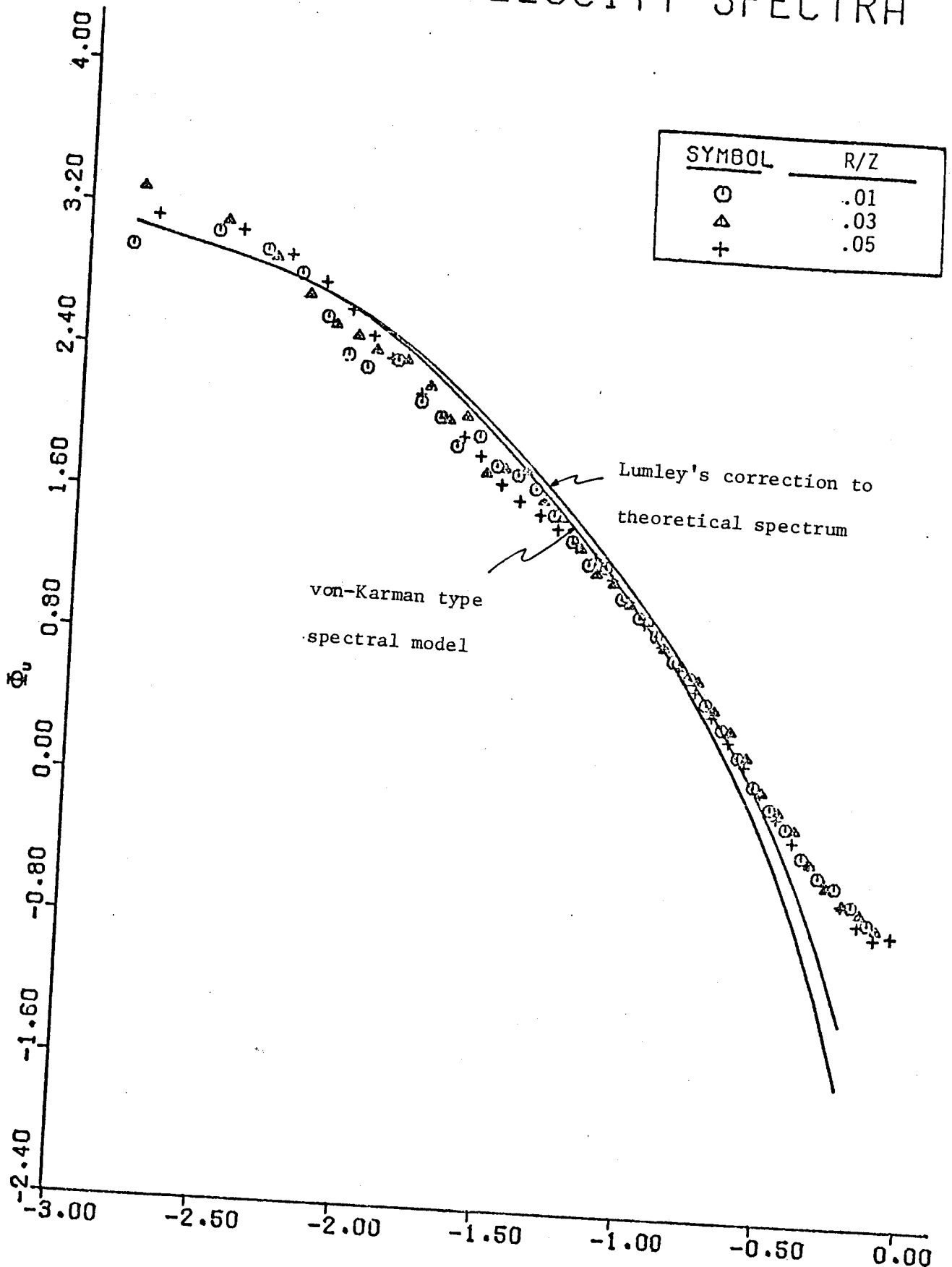

Figure 38

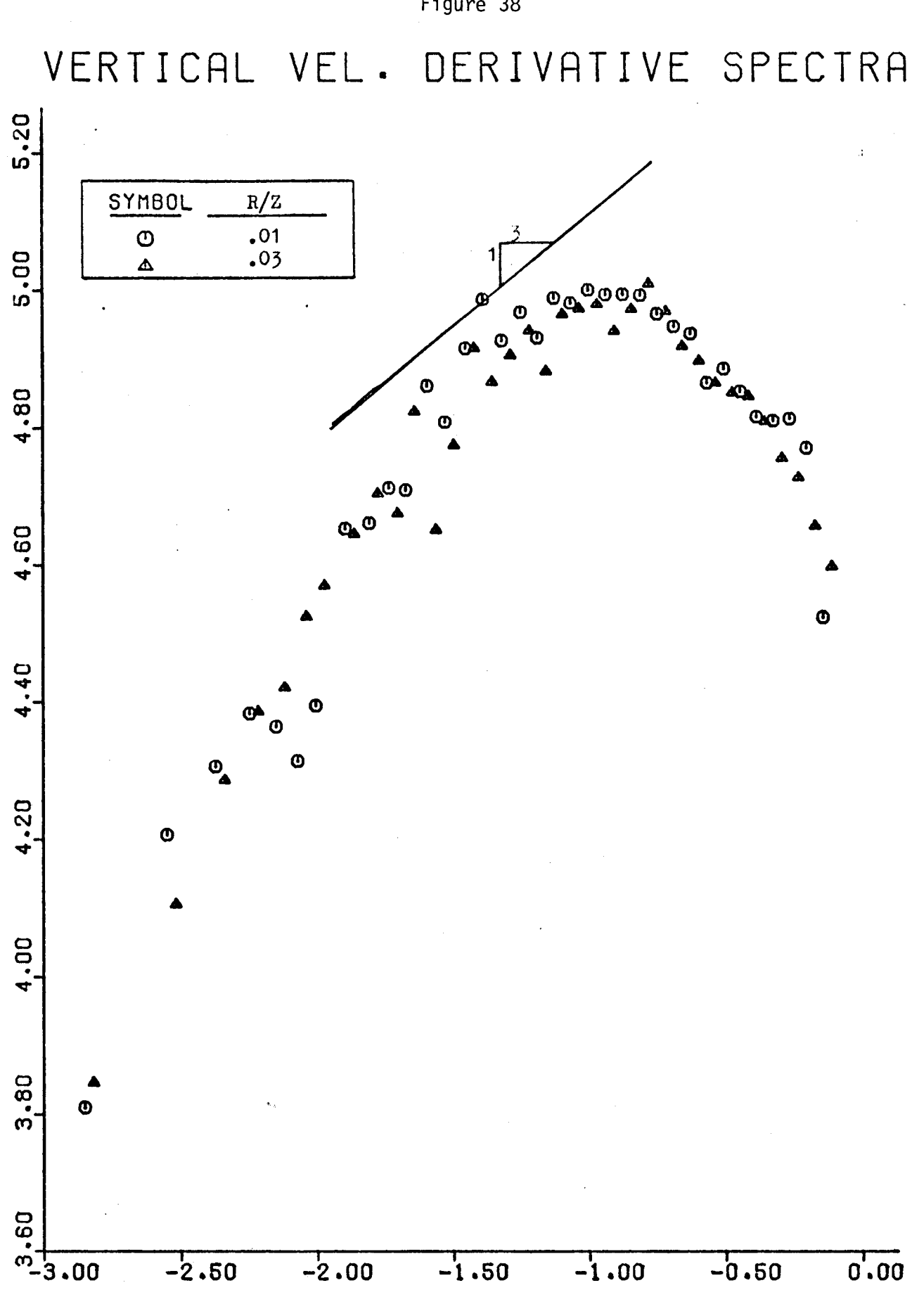
VERTICAL VEL. DERIVATIVE SPECTRA
SYMBOL
R/Z
.01
.03
3
1
5.20
5.00
4.80
4.60
4.40
4.20
4.00
3.80
3.60
-3.00
-2.50
-2.00
-1.50
-1.00
-0.50
0.00

Figure 39 - Comparison of Vertical Velocity and Vertical Velocity Derivative Spectra

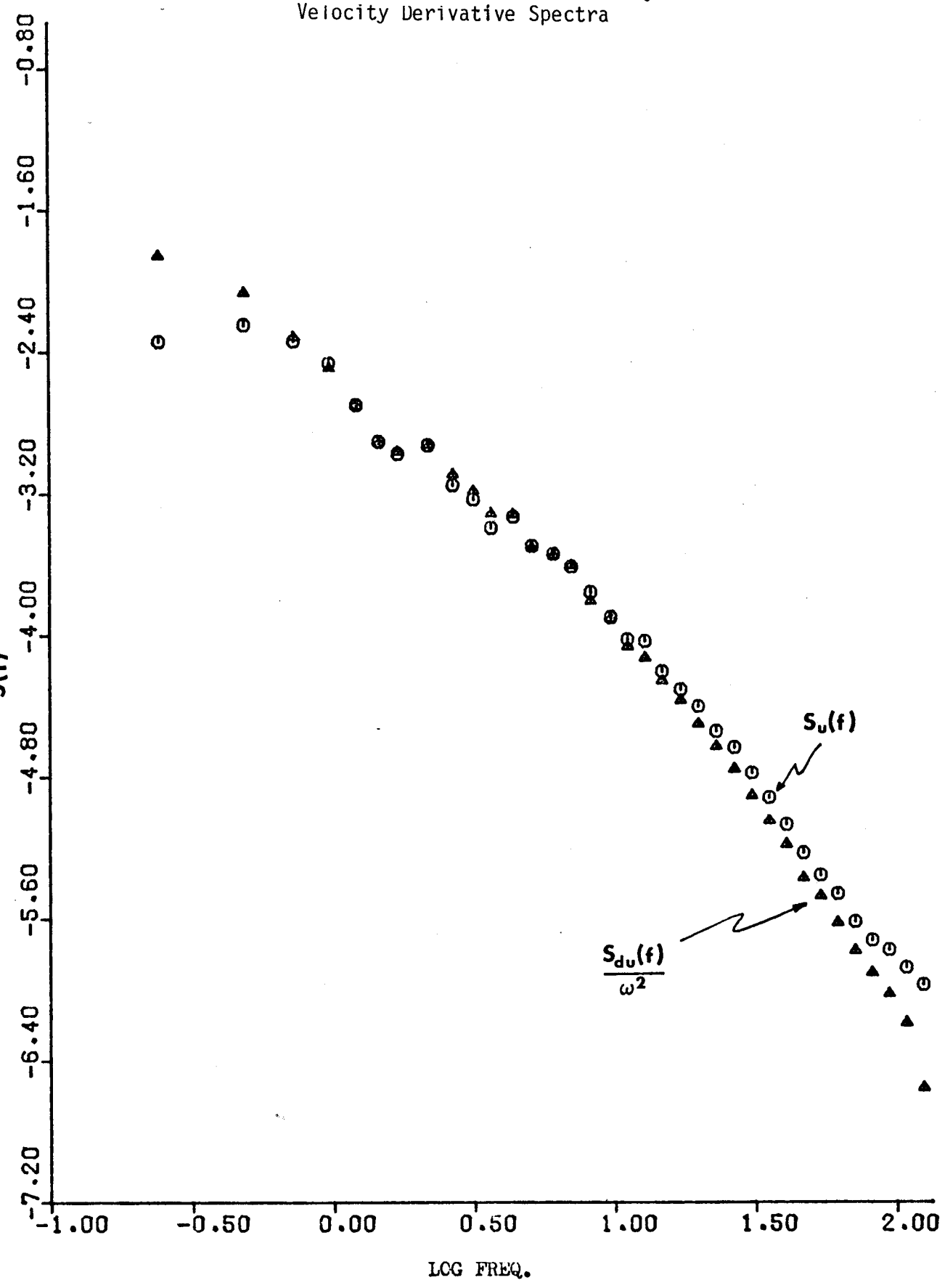

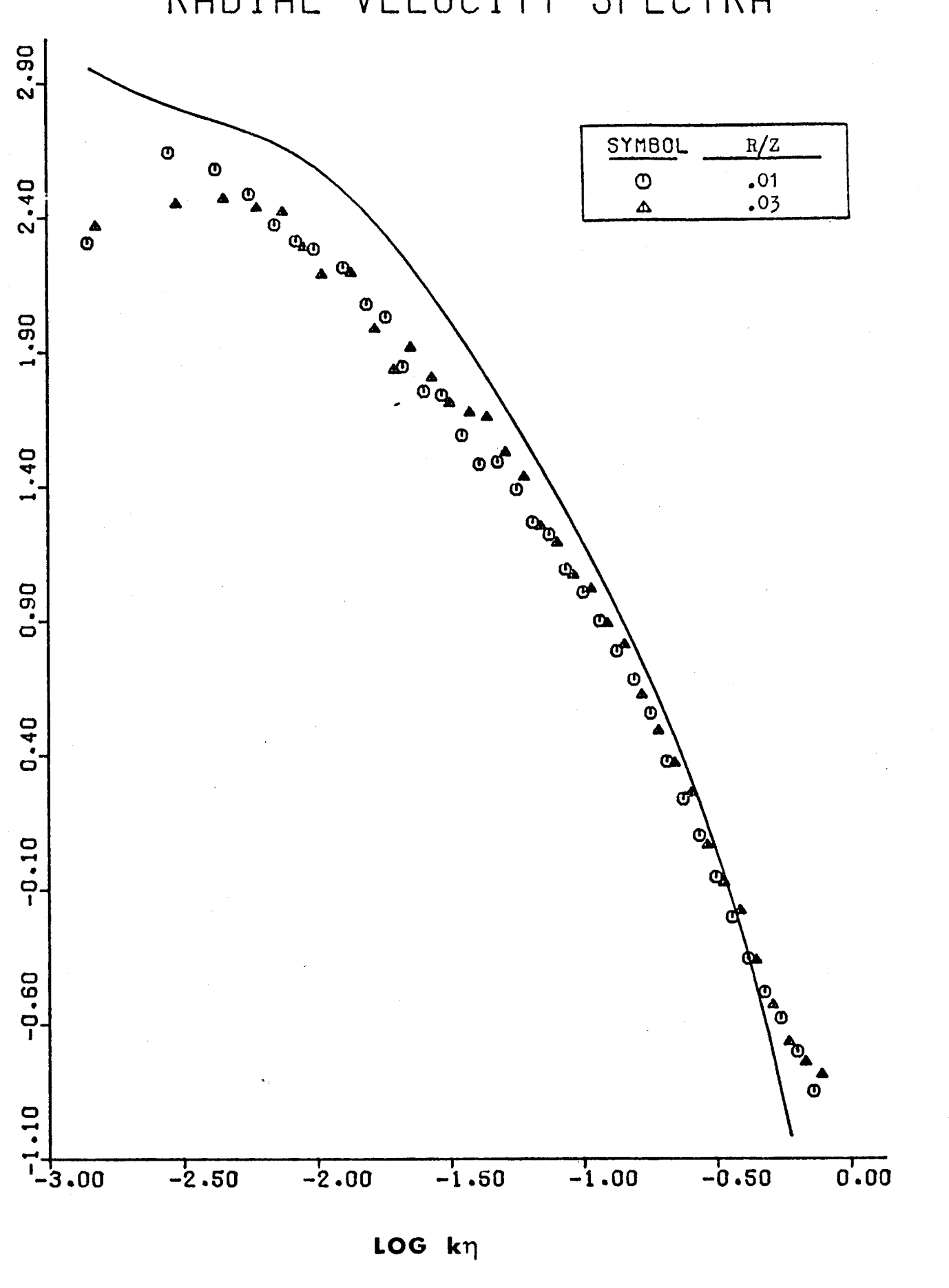
RADIAL VELOCITY SPECTRA
SYMBOL
R/Z
.01
.03
2.90
2.40
1.90
1.40
0.90
0.40
-0.10
-0.60
-1.10
-3.00
-2.50
-2.00
-1.50
-1.00
-0.50
0.00
LOG kη

Figure 41

COMPARISON OF U & V SPECTRA

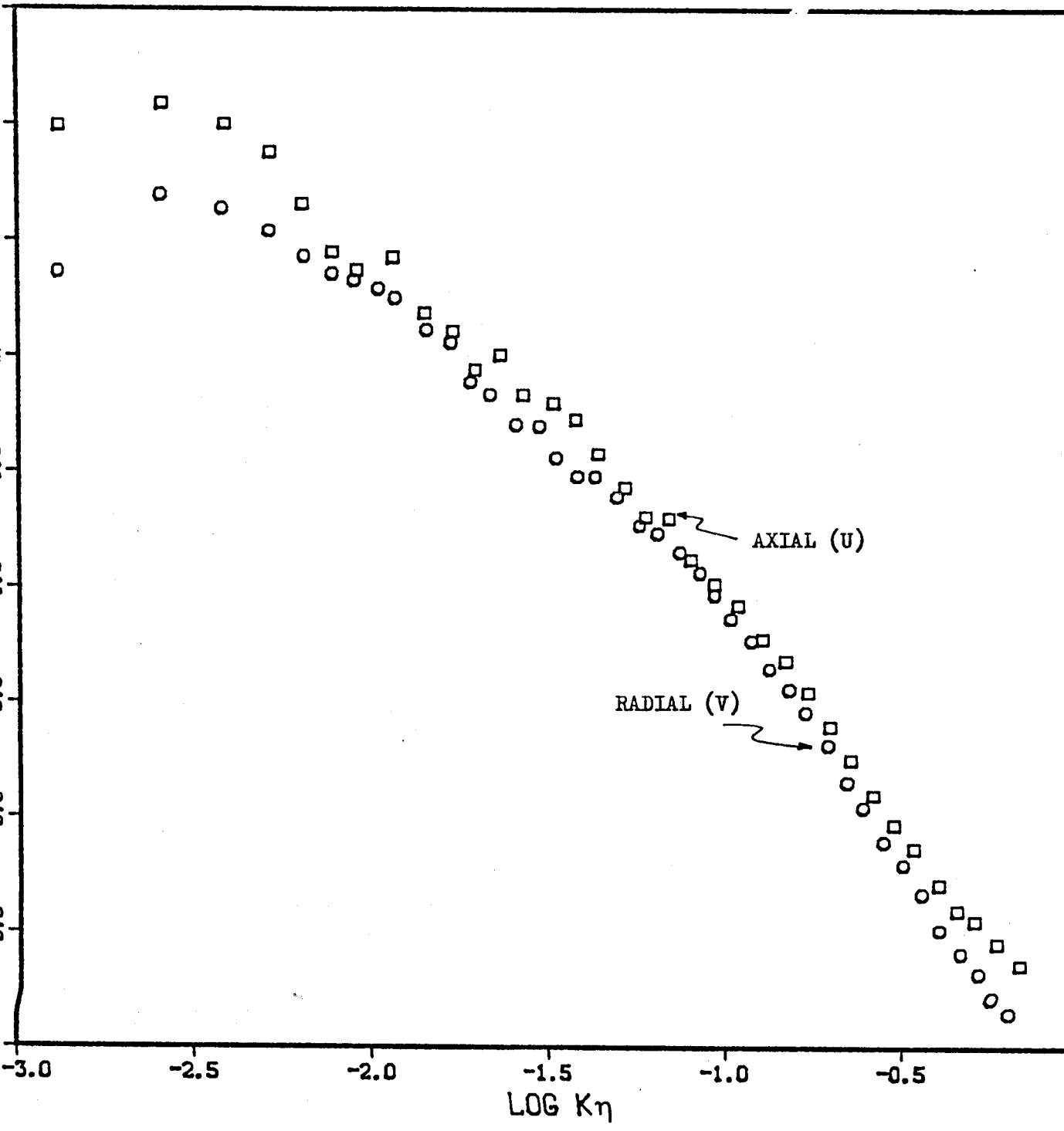

Figure 42 - Comparison of Radial Velocity and Radial Velocity Derivative Spectra.

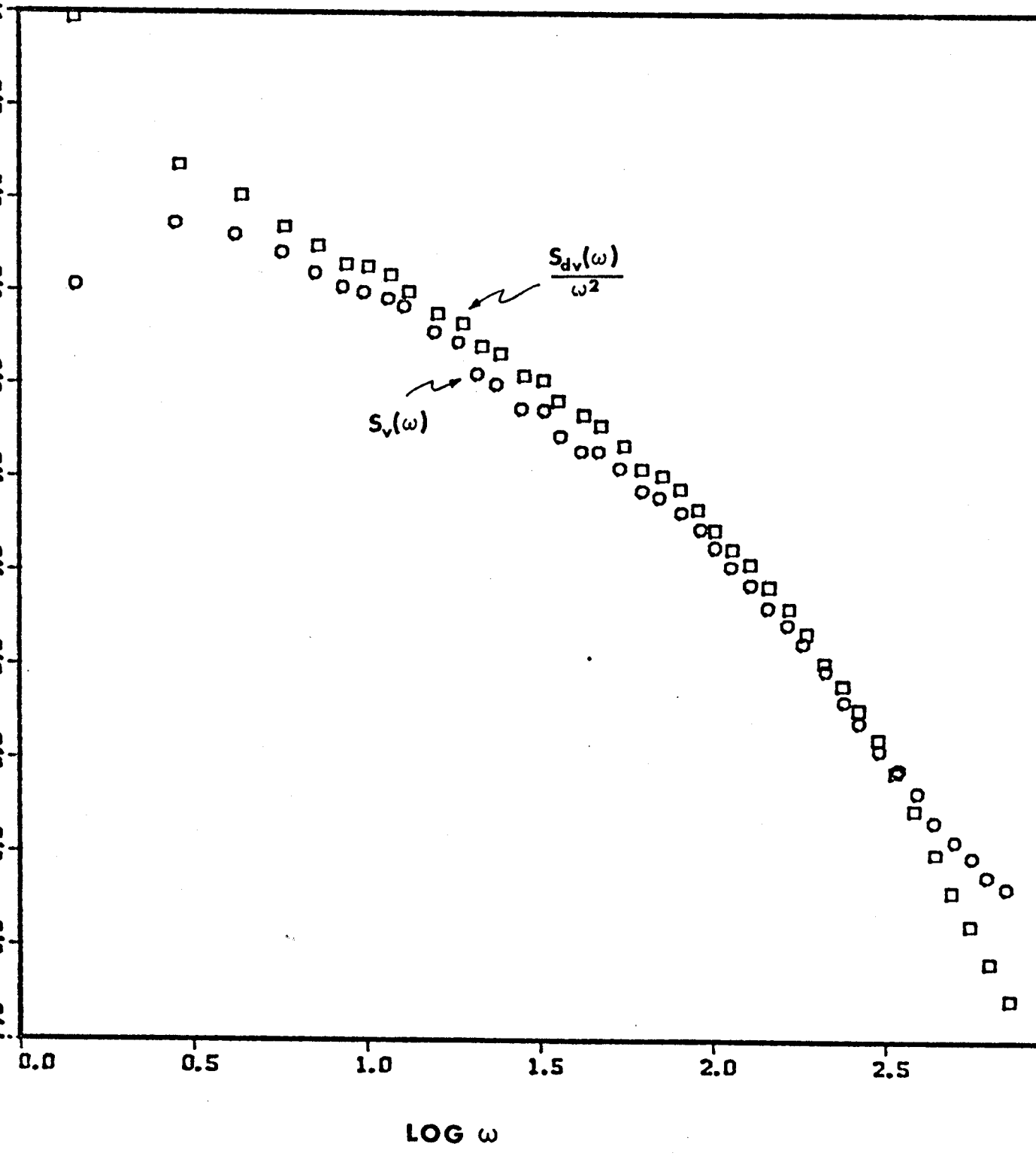

compare the measurements and theory (the theory assumes the data to be valid everywhere, and not just in the high wavenumber region as pointed out above.) The differences between the corrected and uncorrected theory are not that great because of the normalization of Φ_{11}. At $k\eta = 0.1$, the difference is roughly 20%. However, at $k\eta = 0.25$, the error is near 100%. This is very important for the dissipation, since it peaks in this region.

The measured spectrum is consistently too low throughout the inertial subrange. This is due to an overestimate of the dissipation because of the non-isotropy of the small scale motion. In addition, the theory is only valid where the flow can be considered isotropic. Since this flow is non-isotropic at almost all scales, no definite conclusions can be drawn from this comparison. The large deviation at the very high wavenumbers is due to noise (both electronic and quanitization noise).

The spectrum of the spatial derivative of u_z is shown in Figure 38. The peak occurs around $k\eta = 0.2$. To verify that the derivative signal was calculated properly, the frequency spectrum is divided by ω^2 and compared to the u_z spectrum. The agreement is nearly perfect, as is shown in Figure 39. The only deviation is at the high frequency end, where the u_z spectrum contains more noise.

The u_r spectra, along with a corrected theoretical spectrum, are shown in Figure 40. The measured u_r spectra are considerably lower than expected. When compared with a u_z spectrum, as in Figure 41, it can be seen that the isotropic relation $F_{22}^1(k_1) = 4/3\ F_{11}^1(k_1)$ is not valid anywhere. Instead of being larger, the u_r spectrum is smaller than the u_z spectrum. Again, this is due to the anisotropy of the flow. When the derivative spectrum is compared to the velocity spectrum, a difference is noticed (Figure 42). Either $\overline{u_r^2}$ is too small or $\overline{\left(\frac{du_r}{dt}\right)^2}$ is too large. The reason for this discrepency is not known, but the difference is not large enough to explain the differences between the u_z and u_r spectra described above.

Finally, the temperature spectra are plotted in a similar fashion. No theoretical curve is plotted due to the unknown value of the spectral constant β_1. The temperature spectra are plotted in Figure 43. Figure 44 shows a linear plot of $F_t^2(k_1) k_1^{5/3} / \epsilon_t \epsilon^{-1/3}$ vs $\log k_1$. This shows the limited extent of the inertial subrange in this flow, and also provides a value of 0.5 for β_1. (Note: As mentioned, the dissipation is probably over-estimated by as much as 100% due to the anisotropy. If this were taken into account the actual value of β_1 might be closer to 0.4.)

The temperature derivative spectra and the comparison of the derivative spectrum to the temperature fluctuation spectrum are shown in Figures 45 and 46. The agreement in Figure 46 between the two spectra is nearly perfect. This is because the temperature signal is not subject to the problems of cross-flow and drop-out like the velocity signals.

It was hoped that cross-spectra could also be measured, but the problems with drop-out caused this plan to fail. The calculation of the cross-spectra by calculating the cross-correlation matrix involved too much time and memory for our small computer to handle. This was unfortunate.

The small inertial subrange in this flow made it impossible to compare this data to spectral theories in any detail. This is particularly true of the velocity spectrum. Many theories exist relating the effects of buoyancy on the velocity spectrum, but the theoretical curves presented earlier did not include any of these effects; they treated the temperature as a passive scalar contaminant. Lumley (1956b) outlines two spectral theories taking buoyancy into account. These theories, by Bolgiano and Shur, suggest spectral regions at the lower end of the inertial subrange in which the dissipation of temperature fluctuations is a parameter. Shur's model also takes into account the potential temperature gradient. However, it is not likely that either of these two models would be applicable to the

Figure 43 - Temperature Spectra

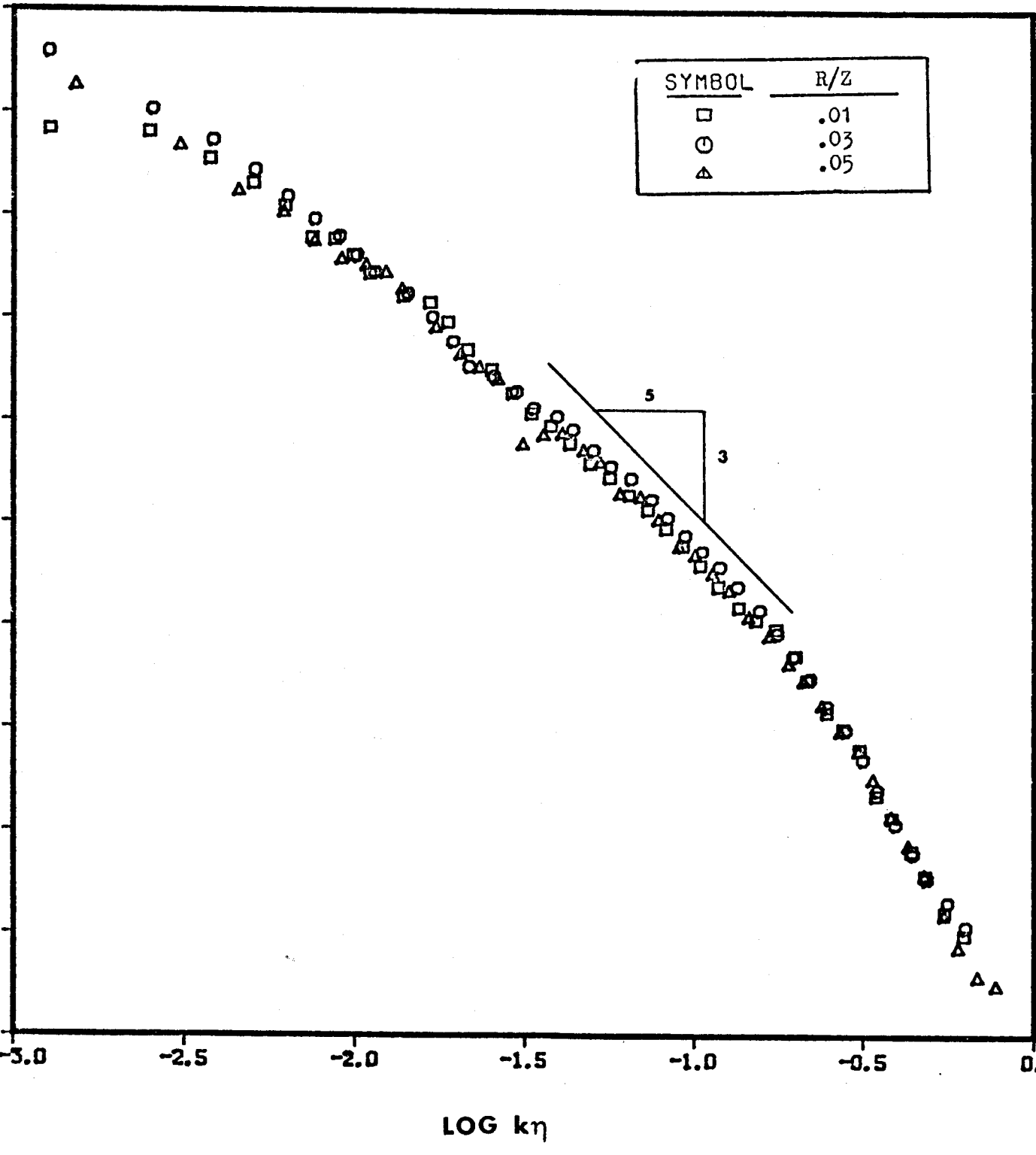

Figure 11 Temperature Spectrum R K

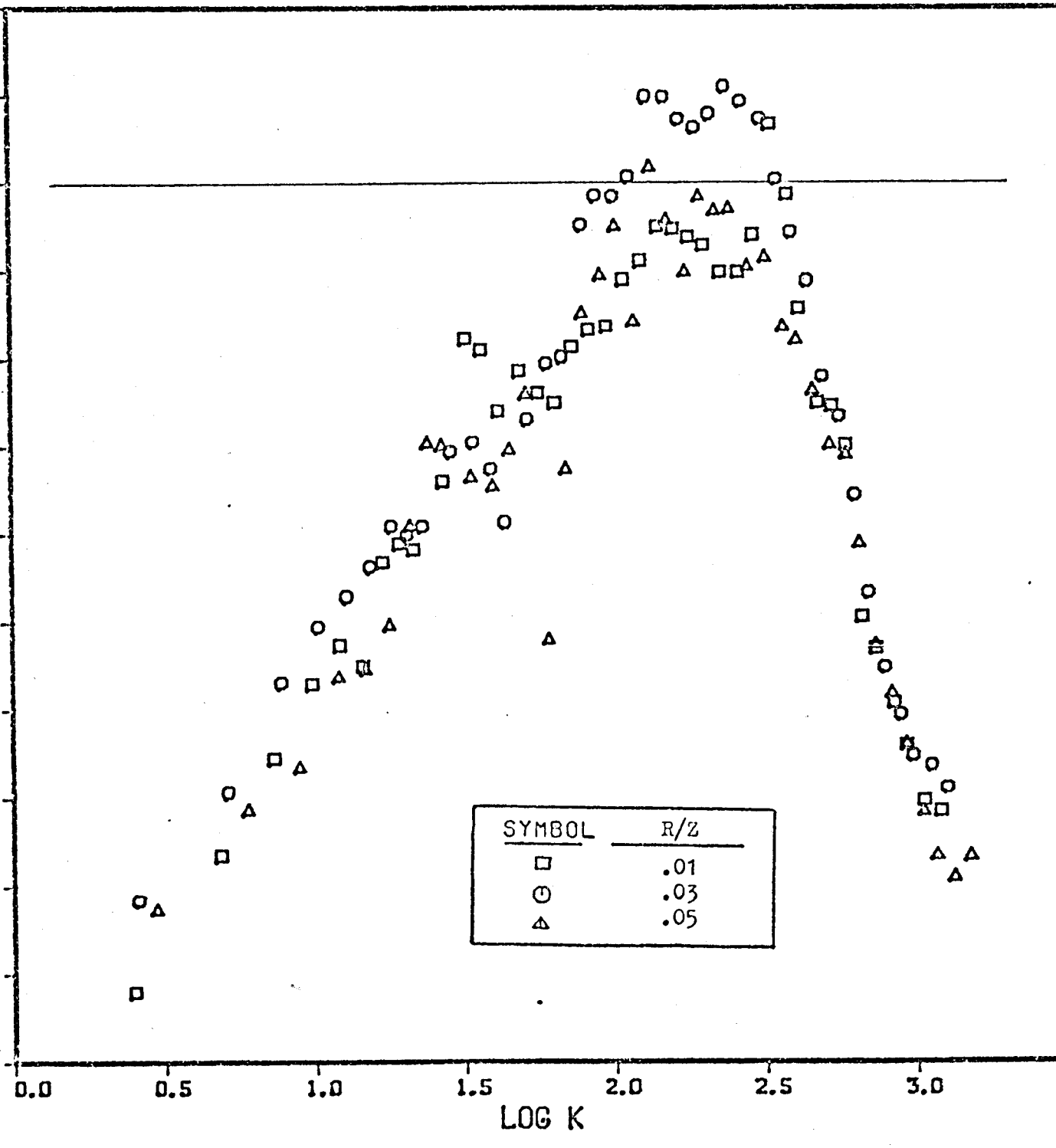

Figure 45

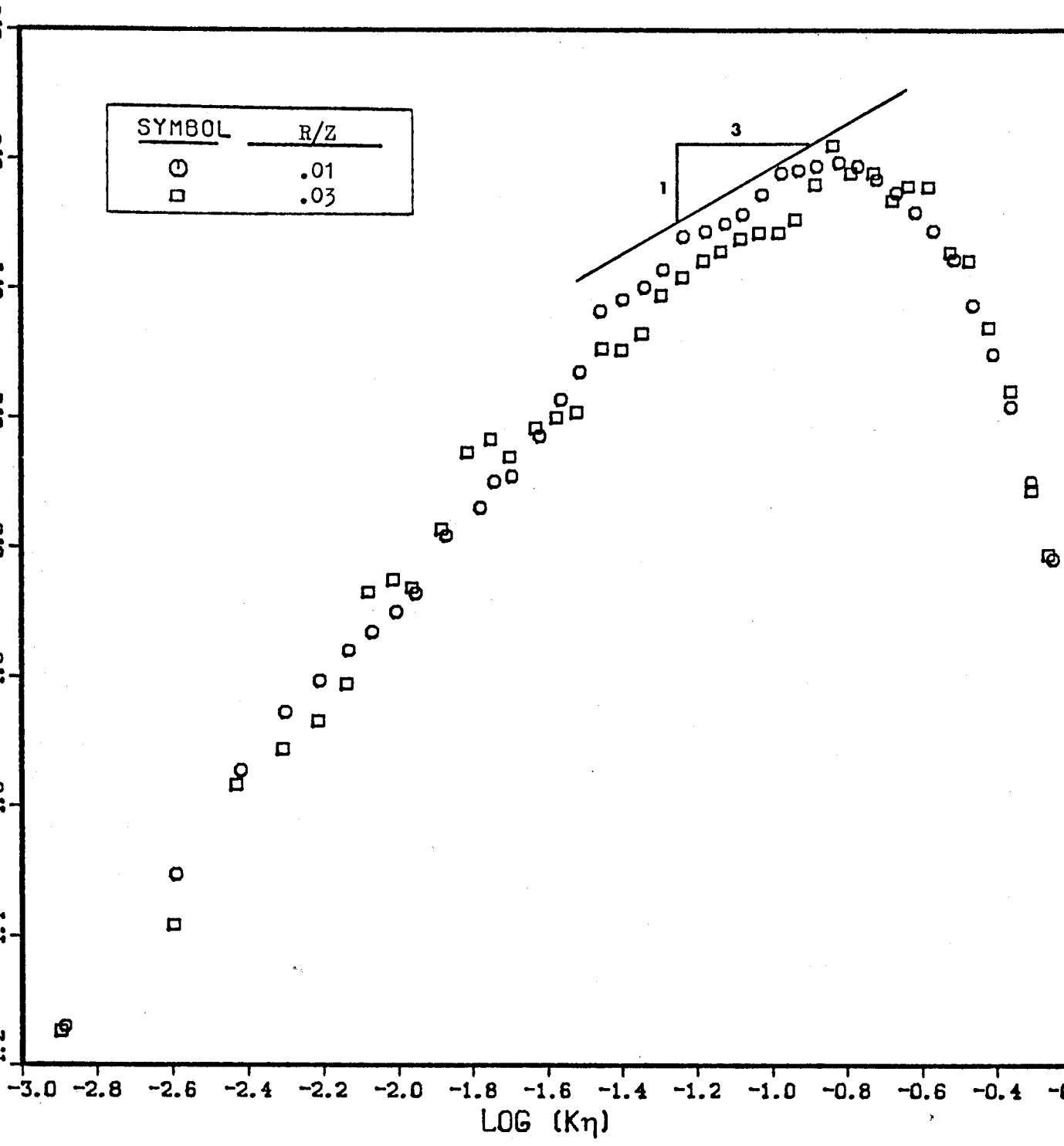
TEMPERATURE DERIVATIVE SPECTRA
SYMBOL
R/Z
.01
.03
3
1
-3.0 -2.8 -2.6 -2.4 -2.2 -2.0 -1.8 -1.6 -1.4 -1.2 -1.0 -0.8 -0.6 -0.4
LOG (Kη)

Figure 46 - Comparison of Temperature and Temperature Derivative Spectra

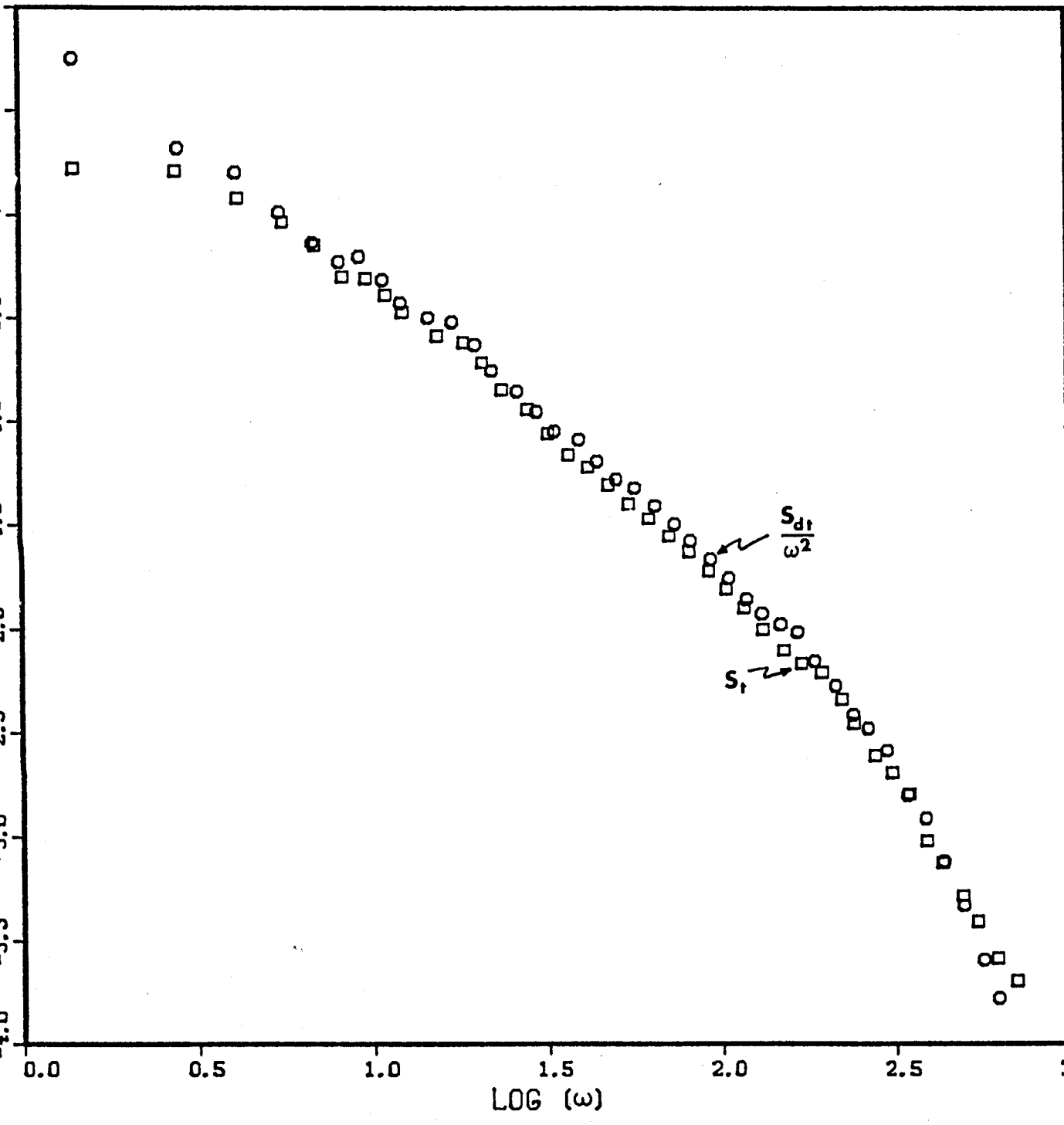

laboratory model presented in this paper because of the strong shear production term that is always present. Since the shear is always dominate the -5/3 law should still hold, and at most, the coefficient might change slightly due to buoyancy effects. To measure this change, the inertial subrange would have to be considerably larger than it is.

5.4 Turbulent energy and fluctuating temperature balance

As discussed in Section 2.3, the balance of turbulent kinetic energy plays an important role in many turbulence models. The equation governing the turbulent kinetic energy is obtained by multiplying the Navier-Stokes Equations by the velocity, u_j, taking the time average of all terms, and subtracting the equation for the mean kinetic energy. Similarly, an equation can be obtained for the mean square temperature fluctuations. These derivations are outlined in Appendix AI, and the results are shown in Equations (5.51) and (5.52).

$$\underbrace{\frac{D}{Dt}\left(\overline{t^2}/2\right)}_{\substack{\text{rate of change of} \\ t^2/2}} = \underbrace{-\tfrac{1}{2}\left(\frac{\partial}{\partial z}\overline{u_z t^2} + \frac{1}{r}\frac{\partial}{\partial r} r\overline{u_r t^2}\right)}_{\text{turbulent transport}} \underbrace{-\left(\overline{u_z t}\frac{\partial T}{\partial z} + \overline{u_r t}\frac{\partial T}{\partial r}\right)}_{\substack{\text{gradient} \\ \text{production}}} \underbrace{-\epsilon_t}_{\text{dissipation}} \qquad (5.52)$$

$$\underbrace{\frac{D}{Dt}\left(q^2\right)}_{\substack{\text{rate of change of} \\ \text{k.e.}}} = \underbrace{\frac{\partial}{\partial z}\left(\frac{\overline{u_z p}}{\rho} + \overline{q^2 u_z}\right) + \frac{1}{r}\frac{\partial}{\partial r}\left[r\left(\frac{\overline{u_r p}}{\rho} + \overline{q^2 u_r}\right)\right]}_{\text{pressure gradient work and turbulent transport}}$$

$$\underbrace{-\left[\overline{u_z^2}\frac{\partial \bar{v}_z}{\partial z} + \overline{u_z u_r}\frac{\partial \bar{v}_z}{\partial r} + \overline{u_z u_r}\frac{\partial \bar{v}_r}{\partial z} + \overline{u_r^2}\frac{\partial \bar{v}_r}{\partial r}\right]}_{\substack{\text{deformation work} \\ \text{(gradient production)}}} \underbrace{+ g_o \beta \overline{u_z t}}_{\substack{\text{buoyancy} \\ \text{production}}} \underbrace{- \epsilon}_{\text{dissipation}} \qquad (5.51)$$

$$q^2 = \tfrac{1}{2}\left(\overline{u_z^2} + \overline{u_r^2} + \overline{u_\phi^2}\right) \qquad (5.53)$$

The rate of change of q^2 is due pressure gradient work, transport by turbulent velocity fluctuations, deformation work, work due to buoyancy, and viscous dissipation. The transport terms are divergences of turbulent energy flux, which must be zero for a closed rigid volume. Thus these terms merely redistribute energy from one point in the flow to another.

The pressure terms play an important role in redistributing the energy between the various velocity components. If one writes an equation governing the kinetic energy of each component, it can be shown that the pressure terms transfer energy from the streamwise component to the radial and azimuthal components. As described above, the overall effect of this term must integrate to zero.

The deformation work terms exchange kinetic energy between the mean flow and the turbulence. The same terms occur in the equation for the mean kinetic energy but with the opposite sign. In the plume, as in most flows, this means a loss to the mean flow and a gain to the turbulence. Thus this term is a production term.

The work done by buoyancy is also a production term, since u_z and t are well correlated everywhere in the plume. Although it accounts for a significant portion of the total production of turbulent kinetic energy, it is still smaller than the deformation work term nearly everywhere in the plume.

The viscous dissipation term is the rate at which viscous stresses perform deformation work, and is always an energy drain. This term is also the most difficult to measure due to the number of components of spatial gradients. As discussed in Section 5.2, it is customary to assume isotropic relations between these components and thus measure only a few. This relationship is given by:

$$\epsilon = 15\nu\overline{\left(\frac{du_z}{dz}\right)^2} \qquad (5.54)$$

However, as shown in Section 5.2, the turbulence in this flow does not obey these isotropic relations. Since all nine components were not measured, it is not possible to directly compute the value of the dissipation. It can be shown (from the measured ratio of $\frac{du_z}{dz}$ to $\frac{du_r}{dz}$ that the dissipation as calculated from equation(5.54)will overestimate the actual value.

The equation for the temperature fluctuations (Equation 5.52) can be described in a similar manner. The rate of change of $t^2/2$ is due to transport by turbulent velocity fluctuations, gradient production, and molecular dissipation. Again, as in the kinetic energy balance, the molecular diffusion term is usually computed with the isotropic relations using the measured value of $(\overline{\frac{dt}{dz}})^2$:

$$\epsilon_t = 3\gamma \overline{\left(\frac{dt}{dz}\right)^2} \qquad (5.55)$$

Since only one component of $\overline{\frac{dt}{dx_i}\frac{dt}{dx_j}}$ was measured, no estimate of the degree of anisotropy can be ascertained. However, unlike the kinetic energy balance all other terms in the temperature fluctuation balance have been measured. Thus the error in this balance gives an indication of the anisotropy. By this method the temperature derivatives show less anisotropy than the energy dissipation, but the isotropic relation still overestimates the dissipation term. This will be illustrated shortly.

For a neutral environment, the terms of the energy balance should obey similarity, but as shown in Section 5.2 , the ambient stratification causes the derivatives to deviate from this scaling considerably. Nevertheless, for convenience the kinetic energy balance is normalized with $F_o^{-1} z^{+2}$ and the temperature fluctuation balance with $\left(\frac{1}{g_o \beta}\right)^2 F_o^{-5/3} z^{14/3}$ where F_o is the local heat flux. Since the balances are not similar, the profiles will be calculated at the highest position. This corresponds to $z \approx 2.1$ m, or $z/D = 3$

The ambient temperature gradient at this height is roughly 1°C/meter. Because the actual values of dissipation cannot be measured the energy balances are computed using the measured data to calculate the convection, turbulent diffusion, and production terms (c.f. Section 5.1). The remainder of the balance will be defined to be the dissipation. Although the kinetic energy balance also has an unknown pressure transport term included in this remainder, it is believed to be small compared to the dissipation term over much of the flow. However, this hypothesis can not be substantiated. It was originally hoped that the directly measureable terms (all but pressure) could be measured accurately enough to estimate the magnitude of the pressure transport from the energy balance, but this is impossible due to the low Reynolds number of the flow and the resulting anisotropy at small scales.

The kinetic energy and temperature fluctuation balances are shown in Figures 47 and 48 respectively. In both balances, the turbulent diffusion terms integrate to zero as they should, and at the outer region of the plume, production is balanced by dissipation and the turbulent diffusion by mean convection. As can be seen from Table VII, the actual dissipation of turbulent kinetic energy is much less than that predicted by equation 5.54 However, the differences in the measured and calculated temperature derivatives are less severe than that of the velocity derivatives. The pressure transport terms might account for some of the discrepancy in the kinetic energy dissipation but it is not believed to be a significant portion. It is disturbing that these measured and calculated values differ so greatly, especially at the centerline. At larger values of r/z it is expected that the higher moments are in serious error due to the drop-out, but their accuracy at the centerline should be to within 10-15%. T hus, the only explanation for the large values of dissipation is the anisotropy of the flow.

Figure 47

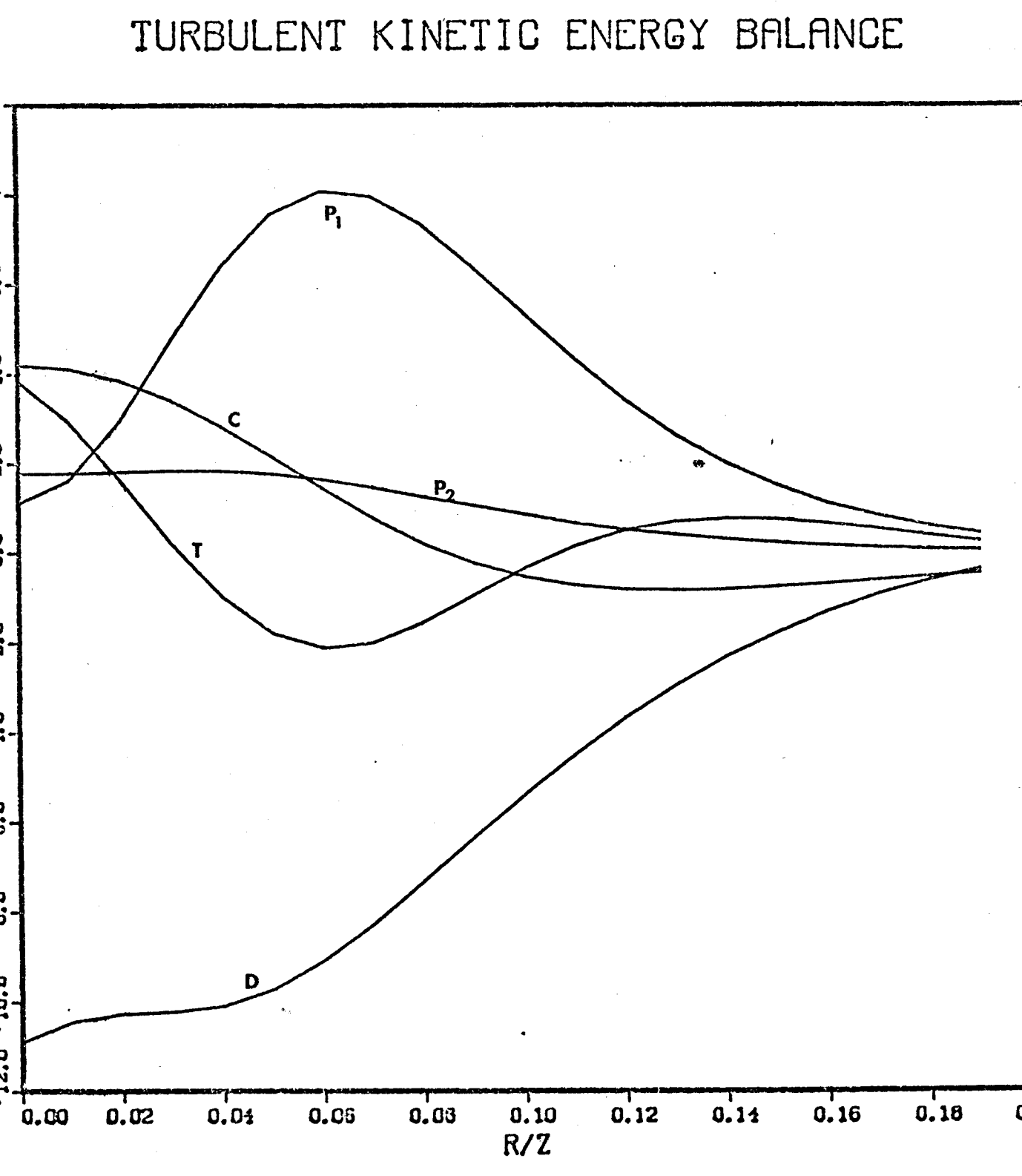
TURBULENT KINETIC ENERGY BALANCE
P1
C
P2
T
D
0.00
0.02
0.04
0.06
0.08
0.10
0.12
0.14
0.16
0.18
R/Z

Figure 48

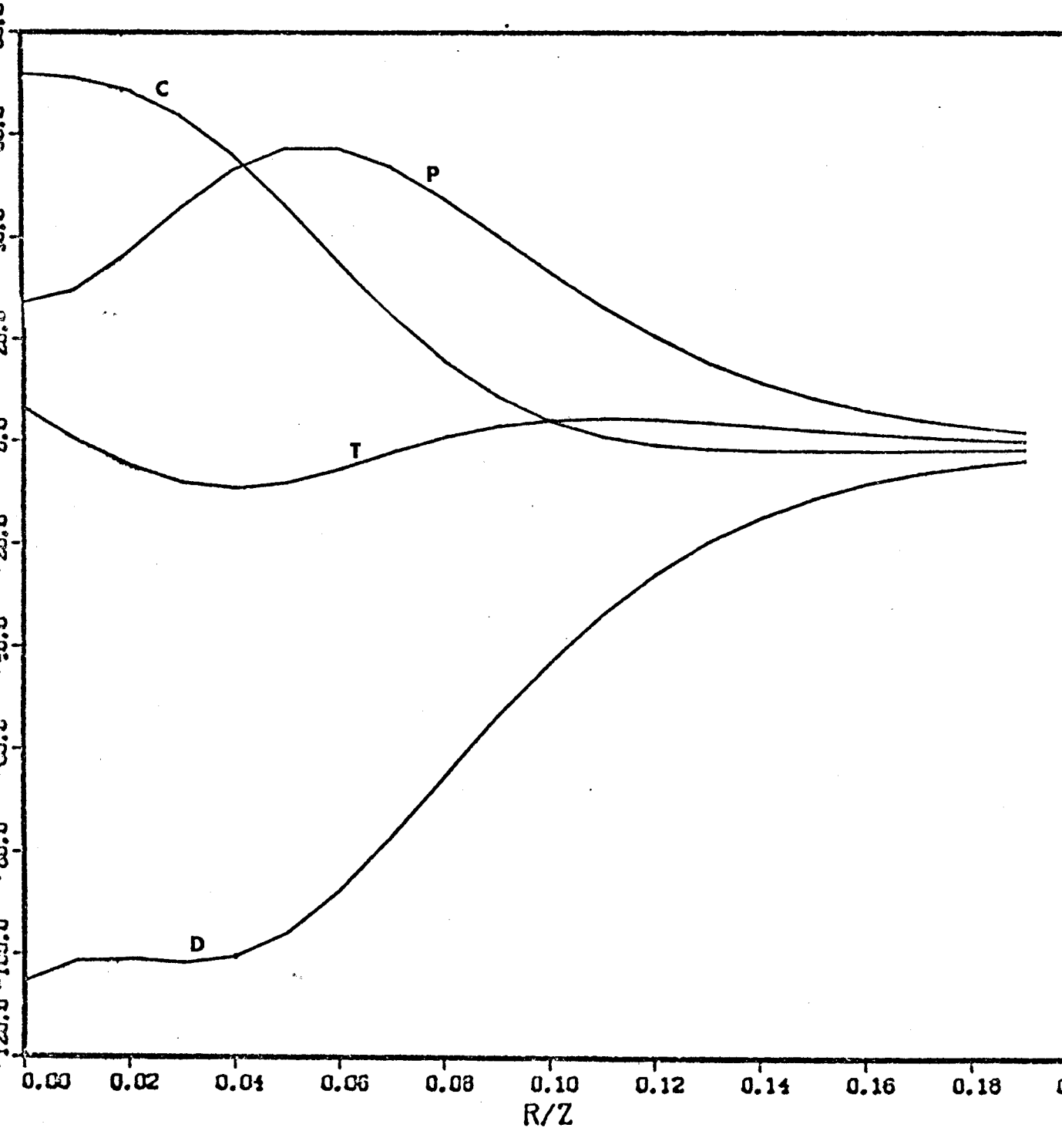
TEMPERATURE FLUCTUATION BALANCE
C
P
T
D
0.00
0.02
0.04
0.06
0.08
0.10
0.12
0.14
0.16
0.18
R/Z

TABLE VII

Comparison of Calculated and Measured Dissipation

Energy Dissipation			Temperature Dissipation	
Measured	Calculated*	r/z	Measured	Calculated
32	10.5	-.005	126	101
30	10	.01	106	100
32	10	.03	109	100
26	9.5	.05	92	94
18	6	.09	39	51
16	3	.13	14.5	18

* Calculated dissipation term also includes the pressure transport term.

It can be seen that earlier spectral scaling using the measured value of dissipation is in error. This is primarily of interest in regard to the spectral measurements. The one-dimensional velocity spectrum is more than 50% too low because of this scaling. By returning to Figure 37, it can be seen that in the inertial subrange the normalized spectrum is roughly 30% too low, which is partly accounted for by the high value of the measured dissipation. Similarly, the normalized temperature spectrum will be roughly 44% too high. This affects the value of β_1 discussed in Section 5.2. The corrected values of β and β_1 based on the computed dissipation are listed in Table III beneath the ones based on the measured dissipation. Although now slightly smaller (β_1 = 0.3 - 0.4), this value is still within the bounds of previous data.

The previous values for the length scale ℓ, and thus the turbulent Reynolds number, R_ℓ are also incorrect, both being too small by a factor of 2.5-3. This explains why our original estimates for these parameters were so different from the measured values. From the computed dissipation, R_ℓ is approximately 1500 at a height of two meters (the height for which

the spectra are presented) while ℓ is approximately 0.15 m. This gives a ratio for ℓ/z of about 0.075. Since the plume spreads faster than a jet, this value is consistent with the value of ℓ/z for a jet of 0.05.

Chapter 6 - Summary and Conclusions

The goal of this investigation was to provide a reliable set of measurements of the mean and fluctuating components of velocity and temperature in an axisymmetric turbulent plume. Also to be measured were the values of the dissipations of turbulent kinetic energy and mean square temperature fluctuation. However, during the course of the project, problems arose. Due to their wide reaching consequences, the discovery of these problems should probably be considered more significant than the measurements themselves. These problems and the results of this investigation are summarized below.

The main unexpected problem encountered in this investigation was the hot-wire's weak sensitivity to angular variations at low flow velocities. This, coupled with the high intensity of the velocity fluctuations, created a problem of drop-out of the velocity signal far in excess of what was expected. (Drop-out occurs when the measured velocities from each wire do not correspond to valid velocities because the instantaneous velocity vector moves outside the cone of acceptance of the probe.) At the outer edges of the plume this drop-out exceeded 50%. Although most of these dropped-out points were probably of low (near zero) velocity, many were strong fluctuations at large angles to the probe axis. This was verified indirectly with earlier temperature measurements using a high overheat for the velocity sensors and a side-by-side arrangement for the temperature wire sensor.* The resulting profiles of the mean temperature displayed considerable contamination from the hot wakes of the velocity sensors, and the measured mean temperature increased from the centerline to $r/z = 0.2$ instead of decreasing. This can only be explained by the presence of strong

* The probe shown in Figure 4 which was used in the measurements reported earlier has the temperature sensor slightly upstream of the velocity sensor.

cross-stream velocity fluctuations; in fact, it is quite probable that the probe was experiencing considerable flow reversal at times.

This drop-out strongly biases the measured radial velocity, and especially the higher cross-moments of the fluctuations. When taking measurements in regions where u and v are highly correlated, it was recommended in Chapter 4 that the hot-wire be deliberately misaligned with the mean flow to reduce the bias in the second and third moments. This is contrary to standard methods, which call for aligning the hot-wire axis with the mean flow.

Associated with the low sensitivity of hot-wire output with angle is a strong dependence of angle calibration velocity. It is standard practice to calibrate an x-wire at a particular velocity (near the mean velocity of interest) and apply this calibration to all measured values. While this is often acceptable for high velocities, the angle calibration of the hot-wire at low velocities is a strong function of the instantaneous velocity making it necessary to calibrate at several velocities. Because of this, it should also be clear that analog methods of measuring the u and v components are unacceptable.

It should be re-emphasized that these problems are due primarily to the low velocities and high turbulence intensities encountered in this investigation. The effects for higher velocity flows need to be examined further, since these problems and their consequences have been overlooked in the past.

Another unrelated problem which was encountered was the non-isotropy of the small scales of the turbulence. As was discussed in Chapter 5, this was much greater than originally expected. The lack of isotropy at the highest measurement position indicates a longer development region than expected. For comparison, the mean profiles are similar within

10 diameters downstream and the turbulence quantities appear similar within 20 diameters, but the derivative quantities showed no indication of similarity even at 40 diameters.

Originally it was planned to estimate the dissipation from the isotropic relations by applying Taylor's hypothesis to the measured time derivatives of the velocity. The derivative measurements were corrected for the deficiencies of Taylor's hypothesis in high intensity shear flows by using the correction scheme of Lumley (1965a). The anisotropy of the velocity derivatives negated this attempt and therefore a direct estimate of the dissipation was not obtained. The measured values of the temperature derivatives showed far less deviation from similarity and isotropy than the velocity derivatives and a direct estimate of the dissipation of the temperature fluctuations was possible.

Part of the non-isotropy may have been increased by the stratification present in the plume. At first the stratification was viewed as a problem, but it was later viewed as an extension of the investigation, since measurements were taken with several degrees of stratification over the course of the investigation. Unfortunately, the cause of the stratification was not determined until after the investigation was over, which prevented measurements of a plume in a neutral environment to be taken.

A major observation associated with the stratification was that the width of the velocity profile narrowed with increasing stratification. This observation was unexpected, and is still not well explained. One possible explanation involves the entrainment, and how it might be affected by the stratification. The stratification was due partly to a restriction of circulation of ambient air in the upper parts of the plume facility. This could have caused air to recirculate inside the screening instead of outside

as it should, and thus make the plume behave as if it were in a confined region instead of an infinite environment. The calculations of Baines and Turner (1969) show that for a plume in a confined box, the plume width is 6-7% narrower than for a similar stratification in an infinite environment, as calculated by Morton, Taylor and Turner (1956). This is in the region where the effects of stratification are small, and the plume width increases linearly.

Why this behavior would exist in this experiment is not clear, especially since only a portion of the air is recirculated. Much of the entrainment air, especially in the lower section of the plume, comes from outside the plume facility via openings at the bottom. It is surprising that the recirculation at the top of the facility can impose such a large effect on the lower region. However, the fact that the entire facility becomes stratified might be an indication that it can.

The balances of turbulent kinetic energy and temperature fluctuations were calculated for a specific vertical height due to the stratification of the ambient air. The anisotropy of the small scale structure required that the dissipation be calculated from the balances instead of using the measured values. For the temperature fluctuations, the differences between the measured and calculated values of dissipation was small, but the differences in the velocity dissipation was considerable. Part of this larger discrepancy was due to the unmeasured pressure-velocity correlation term in the kinetic energy balance.

This experiment provided large amounts of turbulence data of a buoyancy dominated flow. However, to adequately test many of the turbulence models now being developed, more data needs to be taken. As determined by this experiment, much of this data cannot be taken with present state-of-the-art techniques. New methods need to be developed that will enable experimenters

to accurately measure the dissipation and higher moments of the turbulent velocity field. This might include such methods as a shooting probe or a LDA. However many problems must be overcome before either of these would be suitable for general use. The high value of turbulence intensity measured in a 2-D plume with an LDA (Kotsovinos 1977) might indicate greater problems with that method than with hot-wires. Similarly, the engineering and flow disturbance problems associated with large moving probe systems might also significantly bias the results. These problems need to be addressed soon so that more data can be taken.

Appendix A1 Governing Equations for an Axisymmetric Turbulent Plume

Reynolds equations for flow with buoyancy:

Momentum: $$\bar{u}_j \frac{\partial \bar{u}_i}{\partial x_j} + \frac{\partial}{\partial x_j}(\overline{u_i u_j}) = -\frac{1}{\rho}\frac{\partial P}{\partial x_i} + \nu \frac{\partial^2 \bar{u}_i}{\partial x_j \partial x_j} + g_0 \beta \Delta T \, \delta_{iz} \qquad \text{A1.1}$$

Continuity: $$\frac{\partial \bar{u}_i}{\partial x_i} = 0 \; ; \quad \frac{\partial u_i}{\partial x_i} = 0 \qquad \text{A1.2}$$

Temperature: $$\bar{u}_j \frac{\partial T}{\partial x_j} + \frac{\partial}{\partial x_j}(\overline{u_j t}) = \gamma \frac{\partial^2 T}{\partial x_j \partial x_j} \qquad \text{A1.3}$$

Axial momentum equation in cylindrical coordinates:

$$\bar{u}_z \frac{\partial \bar{u}_z}{\partial z} + \bar{u}_r \frac{\partial \bar{u}_z}{\partial r} + \frac{\bar{u}_\phi}{r}\frac{\partial \bar{u}_z}{\partial \phi} + \frac{\partial}{\partial z}(\overline{u_z u_z}) + \frac{1}{r}\frac{\partial}{\partial r}(r\,\overline{u_z u_r}) + \frac{1}{r}\frac{\partial}{\partial \phi}(\overline{u_z u_\phi}) = -\frac{1}{\rho}\frac{\partial P}{\partial z} + \nu\left[\frac{\partial^2 \bar{u}_z}{\partial z^2} + \frac{1}{r}\frac{\partial}{\partial r}\left(r\frac{\partial \bar{u}_z}{\partial r}\right) + \frac{1}{r^2}\frac{\partial^2 \bar{u}_z}{\partial \phi^2}\right] + g_0 \beta \Delta T \qquad \text{A1.4}$$

Radial momentum equation in cylindrical coordinates:

$$\bar{u}_z \frac{\partial \bar{u}_r}{\partial z} + \bar{u}_r \frac{\partial \bar{u}_r}{\partial r} + \frac{\bar{u}_\phi}{r}\frac{\partial \bar{u}_r}{\partial \phi} - \frac{\bar{u}_\phi^2}{r} + \frac{\partial}{\partial z}(\overline{u_z u_r}) + \frac{1}{r}\frac{\partial}{\partial r}(r\,\overline{u_r u_r}) + \frac{1}{r}\frac{\partial}{\partial \phi}(\overline{u_\phi u_r}) - \frac{\overline{u_\phi u_\phi}}{r} = -\frac{1}{\rho}\frac{\partial P}{\partial r} + \nu\left[\frac{\partial^2 \bar{u}_r}{\partial z^2} + \frac{1}{r}\frac{\partial}{\partial r}\left(r\frac{\partial \bar{u}_r}{\partial r}\right) - \frac{\bar{u}_r}{r^2} + \frac{1}{r^2}\frac{\partial^2 \bar{u}_r}{\partial \phi^2} - \frac{2}{r^2}\frac{\partial \bar{u}_\phi}{\partial \phi}\right] \qquad \text{A1.5}$$

Azimuthal momentum equation in cylindrical coordinates:

$$\bar{u}_z \frac{\partial \bar{u}_\phi}{\partial z} + \bar{u}_r \frac{\partial \bar{u}_\phi}{\partial r} + \frac{\bar{u}_\phi}{r}\frac{\partial \bar{u}_\phi}{\partial \phi} + \frac{\bar{u}_r \bar{u}_\phi}{r} + \frac{\partial}{\partial z}(\overline{u_z u_\phi}) + \frac{1}{r}\frac{\partial}{\partial r}(r\,\overline{u_r u_\phi}) + \frac{1}{r}\frac{\partial}{\partial \phi}(\overline{u_\phi u_\phi}) = -\frac{1}{r}\frac{1}{\rho}\frac{\partial P}{\partial \phi} + \nu\left[\frac{\partial^2 \bar{u}_\phi}{\partial z^2} + \frac{1}{r}\frac{\partial}{\partial r}\left(r\frac{\partial \bar{u}_\phi}{\partial r}\right) - \frac{\bar{u}_\phi}{r^2} + \frac{1}{r^2}\frac{\partial^2 \bar{u}_\phi}{\partial \phi^2} - \frac{2}{r^2}\frac{\partial \bar{u}_\phi}{\partial \phi}\right] \qquad \text{A1.6}$$

Continuity equation in cylindrical coordinates:

$$\frac{\partial \bar{u}_z}{\partial z} + \frac{\partial \bar{u}_r}{\partial r} + \frac{\bar{u}_r}{r} + \frac{1}{r}\frac{\partial \bar{u}_\phi}{\partial \phi} = 0 \qquad \text{A1.7}$$

Temperature equation in cylindrical coordinates:

$$\bar{u}_z \frac{\partial T}{\partial z} + \bar{u}_r \frac{\partial T}{\partial r} + \frac{\bar{u}_\phi}{r}\frac{\partial T}{\partial \phi} + \frac{\partial}{\partial z}(\overline{u_z t}) + \frac{1}{r}\frac{\partial}{\partial r}(r\,\overline{u_r t}) + \frac{1}{r}\frac{\partial}{\partial \phi}(\overline{u_\phi t})$$
$$= \gamma\left[\frac{\partial^2 T}{\partial z^2} + \frac{1}{r}\frac{\partial}{\partial r}\left(r\frac{\partial T}{\partial r}\right) + \frac{1}{r^2}\frac{\partial T}{\partial \phi}\right] \qquad \text{A1.8}$$

Neglect viscous terms, azimuthal derivatives, and mean quantities in the azimuthal direction. Integration of the radial momentum equation yields:

$$P = P_\infty + \rho \int_r^\infty \frac{\overline{u_r^2} - \overline{u_\phi^2}}{r'}\,dr' - \rho\overline{u_r^2} \quad ; \quad \frac{dP_\infty}{dz} = 0 \qquad \text{A1.9}$$

Substituting into the axial momentum equation and neglecting the turbulent normal stresses yields:

Momentum: $$\bar{u}_z \frac{\partial \bar{u}_z}{\partial z} + \bar{u}_r \frac{\partial \bar{u}_z}{\partial r} + \frac{1}{r}\frac{\partial}{\partial r}(r\,\overline{u_z u_r}) = g_0 \beta \Delta T \qquad \text{A1.10}$$

Continuity: $$\frac{\partial}{\partial z}\bar{u}_z + \frac{\partial \bar{u}_r}{\partial r} + \frac{\bar{u}_r}{r} = 0 \qquad \text{A1.11}$$

Temperature: $$\bar{u}_z \frac{\partial T}{\partial z} + \bar{u}_r \frac{\partial T}{\partial r} + \frac{\partial}{\partial z}(\overline{u_z t}) + \frac{1}{r}\frac{\partial}{\partial r}(r\,\overline{u_r t}) = 0 \qquad \text{A1.12}$$

By defining a temperature difference, the equations can be coupled.

$$\Delta T = T - T_\infty(z) \qquad \text{A1.13}$$

$$\bar{u}_z \frac{\partial \Delta T}{\partial z} + \bar{u}_z \frac{\partial T_\infty}{\partial z} + \bar{u}_r \frac{\partial \Delta T}{\partial r} + \frac{\partial}{\partial z}(\overline{u_z t}) + \frac{1}{r}\frac{\partial}{\partial r}(r\,\overline{u_r t}) = 0 \qquad \text{A1.14}$$

Derivation of the equation for the temperature fluctuations for an axisymmetric plume.

Heat equation: $$\frac{\partial \tilde{T}}{\partial t} + \tilde{U}_z \frac{\partial \tilde{T}}{\partial z} + \tilde{U}_r \frac{\partial \tilde{T}}{\partial r} = \gamma \left[\frac{\partial^2 \tilde{T}}{\partial z^2} + \frac{1}{r} \frac{\partial}{\partial r} \left(r \frac{\partial \tilde{T}}{\partial r} \right) \right] \qquad \text{A1.15}$$

Let $\tilde{T} = T + t$, $\tilde{U}_z = U_z + u_z$, $\tilde{U}_r = U_r + u_r$

$$\frac{\partial T}{\partial t} + \frac{\partial}{\partial t} t + U_z \frac{\partial T}{\partial z} + u_z \frac{\partial t}{\partial z} + U_z \frac{\partial t}{\partial z} + u_z \frac{\partial T}{\partial z} + U_r \frac{\partial T}{\partial r} + U_r \frac{\partial t}{\partial r} + u_r \frac{\partial T}{\partial r} + u_r \frac{\partial t}{\partial r} = \text{CONDUCTION TERMS} \qquad \text{A1.16}$$

Subtract Reynolds equation for temperature (A1.12)and multiply by t

$$t \frac{\partial T}{\partial t} + t \frac{\partial}{\partial t} t + t u_z \frac{\partial T}{\partial z} + t U_z \frac{\partial t}{\partial z} + t u_z \frac{\partial t}{\partial z} + t u_r \frac{\partial T}{\partial r} + t U_r \frac{\partial t}{\partial r} + t u_r \frac{\partial t}{\partial r} - t \frac{\partial}{\partial z} \overline{u_z t} - t \frac{\partial}{\partial r} \overline{u_r t} = \text{CONDUCTION TERMS} \qquad \text{A1.17}$$

Average

$$\frac{D}{Dt} \left(\overline{t^2}/2 \right) = - \overline{u_z t} \frac{\partial T}{\partial z} - \overline{u_r t} \frac{\partial T}{\partial r} - \overline{u_z t \frac{\partial t}{\partial z}} - \overline{u_r t \frac{\partial t}{\partial r}} - \text{DISSIPATION} \qquad \text{A1.18}$$

Rearranging:

$$\frac{D}{Dt} \left(\overline{t^2}/2 \right) = - \left(\overline{u_z t} \frac{\partial T}{\partial z} + \overline{u_r t} \frac{\partial T}{\partial r} \right) - \tfrac{1}{2} \left(2 \overline{u_z t \frac{\partial t}{\partial z}} + 2 \overline{u_r t \frac{\partial t}{\partial r}} \right) - \epsilon_t \qquad \text{A1.19}$$

But:

$$\frac{\partial}{\partial z} \overline{u_z t^2} = u \overline{\frac{\partial t^2}{\partial z}} + \overline{t^2 \frac{\partial}{\partial z} u} = 2 \overline{u t \frac{\partial t}{\partial z}} + \overline{t^2 \frac{\partial}{\partial z} u} \qquad \text{A1.20}$$

Substitute A1.20 and add continuity equation.

$$\tfrac{1}{2} t^2 \left(\frac{\partial u_z}{\partial z} + \frac{1}{r} \frac{\partial}{\partial r} (r u_r) \right) = 0 \qquad \text{A1.21}$$

$$\frac{D}{Dt} \left(\overline{t^2}/2 \right) = - \left(\overline{u_z t} \frac{\partial T}{\partial z} + \overline{u_r t} \frac{\partial T}{\partial r} \right) - \tfrac{1}{2} \left(\frac{\partial}{\partial z} \overline{u_z t^2} + \frac{1}{r} \frac{\partial}{\partial r} r \overline{u_r t^2} \right) - \epsilon_t \qquad \text{A1.22}$$

The turbulent kinetic energy equation can be derived in a similar manner.

The kinetic energy is defined by:

$$q^2 = \tfrac{1}{2}\left(\overline{u_z^2} + \overline{u_r^2} + \overline{u_\theta^2}\right) \qquad \text{A1.23}$$

The kinetic energy equation reduces to:

$$\frac{D}{Dt}\left(q^2\right) = -\frac{\partial}{\partial x_j}\left(\frac{1}{\rho}\overline{u_j p} + \overline{q^2 u_j}\right) - \tfrac{1}{2}\overline{u_i u_j}\left(\frac{\partial \bar{u}_i}{\partial x_j} + \frac{\partial \bar{u}_j}{\partial x_i}\right) + g_o \beta \overline{u_z t} - \epsilon \qquad \text{A1.24}$$

The above equation neglects the viscous transport terms and all mean quantities in the azimuthal direction. Rewriting in cylindrical coordinates yields:

$$\frac{D}{Dt}\left(q^2\right) = \frac{\partial}{\partial z}\left(\frac{\overline{u_z p}}{\rho} + \overline{q^2 u_z}\right) + \frac{1}{r}\frac{\partial}{\partial r}\left[r\left(\frac{\overline{u_r p}}{\rho} + \overline{q^2 u_r}\right)\right] \qquad \text{A1.25}$$

$$- \overline{u_z^2}\frac{\partial \bar{v}_z}{\partial z} - \overline{u_z u_r}\frac{\partial \bar{v}_z}{\partial r} - \overline{u_z u_r}\frac{\partial \bar{v}_r}{\partial z} - \overline{u_r^2}\frac{\partial \bar{v}_r}{\partial r}$$

$$+ g_o \beta \overline{u_z t} - \epsilon$$

APPENDIX A2

Description of Homemade Electronic Hardware

Four pieces of electronic equipment will be described in this Appendix. All were built specifically for this investigation, and were designed to give high performance at a very low cost. Each unit cost less than fifty dollars and performs on a level equal to commercially available models. The four components are: Resistance Temperature Bridge, Amplifier with Variable D.C. offset, Differentiator, and Analog D.C. Motor Control for Probe Positioning. Each will be described in detail below.

1. Resistance Temperature Bridge: This is designed similar to the units by Wlezien and Way (1977) except only one sensor is included. The second, or ambient sensor, is replaced by a fixed resistor. By employing two of these (one for the flow and another for the ambient) both T and ΔT can be measured. Since the velocity wire calibration depends on the actual flow temperature, a single unit using two sensors to measure only ΔT is not adequate.

The schematic for the flow measuring unit is shown in Figure A2.1. The ambient unit is of identical design but with different values of some resistors due to the differences of resistance between the two wire sensors (1 μm @ 60 Ω vs. 5 μm @ 3.5 Ω). To provide a steady, stable probe current, batteries are used in conjunction with a voltage follower circuit and a large ballast resistor.

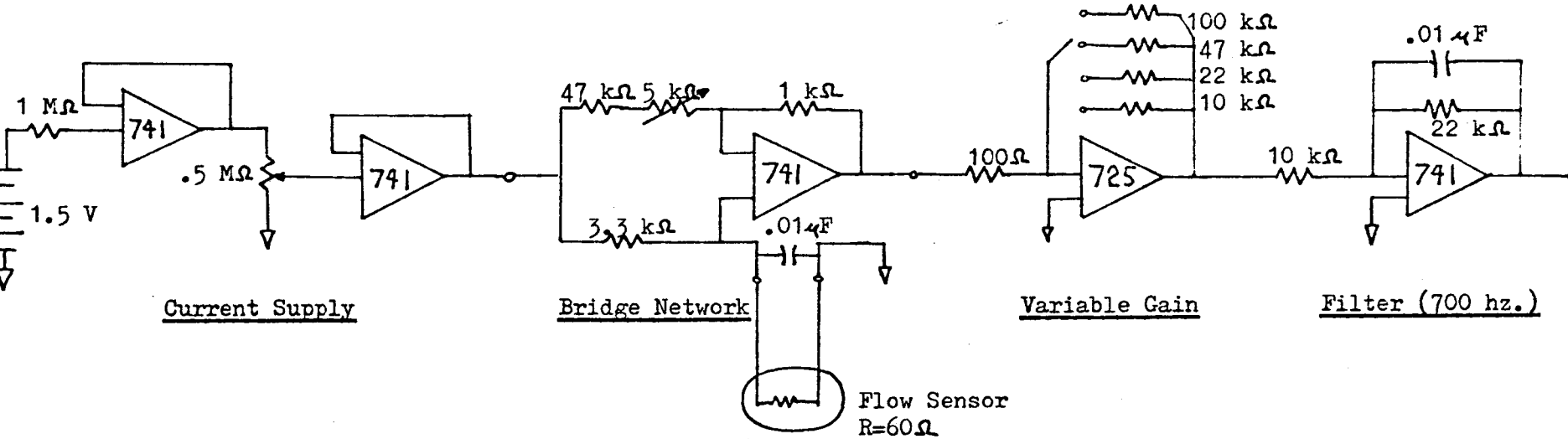
1 MΩ
741
1.5 V
.5 MΩ
741
47 kΩ
5 kΩ
1 kΩ
741
3.3 kΩ
.01μF
100Ω
100 kΩ
47 kΩ
22 kΩ
10 kΩ
725
10 kΩ
.01μF
22 kΩ
741
Current Supply
Bridge Network
Variable Gain
Filter (700 hz.)
Flow Sensor
R=60Ω

Figure A2.1

The unique feature about this design is the feedback bridge arrangement. Most commercial units connect the two sides of the bridge into an amplifier and operate it in an open-loop situation. This causes considerable amounts of temperature drift. By employing a feedback system, many of the characteristics of the amplifier no longer affect the output. The resulting system can be operated with inexpensive components and still maintain high quality performance.

2. Amplifier: To obtain optimum performance from the A/D, the anemometer signals need to be amplified. First, the large D.C. mean voltage has to be removed. Since the magnitude of this D.C. voltage is needed to calculate the velocity, a subtraction circuit is employed to remove a fixed, known voltage. To eliminate problems with drift or noise in this offset, batteries are used in conjunction with a follower circuit to provide a stable, low impedence voltage reference. The schematic for this circuit is shown in Figure A2.2.

3. Differentiator: In the same box that houses the amplifiers are three differentiators. They provide linear response through the dissipation range frequencies. They have a double pole roll-off with break points at 600 hz. and 3400 hz. The schematic is shown in the lower half of Figure A2.2, and the frequency response curve is plotted in Figure A2.3.

4. Position Control: This simple circuit provides a means of analog control of the traverser. An input voltage of 0-5 volts can be supplied through one of the D/A channels of the computer or by an

Figure A2.2

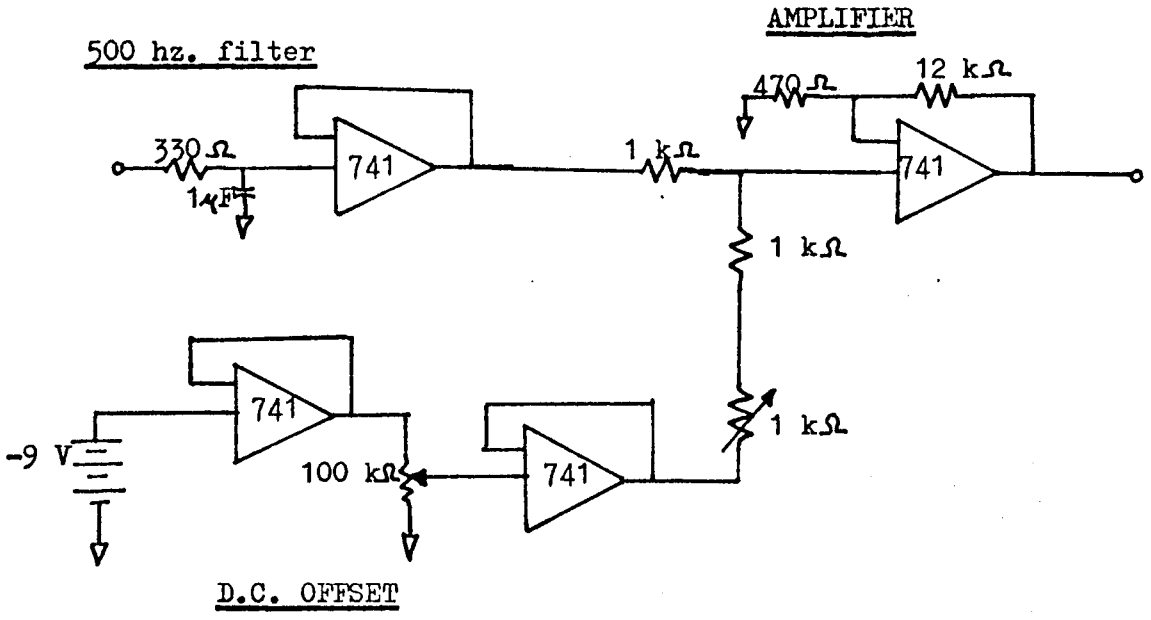
500 hz. filter
AMPLIFIER
330 Ω
1 μF
741
1 kΩ
470 Ω
12 kΩ
741
1 kΩ
741
-9 V
100 kΩ
741
1 kΩ
D.C. OFFSET

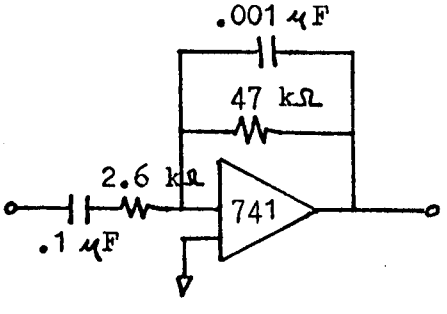
.001 μF
47 kΩ
2.6 kΩ
741
.1 μF
DIFFERENTIATOR

Figure A2.3

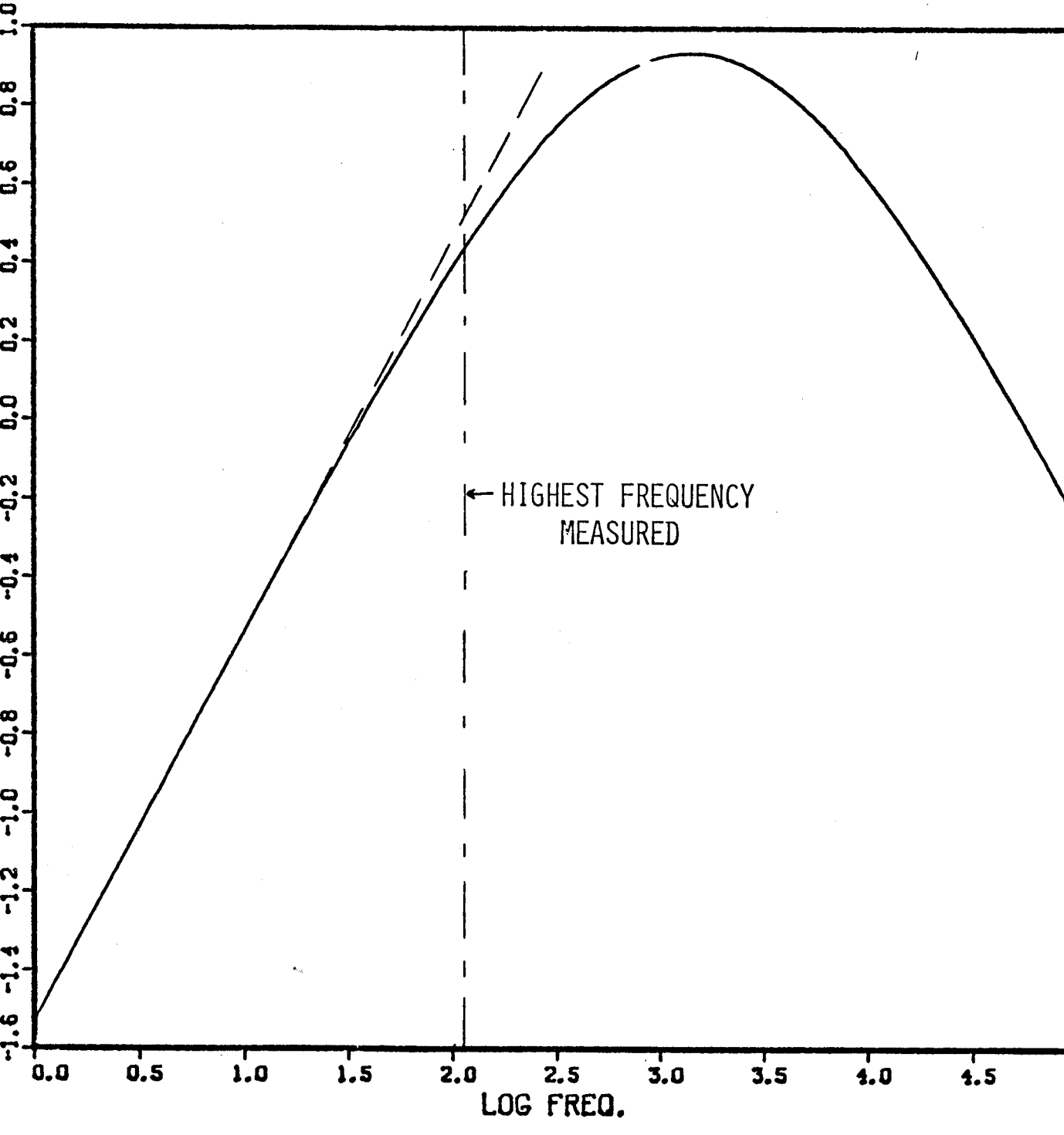
1.0
0.8
0.6
0.4
0.2
0.0
-0.2
-0.4
-0.6
-0.8
-1.0
-1.2
-1.4
-1.6
HIGHEST FREQUENCY
MEASURED
0.0
0.5
1.0
1.5
2.0
2.5
3.0
3.5
4.0
4.5
LOG FREQ.

optional manual control knob on the front face of the unit. Due to the 741 amplifier, the supply voltage is limited to +/- 22 volts. Ideally the supply should be 25-30 volts for the given motors, but by adding counterweights to the traverser, 22 volts is adequate. The D.C. motors are a large source of electronic noise, and since the wires from the comtroller to the traverser were 50 feet long, the traverser would often oscillate somewhat after reaching its final position. To prevent this, a shut-off relay was added. The schematic for one channel (both identical) is shown in Figure A2.4.

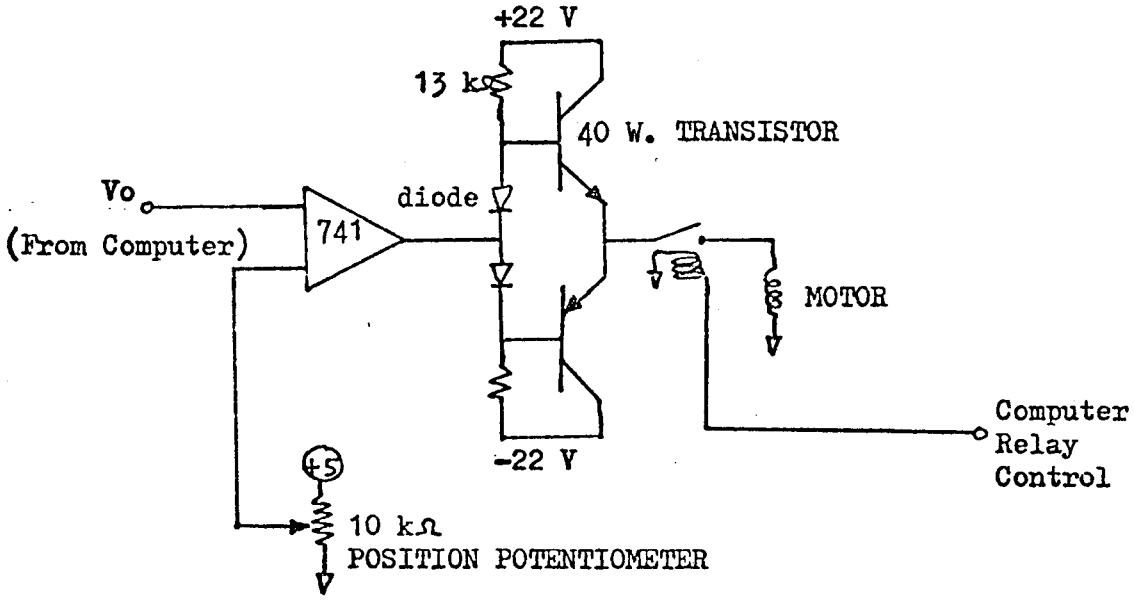
+22 V
13 kΩ
40 W. TRANSISTOR
Vo
(From Computer)
741
diode
MOTOR
Computer
Relay
Control
-22 V
+5
10 kΩ
POSITION POTENTIOMETER

APPENDIX A3

Angle Calibration Techniques

The angle calibration techniques used in this investigation are complicated and are not suited for practical use. They were developed to serve a specific problem - that of angle dependence of an X-wire probe in turbulent flows at low velocities (< 1 m/s) where the velocity derivatives are also of interest. In this flow region the X-wires behaved very non-ideally, and no other calibration scheme was found to be adequate. The form of the relation is given in equation A3.1.

$$U_{EFF} = U_o\left[\cos^2(\phi-\phi_o) + K\sin^2(\phi-\phi_o)\right]^n$$

Both K and ϕ_o are functions of velocity of the form

$$A_1 + B_1 U_o^{1/2} + C_1 U_o^{3/2}$$

This appendix is divided into two sections. The first deals with solving for the calilbration expression, and the second examines how to undo this expression to solve for the velocity components.

Part 1. To determine the values of k, n, and ϕ_o the response of the X-wire has to be measured at several different angles. This is done with the aid of an automated program called ANGLECAL. To determine the velocity sensitivity of the parameters, this calibration data must be taken at several different velocities (8 were used in this investigation, ranging from 0.25 m/s to 1.0 m/s). A non-linear

regression program called "ANGLE" is used to fit equation A3.1 to the data at each velocity. The value of n is a variable, but is kept constant for all velocities.

To simplify things somewhat, the values of ϕ_o are normalized so that a single curve can fit both. Later this will be shown to be equivalent to assuming ϕ_o is zero but the angle between the wires, Θ, is changing with velocity. Physically this is impossible but mathematically it is equivalent, and it is much easier to solve this way.

Another regression program, "CURFIT", is used to fit equation A2.2 to the values of k for each wire, and also to the values of ϕ_o. This entire process is outlined step-by-step in Part 3 of this appendix.

Part 2. Just as difficult is the problem of calculating the values of u and v and their derivatives from the measured anemometer voltages. After the effective velocity of each wire has been calculated from the measured voltage, the effective velocity derivative is calculated from the measured voltage and voltage derivative by differentiating the velocity calibration curve. However, the velocity dependence of k and Θ make it impossible to invert the angle calibration Instead, an estimate of the total velocity, U_o, is made, the values of k and Θ are are calculated, the angle calibration is inverted, and the calculated value of U_o is compared to the estimate. This process is repeated until the error is less than 1-2 cm/s. This is shown graphically in a flow chart in Figure 10b. Once the error is reduced to an acceptable level (usually only one iteration is required), calculation of the u and v components and their derivatives is

straightforward. The mathematics for this follows. Use Figure A3.1 for reference.

$$U_{EFF_i} \equiv U_{o_i} = U_o \left[\cos^2(\gamma_i - \phi_{o_i}) + K_i \sin^2(\gamma_i - \phi_{o_i}) \right]^n \qquad A3.3$$

$$i = 1,2 \quad K_i = K_i(U_o) \; ; \; \phi_{o_i} = \phi_{o_i}(U_o)$$

DEFINE: $\alpha_i \equiv \gamma_i - \phi_{o_i}(U_o)$ A3.4

$$U_{o_i} = U_o \left(\cos^2\alpha_i + K_i \sin^2\alpha_i \right)^n \qquad A3.5$$

$$\alpha_2 = 180^\circ - \alpha_1 - \phi_{o_2} - \phi_{o_2}$$

DEFINE: $\alpha_2 = \Theta^* - \alpha_1$ A3.6

WHERE $\Theta^* = 180^\circ - \phi_{o_2} - \phi_{o_2}$

SOLVE FOR U_o AND α_1

$$\text{LET: } P = \left(\frac{U_{o_1}}{U_{o_2}}\right)^{1/n} = \frac{\cos^2\alpha_1 + K_1 \sin^2\alpha_1}{\cos^2(\Theta^* - \alpha_1) + K_2 \sin^2(\Theta^* - \alpha_1)} \qquad A3.7$$

$$\text{LET: } A = P\left(\cos^2\Theta^* + K_2 \sin^2\Theta^*\right) \qquad A3.8a$$

$$B = P\left(\sin^2\Theta^* + K_2 \cos^2\Theta^*\right) \qquad A3.8b$$

$$C = P(1 - K_2) \sin\Theta^* \cos\Theta^* \qquad A3.8c$$

Figure A3.1

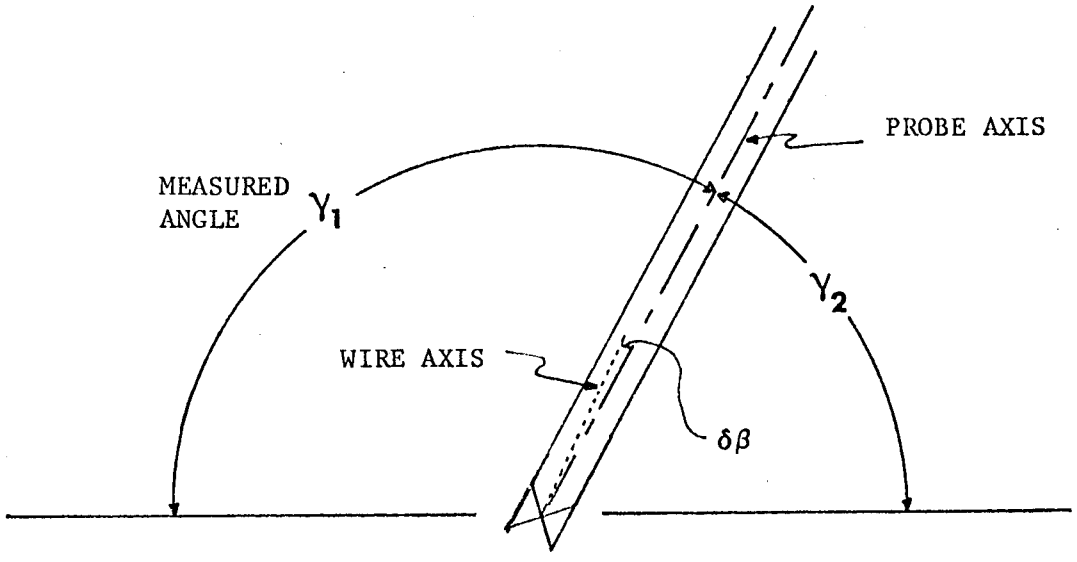
PROBE AXIS
MEASURED
ANGLE
γ_1
γ_2
WIRE AXIS
$\delta\beta$

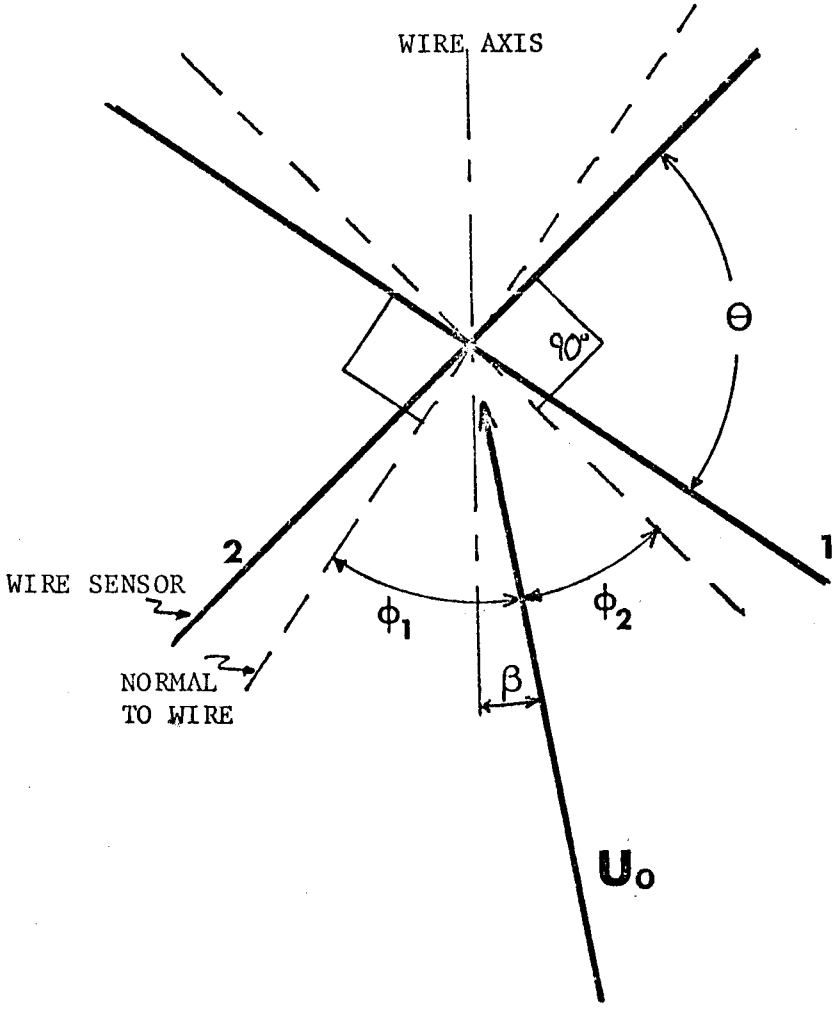
WIRE AXIS
90°
Θ
2
1
WIRE SENSOR
ϕ_1
ϕ_2
NORMAL
TO WIRE
β
U_o

REARRANGING EQUATION A3.7 GIVES:

$$\cos^2\alpha_1 + K_1 \sin^2\alpha_1 = A\cos^2\alpha_1 + B\sin^2\alpha_1 + 2C\sin\alpha_1\cos\alpha_1 \qquad A3.9$$

DIVIDE BY $\cos^2\alpha_1$.

$$(B-K_1)\tan^2\alpha_1 + 2C\tan\alpha_1 + (A-1) = 0 \qquad A3.10$$

$$\alpha_1 = \tan^{-1}\left[\frac{-2C \pm \sqrt{4C^2 - 4(B-K_1)(A-1)}}{2(B-K_1)}\right] \qquad A3.11$$

For velocities within the acceptance angle of the x-wire, the sign of the square root is always positive. Knowing , it is easy to find U and V.

$$U = U_0 \cos\beta$$
$$V = U_0 \sin\beta \qquad A3.12\ a\text{-}b$$

WHERE $\beta = \gamma_1 - 90^\circ - \delta\beta = \alpha_1 - \frac{\Theta^*}{2}$ $\qquad A3.13$

The solution of the velocity derivatives is found in a similar fashion.

ASSUME U_0, α_1, α_2, & β ARE KNOWN FROM ABOVE.

AND:

$$K_i = f_{K_i}(U_0)$$

$$\frac{dK_i}{dt} = f'_{K_i}(U_0)\frac{dU_0}{dt}$$

$$\Theta^* = f_\Theta(U_0) \qquad \text{A3.14 a-e}$$

$$\frac{d\Theta^*}{dt} = f'_\Theta(U_0)\frac{dU_0}{dt}$$

$$\frac{d\beta}{dt} = \frac{d\alpha_1}{dt} - \tfrac{1}{2}\frac{d\Theta^*}{dt}$$

$$U = U_0 \cos\beta$$

$$\frac{dU}{dt} = \frac{dU_0}{dt}\cos\beta - U_0 \sin\beta\left(\frac{d\alpha_1}{dt} - \tfrac{1}{2}\frac{d\Theta^*}{dt}\right) \qquad \text{A3.15}$$

$$\frac{dU}{dt} = \frac{dU_0}{dt}\left[\cos\beta + \tfrac{1}{2}U_0 \sin\beta f'_\Theta\right] + \frac{d\alpha_1}{dt}\left[-U_0 \sin\beta\right] \qquad \text{A3.16}$$

SIMILARLY FOR V,

$$\frac{dV}{dt} = \frac{dU_0}{dt}\left[\sin\beta - \tfrac{1}{2}U_0 \cos\beta f'_\Theta\right] + \frac{d\alpha_1}{dt}\left[U_0 \cos\beta\right] \qquad \text{A3.17}$$

NEED TO FIND $\frac{dU_0}{dt}$ AND $\frac{d\alpha_1}{dt}$

$$U_{o_i} = U_o \left(\cos^2\alpha_i + k_i \sin^2\alpha_i\right)^n \equiv U_o \cdot X_i^n \qquad \text{A3.18}$$

$$\frac{dU_{o_i}}{dt} = \frac{dU_o}{dt}\cdot\frac{U_{o_i}}{U_o} + U_o\left[n X_i^{n-1} - 2\cos\alpha_i \sin\alpha_i \frac{dk_i}{dt}\right.$$

$$\left. + k_i\, 2\sin\alpha_i\cos\alpha_i \frac{d\alpha_i}{dt} + \sin^2\alpha_i f'_{k_i}\frac{dU_o}{dt}\right] \qquad \text{A3.19}$$

$$\therefore \quad \frac{dU_{o_1}}{dt} = \frac{dU_o}{dt}\left[\frac{U_{o_1}}{U_o} + U_o n X_1^{n-1}\sin^2\alpha_1 f'_{k_1}\right]$$

$$+ \frac{d\alpha_1}{dt}\left[U_o n X_1^{n-1} 2(k_1-1)\sin\alpha_1\cos\alpha_1\right] \qquad \text{A3.20}$$

SIMILARLY;

$$\frac{dU_{o_2}}{dt} = \frac{dU_o}{dt}\left[\frac{U_{o_2}}{U_o} + \frac{n U_{o_2}}{X_2}\left(\sin^2\alpha_2 f'_{k_2} + 2(k_2-1) f'_\theta \sin\alpha_2\cos\alpha_2\right)\right]$$

$$+ \frac{d\alpha_1}{dt}\left[-\frac{2n U_{o_2}}{X_2}(k_2-1)\sin\alpha_2\cos\alpha_2\right] \qquad \text{A3.21}$$

IT IS STRAIGHTFORWARD TO SOLVE A3.20 AND A3.21

FOR $\frac{dU_o}{dt}$ AND $\frac{d\alpha_1}{dt}$

THEN A3.16 AND A3.17 CAN BE SOLVED FOR

$\frac{du}{dt}$ AND $\frac{dv}{dt}$.

Part 3. Method for Finding an Analytical Anglecalibration

1. Measure angle dependence of hot wires using program "ANGLECAL". Measure at several different velocities.

   Note: It is helpful to amplify the hot wire signals for angle calibration. The regression program "ANGLE" that follows allows for a linear response amplifier ($E_{out} = C_1 + C_2 E_{in}$) to be compensated for.

2. Find the optimum values of k and ϕ_o with the program "ANGLE" for each wire at each velocity (value of n should be fixed for all situations at a value around 0.5 - 1.0)

3. The values given for the maximum velocity at each given flowrate should be nearly the same for both wires. Average the two values to eliminate any small differences.

4. Average all the ϕ_o values for each wire (denoted $\bar{\phi}_1$ and $\bar{\phi}_2$) and subtract these numbers from all of the ϕ_o values of the corresponding wire.

5. Create a data file (with edit) containing the values of $\bar{U}_o$ and the adjusted values of ϕ_o (with means subtracted). Put all values (both wires) in the data file. The format is F 10.5 format written as follows:

   $\phi_1(1), \bar{U}_o(1)$

   $\phi_2(1), \bar{U}_o(1)$

   $\phi_1(2), \bar{U}_o(2)$

   $\phi_2(2), \bar{U}_o(2)$

   ⋮

6. Run "CURFIT" to fit an appropriate curve to the ϕ_o and $\bar{U}_o$ data. Ex: $\phi_o = A_\phi + B_\phi \bar{U}_o^{1/2} + C_\phi \bar{U}_o^{3/2}$. Then add back the values of $\bar{\phi}_1$ or $\bar{\phi}_2$ for each velocity (do both wires).

7. Again run the program "ANGLE" to find the optimum values of k for each wire, but use the value of ϕ_o as determined in step 6 for each velocity.

8. Create two data files (with edit) containing the k and $\bar{U}_o$ for each wire. (Use the individual values of $\bar{U}_o$ for each wire, not the average). The format for each data file is similar to that in step 5.

   Ex: File 1: $k_1(1), \bar{U}_o(1)$ File 2: $k_2(1), \bar{U}_o(1)$

   $k_1(2), \bar{U}_o(2)$ $k_2(2), \bar{U}_o(2)$

9. Run "CURFIT" to fit an appropriate curve to each data file.
   Ex: $k_1 = A_1 + B \bar{U}_o^{1/2} + C_1 \bar{U}_o^{3/2}$, $k_2 = A_2 + B_2 \bar{U}_o^{1/2} + C_2 \bar{U}_o^{3/2}$

10. Calculate the angle between the wires

    $\Theta = 180 - \bar{\phi}_1 - \bar{\phi}_2 - 2\phi_o(\bar{U}_o)$

Bibliography

Baines, W.D., Turner, J.S. (1969) *Turbulent Buoyant Convection From a Source in a Confined Region*. J. Fluid Mech. 37 Pt. 1, p. 51.

Baker, C.B. (1980). *An Analysis of the Turbulent Buoyant Jet*. Ph. D. Dissertation, SUNY/Buffalo, Buffalo, N. Y.

Baker, C.B., Taulbee, D.B., George, Jr., W.K. (1979). *Eddy Viscosity Calculations of Turbulent Buoyant Plumes*, ASME Public. 79-HT-51.

Batchelor, G.K. (1967). *An Introduction to Fluid Mechanics*, Cambridge University Press, London, England.

Batchelor, G.K. (1954). *Heat Convection and Buoyancy Effects in Fluids*. Quart. J. Royal Met. Soc. V80, p. 339.

Beuther, P.D., Capp, S.P., George, Jr., W.K. (1979) *Momentum and Temperature Balance Measurements in an Axisymmetric Turbulent Plume*, ASME Public. 79-HT-42.

Beuther, P.D., George, Jr., W.K., Arndt, R.E.A., (1977). *Modeling of Pressure Spectra in a Turbulent Shear Flow*. Presented at the 93rd meeting of the Acoustical Soc. of Amer., The Pennsylvania State Univ., June 1977.

Champagne, F.H., Friehe, C.A., LaRue, J.C. (1977). *Flux Measurements, Flux Estimation Techniquis and Fine-Scale Turbulence Measurements in the Unstable Surface Layer Over Land*. J. Atmos. Sci. V.34, No. 3, p. 515.

Champagne, F.H. (1978). *The Fine Scale Structure of the Turbulent Velocity Field*, J. Fluid Mech., 86, Pt. 1, p. 67.

Chen, C.J., Rodi, W. (1975). *A Mathematical Model for Stratified Turbulent Flows and its Application to Buoyant Jets*. IVI Congress, International Assoc. for Hydraulic Research, San Paulo.

Collis, D.C., Williams, M.J. (1959). *Two Dimensional Convection from Heated Wires at Low Reynolds Number.* J. Fluid Mech. 6, p. 357.

Corrsin, S. (1951) *On The Spectrum of Isotropic Temperature Fluctuations in Isotropic Turbulence.* J. Appl. Physics, V. 22, p. 469.

Drubka, R.E., Nagib, H.M., Tan-atichat, J., (1977) *On Temperature and Yaw Dependence of Hot-Wires.* Tech. Report, Illinois Institute of Tech.

George, W.K., Jr., Alpert, R.L., Tamanini, F., (1977). *Turbulence Measurements in an Axisymmetric Buoyant Plume,* Int. J. Heat Mass Trans. V. 20, 1145-1154.

George, W.K., Beuther, P.D. (1979). *Interpretation of Turbulence Measurements in High Intensity Turbulent Shear Flows.* Bulletin of the American Physical Society, V. 24, No. 8, p. 1136.

Gibson, C.H., Schwarz, W.H. (1963). *The Universal Equilibrium Spectra of Turbulent Velocity and Scalar Fields.* J. Fluid Mech. 16 #3, p. 365.

Gibson, C.H., Stegen, G.R., Williams, R.B. (1970). *Statistics of the Fine Structure of Turbulent Velocity and Temperature Fields Measured at High Reynolds Number.* J. Fluid Mech. 41 #1, p. 153.

Grant, H.L., Hughes, B.A., Vogel, W.M. Moilliet, A. (1968). *The Spectrum of Temperature Fluctuations in Turbulent Flow,* J. Fluid Mech. 34 #3 p. 423.

Gurvich, A.S. Yaglom, A.M. (1967). *Breakdown of Eddies and Probability Distributions for Small-Scale Turbulence.* Phys. Fluids, 10, Supplement (Proc. Kyoto Sympos. on Boundary Layers and Turbulence), S59-S65.

Gurvich, A.S. Zubkovskii, S.L. (1966). *Estimate of the Structure Function of Temperature Fluctuation in the Atmosphere.* Izv. Akad. Nauk. SSSR. Fiz. Attiosf. i. Okeana 2 #2, p. 202.

Hamilton, C.M. and George, W.K. (1976) *Eddy Viscosity Calculations for Turbulent Buoyant Plumes*, Bull. Am. Phys. Soc., Ser. II, 21, 10, 1225.

Hill, R. J. (1978) *Models of the Scalar Spectrum for Turbulent Advection* J. Fluid Mechanics, V. 88, 541.

Hinze, J.O. (1975). *Turbulence*, McGraw-Hill, Inc.

Jenkins, G.M., Watts, D.G., (1968) *Spectral Analysis and Its Applications*. Holden-Day, San Francisco.

Jorgensen, F.E., (1971)*Directional Sensitivity of Wire & Fiber-Film Probes*, DTSA Information #11, p. 31.

Kolmogorov, A.N. (1941) *Local STructure of Turbulence in an Incompressible Fluid at Very High Reynolds Numbers*. Dokl. Akad. Nauk SSSR, V30, #4, p.299.

Kotsovinos, N.E., (1977) *Plane Turbulent Buoyant Jets*, Pt. 1, J. Fluid Mech. 81, 1 pp. part 2, p. 45.

Lin, S.C., Lin, S.C. (1973) *Study of Strong Temperature Mixing in Subsonic Grid Turbulence*, Physics of Fluids, 16, p. 1587.

Lumley, J.L. (1965a) *Interpretation of Time Spectra Measured in High-Intensity Shear Flows*, Physics of Fluids, 8, #6, 1056-1062.

Lumley, J.L. (1965b) *Theoretical Aspects of Research on Turbulence in Stratified Flows*, Presentation at the Intl. Coll. on Atm. Turb. and Ra. Wave Propagation, Moscow, 6-15/22, 1965.

Lumley, J.L. (1970) *Stochastic Tools in Turbulence*, Academic Press, N. Y.

Lumley, J.L. (1971) *Explanation of Thermal Plume Growth Rates*, Physics of Fluids, V. 14, p. 2537.

Lumley, J.L., Zeman, O.(1978), *The Influence of Buoyancy on Turbulent Transport*, J. Fluid Mechanics, 84, Pt. 3, 0. 581.

Madni, I.K., Pletcher, R.H. (1977), *Prediction of Turbulent Forced Plumes Issuing Vertically Into Stratified or Uniform Environments*. J. Heat Transfer, p. 99.

Mannis, P.C., (1979), *Turbulent Buoyant Convection From A Source in a Confined Region*, J. Fluid Mechanics, V.91, p. 4, p. 765.

McAdams, W.H. (1954). *Heat Transmission*, Third Edition, Chap. X, McGraw-Hill Book Co., Inc.

Millionshchikov, M.D. (1941). *Theory of Homogeneous Isotropic Turbulence* Dokl. Akad, Nauk SSSR, 32, No. 9, p. 611.

Monin, A.S., Yaglom, A.M. (1971) Statistical Fluid Mechanics, V. 1, MIT Press.

Monin, A.S., Yaglom, A.M., (1975) Statistical Fluid Mechanics, V 2, MIT Press.

Morton, B.R., Taylor, G.I., and Turner, J.S. (1956), *Turbulent Gravitational Correction from Maintained and Instantaneous Sources*, Proc.Roy. Soc. A234, pp. 1-23.,

Nakagome, H. and Hirata, M. (1977), *The Structure of Turbulent Diffusion in an Axi-symmetrical Thermal Plume*, Heat Transfer and Turbulent Buoyant Convection, (Spalding and Afgan, eds.) McGraw-Hill, NY., 367-372.

Oboukhov, A.M., (1962), *Some Special Features of Atmospheric Turbulence*, J. Fluid Mechanics, 13 and #1 p. 77.

Paquin, J.E., Pond, S. (1971) *The Determination of the Kolmogorov Constants for Velocity, Temperature and Humidity Fluctuations from Second and Third-Order Structure Functions*, J. Fluid Mechanics, 50, #2, p. 257.

Reynolds, O. (1895) *On The Dynamical Theory of Incompressible Viscous Fluids and the Determination of the Criterion*, Phil. Trans. Roy. Soc. of London, Ser. A, V.186, p. 123.

Rouse, J., Yih, C.S. and Humphreys, H.W. (1952) *Gravitational Convection From a Boundary Source*, Tellus, 4, pp. 201-10.

Schmidt, W. (1941) *Turbulent Propagation of a Stream of Air*. ZAMM, V21, 6.

Tamanini, F., (1979) *The Effect of Buoyancy on the Turbulence Structure of Vertical Round Jets*, ASME, J. of Heat Trans. V. 100, 4, pp. 659-664.

Taylor, G.I., (1938) *The Spectrum of Turbulence*. Proc. of the Roy. Soc. of London, Series A, V.164, #919, p. 476.

Tennekes, H., Lumley, J.L. (1972). *A First Course in Turbulence*. MIT Press.

Tennekes, H., Wyngaard, J.C. (1972). *The Intermittent Small-Scale Structure of Turbulence: Data-Processing Hazards*, J. Fluid Mech. 55, 1, p. 93.

Townsend, A.A. (1970). *Entrainment and the Structure of Turbulent Flow*, J. Fluid Mechanics, 41, #1, p. 13.

Turner, J.S. (1969). *Buoyant Plumes and Thermals*. Ann. Rev. of Fluid Mechanics, V. 1.

Turner, J.S. (1973) *Buoyancy Effects in Fluids*, Cambridge University Press, Cambridge, England.

Tutu, N.K., Chevray, R. (1975) *Cross-wire Anemometry in High Intensity Turbulence*, J. Fluid Mech. 71, p. 785.

Williams, R.M., Paulson, C.A. (1977). *Microscale Temperature and Velocity Spectra in the Atmospheric Boundary Layer*, J. Fluid Mech. 83, p. 547.

Wills, J.A.B. (1964). *On Convection Velocities in Turbulent Shear Flows*. J. Fluid Mech. 20, #3, 417-432.

Wlezien, R.W., Way, J.L. (1977) *Bridge Circuits for Differential Resistance Measurements and Their Application to Resistance Thermometry*. Presentation at the Inter. Cong. on Instr. in Aerospace Simulation Facilities, Royal Military College of Science, Shrivenham, England. Sept. 6-8, 1977.

Wygnanski, I., Fiedler, H. (1969) *Some Measurements in the Self-Preserving Jet.* J. Fluid Mechanics, 38, p. 3, 0. 577.

Wyngaard, J.C. (1971) *The Effect of Velocity Sensitivity on Temperature Derivative Statistics in Isotropic Turbulence.* J. Fluid Mechanics, 48, Pt. 4, p. 763.

Wyngaard, J.C., Clifford, S.F. (1977) *Taylor's Hypothesis and High-Frequency Turbulence Spectra.* J. Atm. Sci. V.34, p. 922.

Yih, C.S., (1953) *Free Convection Due to Boundary Sources.* Fluid Models in Geophysics, Proc. 1st Symp. on the Use of Models in Geophysical Fluid Dynamics, The John Hoplins Univ., Baltimore, Md. (R.R. Long, ed.)

Yih, C.S. (1977) *Turbulent Buoyant Plumes,* The Physics of Fluids, 20, 8, pp. 1234-1237.